THE EFFECTS OF TURBULENCE ON HABITAT SELECTION AND SWIMMING KINEMATICS OF FISHES

by

Hans M. Tritico

A dissertation submitted in partial fulfillment
of the requirements for the degree of
Doctor of Philosophy
(Civil and Environmental Engineering and Natural Resources and Environment)
in the University of Michigan
2009

Doctoral Committee:

Associate Professor Aline J. Cotel, Co-Chair
Professor Paul W. Webb, Co-Chair
Professor Jonathan W. Bulkley
Professor Steven J. Wright

Acknowledgements

This dissertation could only have been completed with the contributions of many people. The members of my dissertation committee have provided me with generous support and guidance. My two co-chairs, Drs. Aline Cotel and Paul Webb, have been terrific mentors and advisors. I have especially appreciated their high expectations, stimulating conversations, and perspectives on life in academia. Dr. Steve Wright has been a mentor since the junior year of my undergraduate degree, more than a decade ago at this point. His guidance in my professional career has and will always be appreciated. Dr. Jonathan Bulkley has helped me to keep this entire process in perspective and has helped me to understand the importance of this dissertation work.

A special thanks must go to the many students that have helped in this project along the way, including Pratik Pradhan, Jenna Clarke, Stacey Burgtorf, Charles Humpfree, and Lisa Rayle. Rick Burch and the rest of the "coffee crew" provided invaluable practical guidance in building the myriad strange contraptions required for this work. Of course, nothing at this university would function without the support of Jill Miller, Janet Lineer, and Nancy Osugi.

During any journey, the most cherished gifts are the people that you meet and grow fond of along the way. A warm and heartfelt thank you is sent to all of the dear friends from the University and Ann Arbor for being who they are. One special person that I met during this journey is my wife, Lori Kumler, who continues to inspire me daily – thank you. Finally, my family has continued to find ways to support and problem-solve for me: you can rest assured that while this adventure is coming to a close that many more are just beginning!

Chapter 2 has been published in the Transactions of the American Fisheries Society Vol. 135, pp 610-619, 2006 as "Do Brown Trout Choose Locations with Reduced Turbulence" by Aline J. Cotel, Paul W. Webb, and Hans M. Tritico. Chapter 7 has been published by the journal Measurement, Science, and Technology Vol. 18, pp 2555-2562,

2007 as “Development, Testing, and Demonstration of a Portable Submersible Miniature Particle Imaging Velocimetry Device” by Hans M Tritico, Aline J. Cotel, and Jenna N Clarke.

Table of Contents

Acknowledgements ii

List of Figures vi

List of Tables viii

Abstract ix

Chapter

I. Introduction 1

Background 3

II. Do Brown Trout Choose Locations with Reduced Turbulence? 14

Introduction 14

Methods 15

Results 19

Discussion 31

III. The Effects of Turbulent Eddies on Stability and the Critical Swimming Speed of Creek Chub (*Semotilus atromaculatus*) 38

Introduction 38

Materials and Methods 39

Results 48

Discussion 66

Conclusions 73

IV. Relationships between Body-Caudal Fin Swimming Kinematics and the Eddy Composition of Turbulent Flow 81

Introduction 81

Materials and Methods 81
Results 86
Discussion 93
Conclusions 98

V. The Effects of Turbulent Flow Eddy Composition on Median and Paired-Fin Use 104
Introduction 104
Materials and Methods 105
Results 109
Discussion 119

VI. Development, Testing, and Demonstration of a Portable Submersible Miniature Particle Imaging Velocimetry Device 129
Introduction 129
System Overview 130
Validation 134
Field Demonstration 138
Conclusions 140

VII. Conclusion 146
Future Work 150

List of Figures

Figure

2.1: Relationships between turbulence intensity (TI) and current speed (u) for various locations with brown trout and similar locations with no fish 24

2.2: Depth distribution of the locations occupied by fish and the chosen locations without fish sampled in 2002 and 2003 25

2.3: Sketch map (A) and flow characteristics (B, C) of a cross-stream transect with large accumulations of large woody debris (LWD) 28

2.4: Sketch map (A) and flow characteristics (B, C) along a cross-stream transect over a sandy area of stream bed with little in-flow structures 30

3.1: Flume and Test Section Configuration 41

3.2: Test Section Regions 42

3.3: Location of PIV Interrogation Windows 45

3.4: A comparison of local velocity to cross-sectionally averaged velocity for flow regions and treatment 49

3.5: The distribution of eddy diameters varied across cylinder treatment 51

3.6: The 95th percentile eddy diameter varied across treatment and flow region 52

3.7: The 95th percentile eddy vorticity varied across treatment and flow region 55

3.8: Flow Region Preference 58

3.9: The body centerline is plotted across 67 ms time-steps for a representative spill and recovery 61

3.10: The critical swimming speed and speed of first spill varied across treatment 64

3.11: The percentage time fish were observed in a region for cross-sectionally averaged velocities that spills occurred and the

percentage of total failures observed varied across flow region 65

3.12: The ratio of the 95th percentile eddy to fish momentum varied across treatment and region 71

4.1: Large Cylinder Test Section Regions 85

4.2: Variation of local velocity, vorticity, and eddy diameter with cross-sectionally averaged velocity and flow region 89

4.3: Tail beat frequency and amplitude across speed and turbulent regime 91

4.4: Fish based Strouhal number increases linearly with 95th percentile fish based persistence parameter 97

5.1: Median-Fin Usage 111

5.2: Paired-Fin Usage 114

5.3: Mean Pectoral-fin % Time Deployed vs 95th Percentile Eddy Momentum Ratio 116

5.4: Pectoral-Fin Deployment Pattern 118

6.1: System Schematic 131

6.2: Selected vorticity plots from lab PIV (left) and underwater PIV (right) for discharge Reynolds numbers of a) 3.3x10^4 b) 1.4x10^5 and c) 7.9x10^5 136

6.3: Image of underwater PIV being used in the Huron River, MI 140

6.4: Field data 141

List of Tables

Table

1.1: **A selection of studies investigating the effects of increased turbulent velocity fluctuations on various fish response characteristics** 4

2.1: Summary of observations and methods used to determine turbulence intensity in brown trout habitat 17

6.1: Comparisons of free stream velocity, vorticity, mean eddy diameter and maximum eddy diameter between Laboratory and Underwater PIV for flow downstream from a 1.6 cm cylinder 139

Abstract

This dissertation has investigated the role of turbulent eddies on habitat selection and swimming kinematics of fish. First, the level of turbulent velocity fluctuations in habitat selected by brown trout (*Salmo trutta*) was investigated in the field. It was found that turbulent velocity fluctuations were lower in areas that fish selected compared to areas that were not inhabited but were believed to be viable habitat based on standard habitat suitability indices. Based on the results from these field observations, a series of laboratory experiments tested the effects of turbulent eddies on fish swimming kinematics. Specifically, a series of increasing velocity tests were conducted such that creek chub (*Semotilus atromaculatus*, total length = 12.2 cm) were swum downstream from either a control grid or one of three cylinder arrays (diameters of 0.4, 1.6, and 8.9 cm, with gaps equal to cylinder diameter) which were oriented either vertically or horizontally. The control grid and cylinder arrays produced turbulent flow regimes with 95^{th} percentile eddy diameters ranging from 1/6 to 1 fish length and 95^{th} percentile eddy vorticity ranging from 1.5 to 11.3 s^{-1} across cross-sectionally averaged flow speeds ranging from 8.5 to 50.2 $cm.s^{-1}$. As eddy diameter and vorticity increased (and hence eddy momentum), the fish critical swimming speed and tail beat frequency decreased. Conversely, increasing eddy momentum resulted in increased tail beat amplitude, rates of spill, and pectoral and pelvic fin percentage area and time deployed. In the presence of eddies with high momentum the fish based Strouhal number was found to increase linearly with the fish based persistence parameter. Further, it was found that changes in the orientation of the eddies, which either rotated about a horizontal or vertical axis, produced changes in critical swimming speed, spill rates, and the pattern of pectoral fin deployment. It was shown that the primary mechanism which links the features of turbulence to the response of fish was the relative momentum of the 95^{th} percentile turbulent eddies with respect to the fish. Finally, in order to apply the results from these

laboratory experiments in the field, a portable, submersible, miniature particle image velocimetry device was developed and tested allowing for the collection of turbulent eddy metrics in fluvial environments.

Chapter I

Introduction

Civil engineering designs are increasingly required to mitigate impacts on aquatic ecology; as such, stream restoration and the design of fishways (fish ladders, fish screens, and road culverts) are becoming increasingly important (Pearson et al. 2005). These new societal and governmental mandates (e.g. EPA 40 CFR Part 30, 2008) push engineering projects to be more sustainable, have a lower impact on the environment, and meet the demands of a growing population. A major component of stream restoration is the design of micro-habitat, sub-reach scale designs which often include flow obstructions such as large-woody debris, rock barbs, and boulder clusters (Rosgen 1996, Papanicolaou et al. 2003, Shields et al. 2004). The primary purpose of these engineered obstructions is usually three-fold in that they provide a time-averaged velocity refuge, provide cover from predation, and provide increased diversity of habitat choices (Huston 1979, Shields et al. 2003, Palmer and Allan 2006). To understand the role of such engineering obstructions, they must be viewed in the context of eddies and turbulence.

When the obstruction-based Reynolds number (the ratio of inertial to viscous forces in a flow, $Re=UL/\upsilon$, where Re is the obstruction-based Reynolds number, U is the velocity approaching the obstruction, L is the obstruction diameter and υ is the kinematic viscosity of water) is greater than 60, turbulent eddies will be shed from the obstruction (von Kàrmàn 1937). These turbulent eddies are coherent rotating structures in the fluid. A two-dimensional slice through these rotating fluid bodies appears as a rotating disk which can be described by its diameter and rate of rotation, vorticity (ω_e). A required feature of eddies is that they must either connect to an interface (either solid-liquid such as the bed surface, or an interface between two fluids such as the air-water interface) and hence can be visualized as cylinders or ‘strings’ of fluid spanning two interfaces (Robinson 1991,

Zhou et al. 1999, Roushan and Wu 2005) or they must connect to themselves in a toroidal or 'vortex ring' shape (Zhou and Antonia 1992, Linden and Turner 2004). While turbulence is ubiquitous in the environment and laboratory settings, a universal definition of turbulence remains elusive (Tennekes and Lumley 1972, Brown and Roshko 1974, Roshko 1993). For the purpose of this dissertation, turbulent flow is defined to be flow which is composed of a continuum of eddies. These eddies can be described by their diameter, vorticity, and orientation in the flow.

The term continuum is necessary in this definition of turbulent flow in order to differentiate it from simple periodic flow such as that occurring downstream from cylinders with cylinder-based Reynolds numbers between 50 and 1000 (Schlichting 1979 and Williamson 1996). These flows, while unsteady, are distinguished by the presence of nearly uniform diameter, uniform orientation eddies which progress downstream from the cylinder in a zigzag pattern, termed the Kàrmàn vortex street (von Kàrmàn 1937). The nearly unimodal composition of these flows (in the sense of eddy diameter, orientation, and frequency) indicates that, while unsteady, flow is likely to be predictable by the fish. In fact, recent studies by Liao et al. (2003a, 2003b) and Liao (2007) describe fish swimming in Kàrmàn vortex streets. The range of Reynolds numbers (5,600 to 20,000) that these experiments were conducted at suggests that the flow was likely complicated by three-dimensional vortices (vortices with rotational axes not aligned with the cylinder axis) which would interact with the Kàrmàn street inducing a continuum of eddy sizes (Bernal and Roshko 1986, Williamson 1988). Nevertheless, the flow as described by Liao et al. (2003a, 2003b) and Liao (2007) was dominated by unimodal Kàrmàn eddies. Fish were shown to adjust their gait such that the tail beat amplitude, frequency, and wavelength matched the diameter, frequency, and spacing of eddies in the flow. Liao (2003a) further showed that by matching their gait to the dynamics of the flow, muscle use was substantially reduced compared to swimming in the free stream. While these studies are important in showing the ability of fish to adapt to unsteady flow in order to minimize energy expenditures, these highly predictable, unimodal eddies are not the most common form of unsteadiness in natural fluvial environments. Rather, flow is typically composed of a continuum of eddies due to higher Reynolds-numbers, interactions between the bed and flow obstructions, complex bed topography, and inter-eddy

interactions which cause eddies of various sizes, vorticities, and orientations to be formed (Nowell and Jumars, 1984, Shamloo et al. 2001, Tritico and Hotchkiss 2005). Given the ubiquity of turbulence in the fluvial environment, it is prudent to work toward a better understanding its impact on fish behavior.

The research described here investigated the effects of turbulence on fish locomotion. Locomotion is recognized to underlie most fish behavior (Webb and Gerstner 2000, Drucker and Lauder 2002). While turbulence has long been known to be characteristic of aquatic environments, only in the last 25 years have the ecological effects of turbulence on animal behavior been recognized (Pavlov et al. 1982, Mackenzie and Kiorboe 1995, Smith et al. 2005). Studies quantifying turbulence effects large enough to impact fish behavior are sparse.

This work first establishes a role for turbulence in habitat selection, for which swimming ability is essential (Chapter 2). Second, the mechanisms whereby turbulence affects swimming are explored, first evaluating the effects of the momentum of eddies comprising turbulent flow on performance (Chapter 3), and subsequently determining how turbulent flow affects swimming kinematics (Chapter 4) and deployment of control surfaces used in stabilizing posture (Chapter 5). A missing link between these laboratory studies, which quantified the effects of turbulence on fish through the visualization of eddies, and application to field research was the ability to resolve flow fields in terms of eddy composition in the field. To bridge this gap, a new underwater portable particle image velocimetry (PIV) system is described (Chapter 6).

Background

Using a variety of point measurement devices (e.g. Marsh-McBirney, Acoustic Doppler Velocimeters (ADV)), turbulent velocity fluctuations have been shown to affect habitat selection (Smith et al. 2005, Fulton et al. 2005), the energy budget of individuals (Standen et al. 2002 and 2004, Enders et al. 2003), gamete dispersal (Montgomery et al. 1996), and food availability (Mackenzie et al. 1994, Mackenzie and Kiorboe 1995, 2000, Landry et al. 1995). While turbulent velocity fluctuations have been shown within a single study to correlate with fish response, whether each response is positively or negatively affected by increasing levels of turbulent velocity fluctuations often varies

across studies (Table 1.1). For instance, Pavlov et al. (various articles summarized in 2000) and Enders et al. (2003, 2004) have reported that as the intensity of velocity fluctuations (turbulence intensity) increases, the swimming costs increase. Conversely, Liao, et al. (2003a, 2007) and Standen et al. (2004) argue from their data that turbulence results in increased swimming efficiencies due to the potential for fish to extract momentum from eddies.

Table 1.1: **A selection of studies investigating the effects of increased turbulent velocity fluctuations on various fish response characteristics**. Arrows represent whether increasing levels of turbulent velocity fluctuations have positive (↑), negative (↓), no (↔), or a mixed impact (↕) on fish response.

Parameter	Result
Swimming Ability	↓ Pavlov et al. (1982, 2000), Cada and Odeh (2001), Enders et al. (2003, 2004), Lupandin (2005) ↑ Liao et al. (2003a, 2003b, 2007), Standen et al. (2004) ↔ Nikora et al. (2003)
Feeding Efficiency	↓ Landry et al. (1995), Mackenzie and Kiorboe (2000) ↑ Mackenzie and Kiorboe (1995), Kato et al. (2008)
Habitat Choice	↕ Smith et al. (2005), Fulton et al. (2005), Smith and Brannon (2008)

The second chapter of this dissertation indicated an inverse relationship between increased turbulence intensity (temporal variance of velocity divided by the time-averaged velocity) of a sand bed river in northern Michigan and habitat selection of brown trout (*Salmo trutta*). A snorkel survey was conducted identifying locations where adult brown trout were holding station in the flow. Turbulent velocity fluctuations were measured in these locations along with other locations that, according to habitat suitability criteria, should be equivalent habitat but were unoccupied. The turbulence intensities in inhabited locations were compared to the turbulence intensities in vacant but otherwise suitable areas. Additionally, instantaneous velocity data were collected in two exemplary cross-sections of the stream to characterize the range of flow habitats in the stream. The results support the conclusion that turbulence is an important factor (in addition to standard habitat suitability indices such as current speed, water depth, and cover) in determining fish habitat suitability, which generally is a function of energy

requirements, access to food, and avoidance of predation for non-spawning adult salmonids.

This study, like those of others using velocity fluctuations to quantify turbulence, added to observations showing a role for turbulence in the distribution of fishes. However, it did not provide a basis for understanding how turbulence affects fishes, nor any unifying principles that could explain both positive and negative effects. Results from studies such as those noted in Table 1.1, notably by Cada and Odeh (2001), Nikora et al. (2003), Liao et al. (2003a, 2007), Lupandin (2005), had suggested that the key to understanding effects of turbulence might be related to the size of eddies relative to the size (total length) of a fish.

Cada and Odeh (2001) theorized, based on first principles, that the scale of turbulent eddies would affect migrating salmon in different ways depending upon the relative diameter of the eddy to the fish length. Specifically, they proposed that eddies which are much smaller in diameter than the fish length will lack a sufficient moment arm to provide a substantial torque on the fish body. They also argued that the combination of a number of small eddies rotating in different directions along a fish body would tend to negate any moments induced by a single eddy. Furthermore, they predicted that eddies which are much larger than the fish will be perceived as secondary currents, which may act to give incorrect migratory guidance cues but would induce destabilizing perturbations on the fish, while eddies of approximately the same diameter as the fish length have the appropriate scale to provide a torque about the fish center of mass.

Anecdotal support for this theory has been provided by Liao et al (2003a,b) who showed that fish swimming in the Kàrmàn vortex street downstream from cylinders 0.25 and 0.5 body-lengths in diameter adjusted body wavelength, tail beat amplitude, and tail beat frequency compared to those swimming in the free stream. These results are anecdotal since the eddy diameter was not determined, although expected to be proportional to the cylinder diameter.

Lupandin (2005) looked at the effects of turbulence length scale on the critical swimming speed of perch (*Perca fluviatilis*). The critical swimming speed is a measure of swimming performance and is the speed at which fish exhaust after a sequential increases in flow speed within a flume. The turbulence length scale is a measure of the spatial

similarity of velocity across a flow. While related to the eddy radius, since flow inside an eddy is coherent and therefore spatially correlated, a direct connection between the turbulent length scale and an eddy diameter is difficult to draw since eddies are defined by their angular velocity rather than a linear velocity correlation (Taylor 1935a and b, Hill 1996, Roy et al. 2004). In spite of this discrepancy, which was necessary given that flow was characterized using a point measurement device, Lupandin (2005) found that when the turbulent length scale of the flow was less than 2/3 of fish body length, there was no effect on the critical swimming speed of the fish. When the turbulent length scale was greater then 2/3 of fish length, the critical swimming speed of the fish declined. In another study, Nikora et al. (2003) examined the effects of turbulence produced by wavy walls on the fatigue time of *Galaxias maculatus*. They found no effect of the walls in spite of increased levels of turbulence intensity and proposed that the reason for the lack of effect was related to the scale of the turbulence that they created.

To date, there has been no systematic evaluation of how eddy characteristics affect fish swimming. The work by Liao et al. (2003a) reported fish swimming in flows at Reynolds numbers between 5,600 to 20,000, yet the classic Kàrmàn vortex street occurs below this range, at Reynolds numbers between 50 and 1000 (Schlichting 1979 and Williamson 1996). Above a Reynolds number of 1000, three dimensional instabilities in the shear layer interact with the Kàrmàn and shear layer vortices to induce a continuum of eddy sizes (Bernal and Roshko 1986, Williamson 1988). Liao et al (2003a) do not report eddy diameter or vorticity distributions. The Kàrmàn vortex street, as reported by Liao et al. (2003a) and Liao (2007), was a highly predictable flow with a single eddy shedding frequency; one must thus assume it lacks the complexity found in most aquatic environments. To address this issue of complexity, the core of this dissertation (Chapters 3, 4, and 5) reports on experimental studies in which arrays of cylinders of different sizes were used to induce a continuum of turbulent eddies with increasing ranges of eddy sizes (cylinder based Reynolds numbers ranged from 340 to 45,000), especially increasing the proportion of eddies with diameters similar to fish length. In addition, it considers the consequences of turbulent perturbations in vertical and horizontal planes by orienting the turbulence producing cylinder arrays in the vertical and horizontal planes respectively. These experiments use two-dimensional PIV (Raffel

et al. 1998, Gharib and Dabiri 2000, Samothrakis and Cotel 2006) to identify and characterize eddies.

The third chapter describes the flow patterns induced by cylinder arrays, quantifying flow in terms of eddy diameter and vorticity. These were related to the critical swimming speed of creek chub (*Semotilus atromaculatus*). Eddy size alone was considered an incomplete measure of turbulence-fish interactions. An additional measure that accounted for the momentum of an eddy relative to that of the fish, defined as the momentum ratio, was introduced to explain results. The orientation of larger eddies also affected swimming performance, with fish being able to recover faster from eddy-induced perturbations in the vertical plane where a fish could harness large forces produced by the vertical caudal fin to re-establish control.

The fourth chapter relates swimming kinematics of tail beat amplitude, frequency, wavelength, tail depth, and tail angle of attack during swimming at constant speed and body posture in various turbulent regimes. Again the momentum ratio proved important, such that when eddy momentum was of the same order of magnitude as fish momentum, tail beat frequency decreased and amplitude increased. Furthermore it was shown that the tail beat frequency was proportional to eddy vorticity for fish swimming in a given flow regime.

In the last of the three chapters on fish responses to various turbulence regimes, the deployment of non-caudal-fin control surfaces was explored. No significant changes were found in usage patterns across turbulent eddy diameter or vorticity for the anal and dorsal fins. However, both the percentage of time for which the paired pectoral and pelvic fins were deployed, and the area deployed, increased with the momentum ratio. Additionally, the pattern of pectoral fin deployment was observed to change based on eddy orientation in the flow.

The success of these studies demonstrates the need for a tool to make similar quantitative recordings of eddies in the field. In accordance, Chapter VI describes the development, testing, and demonstration of an underwater PIV device that can be used in rivers to quantify turbulent eddies.

Finally, a Conclusions Chapter (Chapter VII) relays the major findings and implications of this dissertation. The chapter also lays out paths for future research and

specific recommendations for incorporating these results into stream restoration and fish ladder design.

It is the goal of this dissertation to show that the relative size, vorticity, and orientation of turbulent eddies affects the swimming performance of fishes. This dissertation therefore hopes to transition the discussion of the effects of turbulence on fish habitat selection and swimming kinematics away from a turbulent fluctuations based description of turbulence to one based on eddies. It is hoped that through this new lens that many of the inconsistencies described previously will be clarified allowing biologists and engineers to more readily incorporate these and previous findings into future research and applications.

References

Bernal, L. P. and Roshko A. (1986). Streamwise vortex structure in plane mixing layers. *Journal of Fluid Mechanics* **170**, 499.

Brown, G. L. and Roshko, A. (1974). On Density Effects and Large Structure in the Turbulent Mixing Layers. *Journal of Fluid Mechanics* **64**: 775-816.

Cada, G. F. and Odeh, M. (2001). Turbulence at hydroelectric power plants and its potential effects on fish. *Report to Bonneville Power Administration*, Contract No. 2000AI26531, Project No. 200005700: 1-37.

Drucker, E. G. and Lauder, G. V. (2002). Wake dynamics and locomotor function in fishes: Interpreting evolutionary patterns in pectoral fin design. *Integrative and Comparative Biology* **42(5)**, 997-1008.

Enders, E. C., Boisclair, D. and Roy, A. G. (2003). The Effect of Turbulence on the Cost of Swimming for Juvenile Atlantic Salmon. *Canadian Journal of Fisheries and Aquatic Science* **60**, 1149-1160.

Enders, E. C., Boisclair, D. and Roy, A. G. (2004). The Costs of Habitat Utilization of Wild, Farmed, and Domesticated Juvenile Atlantic Salmon. *Canadian Journal of Fisheries and Aquatic Science* **61**, 2302-2313.

Environmental Protection Agency. (2008). *Federal Register: Compensatory Mitigation for Losses of Aquatic Resources; Final Rule*. 40 CFR Part 30.

Fulton, C. J., Bellwood, D. R. and Wainwright, P. C. (2005). Wave Energy and Swimming Performance Shape Coral Reef Fish Assemblages. *Proceedings of the Royal Society B* **272**, 827-832.

Gharib, M. and Dabiri, D. (2000). *An overview of digital particle image velocimetry Flow Visualization: Techniques and Examples* ed Smits A and Lim T T (London: Imperial College Press).

Hill, R. J. (1996). Corrections to Taylor's Frozen Turbulence Approximation. *Atmospheric Research* **40**, 153-175.

Huston, M. (1979). A general hypothesis of species diversity. *The American Naturalist* **113(1)**, 81-101.

Karman, T. von (1937). The fundamentals of the statistical theory of turbulence. *J. Aero. Sci.* **4**, 131-138.

Kato, Y., Takebe, T., Masuma, S., Kitagawa, T. and Kimura, S. (2008). Turbulence effect on the survival and feeding of Pacific bluefin tuna (Thunnus orientalis) larvae, on the basis of a rearing experiment. *Fisheries Science* **74,** 48-53.

Landry, F., Miller, T. J. and Leggett, W. C. (1995). The effects of small-scale turbulence on the ingestion rate of fathead minnow larvae. *Canadian Journal of Fisheries and Aquatic Sciences* **52**, 1714-1719.

Liao, J. C., Beal, D. N., Lauder, G. V. and Triantafyllou, M. S. (2003a). The Karman gait: novel body kinematics of rainbow trout swimming in a vortex street. *Journal of Experimental Biology* **206**, 1059-1073.

Liao, J. C., Beal, D. N., Lauder, G. V. and Triantafyllou, M. S. (2003b). Fish Exploiting Vortices Decrease Muscle Activity. *Science* **302**, 1566-1569.

Liao, J. C. (2007). A review of fish swimming mechanics and behavior in altered flows. *Philosophical Transactions of the Royal Society B.* **362(1487)**, 1973-1993.

Linden, P. F. and Turner, J. S. (2004). 'Optimal' vortex rings and aquatic propulsion mechanisms. *Proc. R. Soc. Lond. B* **271**, 647-653.

Lupandin, A. I. (2005). Effect of Flow Turbulence on Swimming Speed of Fish. *Biology Bulletin* **32(5)**, 558-565.

Mackenzie, B. R. and Kiorboe, T. (1995). Encounter Rates and Swimming Behavior of Pause-Travel and Cruise Larval Fish Predators in Calm and Turbulent Laboratory Environments. *Limnology and Oceanography* **40(7)**, 1278-1289.

Mackenzie, B. R. and Kiorboe, T. (2000). Larval Fish Feeding and Turbulence: A Case For the Downside. *Limnology and Oceanography* **45(1)**, 1-10.

Mackenzie, B. R., Miller, T. J., Cyr, S. and Leggett, W. C. (1994). Evidence for a Dome Shaped Relationship Between Turbulence and Larval Fish Ingestion Rates. *Limnology and Oceanography* **39(8)**, 1790-1799.

Montgomery, D. R., Buffington, J. M., Peterson, N. P., Schuett-Hames, D. and Quin, T. P. (1996). Stream-bed Scour, Egg Burial Depths, and the Influence of Salmonid Spawning on Bed Surface Mobility. *Canadian Journal of Fisheries and Aquatic Sciences* **53**, 1061-1070.

Nikora, V. I., Aberlee, J., Biggs, B. J. F., Jowett, I. G. and Sykes, J. R. E. (2003). Effects of Fish Size, Time to Fatigue, and Turbulence on Swimming Performance: A Case Study of *Galaxias maculatus. Journal of Fish Biology* **63**, 1365-1382.

Nowell, A. R. M. and Jumars, P. A. (1984). Flow environments of aquatic benthos. *Annu. Rev. Ecol. Syst.* **15**, 303–328.

Palmer, M. A. and Allan, J. D. (2006). Restoring rivers. *Issues in Science and Technology* **Winter 2006**, 40-48.

Papanicolaou, A., Strom, K., Schuyler, A. and Talebbeydokhti, N. (2003). The Role of Sediment Specific Gravity and Availability on Cluster Evolution. *Journal of Earth Surface Processes and Landforms* **28(1)**, 69-86.

Pavlov, D. S., Skorobogatov, M. A. and Shtaf, L. G. (1982). Effect of Tubulence Degree on the Critical Flow Rate for Fishes, *Dokl. Akad. Nauk SSSR* **267(4)**, 1019–1021.

Pavlov, D. S., Lupandin, A. I. and Skorobogatov, M. A. (2000). The Effects of Flow Turbulence on the Behaviour and Distribution of Fish. *Journal of Ichthyology* **40(S2)**, S232-261.

Pearson, W., Richmond, M., Johnson, G., Sargeant, S., Mueller, R., Cullinan, V., Deng, Z., Dibrani, B., Guensch, G., May, C., O'Rourke, L., Sobocinski, K. and Tritico, H. M. (2005). *Protocols for Evaluation of Upstream Passage of Juvenile Salmonids in an Experimental Culvert Test Bed*. Final Report for Washington Stated Department of Transportation, PNWD-3525.

Raffel, M., Willert, C. and Kompenhans, J. (1998). *Particle Image Velocimetry: A Practical Guide* (Berlin: Springer-Verlag).

Robinson, S. K. (1991). Coherent motions in the turbulent boundary layer. *Annu. Rev. Fluid Mech.* **23**, 601-639.

Rosgen, D. L. (1996). *Applied river morphology*, Wildland Hydrology, Pagosa Springs, Colo.

Roshko, A. (1993). Perspectives on bluff body aerodynamics. *J. Wind Ind. Aerodyn.* **49**, 79.

Roushan, P. and Wu, X. L. (2005). Universal wake structures of Karman vortex streets. *Physics of Fluids* **17**, 073601.

Roy, A. G., Buffin-Belanger, T., Lamarre, H. and Kirkbride, A. (2004). Size, Shape, and Dynamics of Large Scale Turbulent Flow Structures in a Gravel Bed River. *Journal of Fluid Mechanics* **500**, 1-27.

Samothrakis, P. and Cotel, A. J. (2006). Finite volume gravity currents impinging on a stratified interface *Exp. Fluids* **41**, 991-1003.

Schlichting, H. (1979). *Boundary-Layer Theory*. McGraw-Hill Publishing Co., New York, NY.

Shamloo, H., Rajaratnam, N. and Katopodis, C. (2001). Hydraulics of simple habitat structures. *J. Hydraul. Res.* **39(4)**, 351–366.

Shields, F. D., Morin, N. and Cooper, C. M. (2004). Large woody debris structures for sand-bed channels. *J. Hydraul. Eng.* **130(3)**, 208–217.

Smith, D. L. and Brannon, E. L. (2008). Growth and habitat occupancy of hatchery coho salmon in an engineered stream. *Transactions of the American Fisheries Society* **137(4)**, 1108-1119.

Smith, D. L., Brannon, E. L. and Odeh, M. (2005). Response of Juvenile Rainbow Trout to Turbulence Produced by Prismatoidal Shapes. *Transactions of the American Fisheries Society* **134**, 741-753.

Standen, E. M., Hinch, S. G., Healey, M. C. and Farrell, A. P. (2002). Energetic Costs of Migration through the Fraser River Canon, British Columbia, in Adult Pink and Sockeye Salmon as Assessed by EMG Telemetry. *Canadian Journal of Fisheries and Aquatic Sciences* **59**, 1809-1818.

Standen, E. M., Hinch, S. G. and Rand, P. S. (2004). Influence of River Speed on Path Selection By Migrating Adult Sockeye Salmon. *Canadian Journal of Fisheries and Aquatic Science* **61**, 905-912.

Taylor, G. I. (1935a). Statistical Theory of Turbulence I. *Proceedings of the Royal Society of London, Series A: Mathematical and Physical Sciences* **151**, 421-444.

Taylor, G. I. (1935b). Statistical Theory of Turbulence II. *Proceedings of the Royal Society of London, Series A: Mathematical and Physical Sciences* **151**, 444-454.

Tennekes, H. and Lumley, J. L. (1972). *A First Course in Turbulence*. The MIT Press, Cambridge, MA.

Tritico, H. M. and Hotchkiss, R. H. (2005). Unobstructed and Obstructed Turbulent Flow in Gravel Bed Rivers. *Journal of Hydraulic Engineering* **131**, 635-645.

Webb, P.W. and C.L. Gerstner. (2000). Swimming behaviour: Predictions from biomechanical principles. *In* P. Domenici and R.W. Blake (eds.), *Biomechanics in animal behaviour*, pp. 59–77. Bios Scientific Publishers Ltd., Oxford.

Williamson C. H. K. (1988). The existence of two stages in the transition to three-dimensionality of a cylinder wake. *Phys. Fluids* **31,** 3165.

Williamson, C. H. K. (1996). Vortex dynamics in the cylinder wake. *Annual Review of Fluid Mechanics* **28**, 477-539.

Zhou, Y. and Antonia, R. A. (1992). Convection velocity measurements in a cylinder wake. *Experiments in Fluids* **13**, 63-70.

Zhou, J., Adrian, R. J., Balachandar, S. and Kendall, T. M. (1999). Mechanisms for generating coherent packets of hairpin vortices. *J. Fluid Mech*. **387**, 353–396.

Chapter II

Do Brown Trout Choose Locations with Reduced Turbulence?

Introduction

Current velocity, water depth, substrate, cover, and shade are major features used to codify the physical habitat requirements for many species of salmonids as indicated, for example, by habitat suitability indices (HSI), habitat diversity criteria (HSC), and the habitat probabilistic index (HPI) (Raleigh 1982; Raleigh et al. 1986; Baker and Coon 1995; Girard et al. 2003; Guay et al. 2003; Williams et al. 2004).

Turbulence is also a physical characteristic of streams (Hawkins et al. 1993). As seen in laboratory situations, locations chosen by fishes are affected by the levels of turbulence (Pavlov et al. 1982, 1983, 2000; Shtaf et al. 1983; Pavlov and Tyurukov 1988; Odeh et al. 2002; Enders et al. 2003; Liao et al. 2003). Smith (2003) and Smith et al. (2005) showed that trout, while apparently attracted to shear zones, chose locations with reduced turbulence. However, there are relatively few observations on turbulence in streams or on the effects of turbulence on the choice of locations by trout in their natural habitat.

The present research addresses two questions to determine whether turbulence affects habitat choice by brown trout *Salmo trutta* in a sand-bed stream (Table 2.1). First, is turbulence lower in locations occupied by brown trout than in otherwise similar locations unoccupied by brown trout? Second, how do levels of turbulence in locations occupied by brown trout compare with those in other sections available within the same stream? The second question is an essential corollary to the first because hydrodynamic theory suggests that optimal habitat requirements (HIS, HSC, and HPI) place brown trout in high turbulence situations. As such, there may be limited choices, if any, for brown trout to avoid turbulence in natural settings.

Methods

Stream habitat.—Observations were made within a 500-m reach of the west branch of the Maple River in Emmet County, Michigan, during July and August 2002, 2003, and 2004. The West Maple River is a third-order, cold-water stream, with substantial input of cold groundwater supplemented with surface input from wetlands (Wiley et al. 2002; Zorn et al. 2002). The predominant land cover is mixed hardwood, with aspen *Populus tremuloides*, red pine *Pinus resinosa*, and beech *Fagus grandifolia* shading much of the stream.

Stream habitat composition (Bain and Stevenson 1999) was based on detailed analysis of a 50-m stretch of stream 6–12 m in width within the 500-m reach studied in 2002. Observations were made at grid points occurring at 2-m intervals along the thalweg, and 1-m intervals along transects from bank to bank at each 2-m interval. At each point, substrate, cover (usually occurring as instream large woody debris, LWD), and the presence of aquatic plants (primarily *Vallisneria americana*) were recorded. In addition, water depth and mean current speed were measured. Mean current speed in the water column was measured at 60% of the total depth from the water surface by means of a Marsh-McBirney electromagnetic flowmeter (model 2000). Current speed was sampled at 20 Hz for a 2-min period. The Marsh-McBirney flowmeter sensor head was 35 mm in diameter and was precise to ± 2% of mean current speed. The flowmeter was deployed on a wading pole and oriented upstream, avoiding possible interference of the pole on the flow near the sensor. These data were used to describe the coarse-scale stream features at each grid point: run, riffle, shallow sandbar and shallow margin (Bain and Stevenson 1999).

Discharge.—Discharge was determined for each year. In 2002 and 2003, the mean current speed was measured as described above at 1-m intervals across three stream cross-sections. In 2004, the current speeds were determined by means of an acoustic Doppler velocimeter (ADV, Sontek Field ADV Serial Number A525). We took measurements throughout the water column at 1-m intervals across the stream at two locations. These measurements were needed to determine the range of turbulence intensity (TI) and current speed available within a stream as described below. The mean

current speeds at 60% of the water depth were summed for the 1-m intervals across the stream to obtain discharge (Bain and Stevenson 1999).

Turbulence.—Turbulence is most commonly quantified in studies using fishes in terms of a nondimensionalized measure of variation in velocity magnitude relative to the local average speed where the measurement is made (Sanford 1997; Pavlov et al. 2000; Odeh et al. 2002). This statistical measure of turbulence is defined as the turbulence intensity, TI, which is derived from the following equation:

$$TI = \sigma / u_{local} \qquad (2.1)$$

where σ = standard deviation of the instantaneous velocity and u_{local} = average local current speed.

As mentioned above, we switched to using the ADV in 2004 to measure current velocity and its variation. The ADV is used in field situations to sample velocities from 0.1 to 250 cm/s within a standard cylindrical sampling volume with a diameter of 6 mm and a height of 9 mm (e.g., Kraus et al. 1994; Nikora and Goring 1998, 2000; Nikora et al. 2002a, 2002b). The ADV uses the principle of the Doppler effect to measure velocity, detecting changes in wave characteristics caused by the flow of the water relative to a 10 MHz carrier wave. The typical noise level is 1% of the velocity range when transmitting data at 25 Hz, as in this application. At this rate we recorded more than 1,800 instantaneous measures of velocity from the ADV for each sample location. Mean velocity was determined at each location and TI was calculated from equation (2.1). The ADV was supported on a tripod, and oriented in the direction of the overall stream flow. The tripod was arranged with two upstream legs, spread maximally to be as far as possible from the flow incident to the sensor volume. Therefore, there was no interference between the sampling volume and the legs of the tripod. Data from the ADV were filtered (Wahl 2000) to increase signal to noise ratios (SNR) by removing measurements less than 15 and were despiked with the phase space de-spiking method described by Goring and Nikora (2002).

Fish.—Brown trout were located by snorkeling. Two snorkelers moved side-by-side slowly upstream over the 500-m stream length (Smith 1994; Dolloff et al. 1996; McMahon et al. 1996). Some brown trout darted into cover, but most did not appear to notice the snorklers.

Table 2.1: Summary of observations and methods used to determine turbulence intensity in brown trout habitat. To compare current speed and turbulence intensity (1) between locations with and without fish and (2) between locations with fish and typical stream locations; ADV = acoustic Doppler velocimetry.

Measurement(s)	Fish versus no fish		Fish versus streamwide (2004)
	2002	2003	
Measurement of turbulence intensity (TI) and current speed (u) at the nose of brown trout in natural habitat locations. Water depth, temperature, cover, presence of aquatic plants (primarily *Vallisneria americana*), local bathymetry, and substrate also recorded.	Using Marsh-McBirney flowmeter	Using Marsh-McBirney flowmeter	Using ADV
Measurement of TI and u at similar locations in which no trout were seen.	Using Marsh-McBirney flowmeter	Using Marsh-McBirney flowmeter	
Measurement of u and TI throughout the water column at 1-m intervals across the stream to determine typical ranges for a small sand-bed trout stream.			Using ADV
Calculation of discharge from measurement of mean current speed at 60% of depth at 1-m intervals across the stream.	At three locations using Marsh-McBirney flowmeter	At three locations using Marsh-McBirney flowmeter	Obtained from ADV data for whole water column
Stream habitat composition recorded at 2-m intervals along the thalweg and 1-m cross-stream intervals for a typical 50-m reach. Mean current speed at 60% of depth, water depth, temperature, cover, presence of aquatic plants, local bathymetry, and substrate recorded.	Current speed recorded using Marsh-McBirney flowmeter		

When a brown trout was found, it was observed for at least 2 min to ensure that it was holding station at that location and was not affected by the observer's presence. Brown trout were often found at the same locations on successive days, but data were only obtained once. Total length (TL) was estimated to about the nearest 2 cm (Dolloff et

al. 1996). The accuracy of estimates was determined using fish-shaped objects of known length in typical stream situations. The positions of the noses of the brown trout relative to the location in the stream were recorded. Water depth, temperature, cover, local bathymetry and substrate also were recorded. Measurements of current velocity and its variation were made as described above while the snorkelers continued upstream to locate another brown trout.

Fish locations (2002 and 2003 observations).—The question of whether brown trout were found in locations with lower turbulence than similar locations lacking fish was addressed by measuring TI at the nose positions of brown trout and comparing these with minimal values measured in similar no-fish locations. Observations were made over 7 d in July 2002 and 14 d in July-August 2003. A brown trout location was sampled only once.

When a brown trout was located by snorkelers, the Marsh-McBirney flowmeter was deployed at the position of the fish's nose, and current speed (u_{nose}) and TI were measured. Water depth, temperature, stream cover (e.g., large woody debris [LWD]), the presence of aquatic plants (primarily *V. americana*), local bathymetry and substrate also were recorded.

All brown trout occupied substratum dips over a sandy bottom with some gravel, at locations that were shaded and had instream cover, usually as LWD, but lacking aquatic plants. Differences occurred among brown trout locations in u_{nose}, TI, water depth and brown trout length. Multiple regression with TI as the dependent variable was used to show that alternative or confounding factors, such as length and water depth, were not key explanatory factors for our experimental design. The relationship between current speeds and TI was best described as a power function, so that log-transformed current speed and TI were also examined using regression analysis. Only u_{nose} proved to have a significant effect on TI and the best fit relationships between these two variables was determined using nonlinear regression analysis.

No-fish locations (2002 and 2003 observations).—During the sampling period each year, snorkelers also identified locations that were as similar as possible to the occupied locations but lacking brown trout. Before using data from these no-fish locations, repeated observations were made to ensure that trout were absent from these

sites. At no-fish sites, u_{local} and TI were measured using the Marsh-McBirney flowmeter at several positions, each of which was typical of locations chosen by brown trout. We conservatively report the smallest TI values for these no-fish locations. Water depth, temperature, stream cover, presence of aquatic plants, local bathymetry, and substrate also were recorded. Relationships among variables differing among no-fish sites were examined as described above for fish sites.

Comparisons of fish and no-fish locations (2002 and 2003 observations).—While multiple regression showed relationships among variables within the fish and no-fish sites, differences between brown trout and no-brown-trout locations were further tested for significance by means of analysis of covariance (ANCOVA; Zar 1997) with current speed and depth as covariates.

TI variation for exemplary stream transects (2004).—Two transects were found that included the range of habitat features typical of the trout stream as determined from the stream survey in 2002. Measurements of u_{local} and TI were made at 1-m intervals across the stream at each transect, and at heights above the substratum of 1, 3, 5, 10, 15, 20, 30, 40, and 50 cm, as applicable. No measurements were made within 10 cm of the water surface as the volume needed to measure velocity by the ADV lies 10 cm below the transducers. These data were also used to determine the mean water-column current speed at 60% of the water depth at 1-m intervals in order to calculate discharge as described above (Bain and Stevenson 1999). These measurements were made for three stream cross-sections in 2002 and 2003, and two stream cross-sections in 2004.

TI variation and fish locations (2004 observations).—Brown trout were located as described above for 2002 and 2003. Values for u_{nose} and TI for 17 brown trout were compared with data from the years 2002 and 2003.

The relationships between TI, u_{local}, and u_{nose} also were analyzed and compared as described above for fish and no-fish locations.

Results

Stream Habitat-The 500-m length of stream was comprised of pools and runs, shallow sandbars often supporting patches of *V. americana*, and edge habitat. In the intensively sampled 50-m length of stream, pools occupied 35% of the reach area, with

mean water column current speed (60% of depth averaging 13.5 ± 0.2 cm/s [mean ± 2 SEs]) and depths averaging 49.0 ± 0.4 cm. Depths for runs were smaller, averaging 33.3 ± 0.5 cm while average current speeds for the water column were larger averaging 24.3 ± 0.2 cm/s. The runs represented 33% of the 50-m reach area. Shallow areas with *V. americana* represented 24% of the reach area, with water-column mean current speeds of 14.2 ± 4.2 cm/s and depth 22.2 ± 0.4 cm. Shallow edge habitat, which was a shallow, mucky area of the stream lacking aquatic plants, totaled 8% of the sampled reach area. Mean current speeds for the water column of edge habitat were 10.0 ± 0.7 cm/s and mean depth was 10.9 ± 0.6 cm. Large woody debris was present in 20% of locations sampled. Overall, the stream was typical of other Michigan sand-bed streams (Wiley et al. 2002; Zorn et al. 2002).

Fish-Three species of trout were found in the West branch of the Maple River: brown trout, brook trout *Salvelinus fontinalis*, and rainbow trout *Oncorhynchus mykiss*. Data are reported here only for the most abundant species, brown trout. Mottled sculpin *Cottus bairdii* and Johnny darter *Etheostoma nigrum* also were observed.

Over the 3 years of sampling, observations were made on brown trout ranging in total length from 5 to 25 cm. Brown trout were found in water with depths ranging from 16 to 57 cm and values of u_{nose} ranging from 1 to 37 cm/s with a mean of 14 ± 3 cm/s. All locations where brown trout were present were shaded and had cover in the form of LWD. No brown trout were found in locations with aquatic plants. Physical attributes generally were within the range considered optimal in use-based and bioenergetics-based HSC (Baker and Coon 1995).

All brown trout were found in dips in the substratum, which were predominantly comprised of sand but which sometimes contained small amounts of gravel. Of these brown trout, 40% were seen on the upstream slope, 27% at the deepest point of a dip, 13% on ledges created by embedded solid materials on the side of a dip, 10% associated with LWD located above the streambed, and 10% were found in various other locations. The few brown trout swimming at increased heights above the bottom were seen within logjams. The distance between the ventral surface of the brown trout and the stream bottom ranged from 0 to 15 cm, with a mean of 2.3 cm, and a modal height of 0 cm. The noses of the brown trout were from 1 to 16 cm from the bottom. Eighty-five percent of

these nose-points were within 5 cm of the bottom. Thus, brown trout were found in habitats where shear rates were expected to be high.

Most brown trout (80%) swam with steady undulations of the body and caudal fin, even when in contact with the bottom. The remaining brown trout rested on the bottom in the parr posture (Arnold et al. 1991) without swimming motions. One brown trout was observed using the Karman gait (Liao et al. 2003) and another sat on the bottom, leaning against LWD, a stabilizing posture seen in laboratory situations (Eidietis et al. 2002). All these behaviors are typical in our observations of healthy fishes in other field situations.

Fish Locations (2002 and 2003 Observations)-All sampled sites occupied by brown trout were typical of a sand-bed stream, in that fish were found in substratum dips over a sandy bottom with some gravel. Sites were shaded and instream cover was present usually as LWD, but *V. americana* was absent.

Current speed at the nose, TI, and other habitat variables (Table 2.1) were measured for 20 brown trout in 2002 and 14 in 2003 with the Marsh-McBirney flowmeter. Brown trout were solitary, except in 2002 when one group of three and another of four brown trout were found sharing a habitat. In these situations, u_{nose} and TI were measured for lead (upstream) brown trout.

At each location we also measured and noted the variability in water depth and brown trout length. Multiple regression using TI as the dependent variable showed no significant relationships between TI and brown trout length and water depth (multiple linear regression, $P > 0.65$). In addition, brown trout length was not correlated with u_{nose}, water depth, or other physical variables (Table 2.1) (multiple linear regression, $P > 0.5$ and Pearson Correlation followed by Bonferroni test for significance, $P > 0.1$). Thus brown trout location varied with TI and u_{nose}.

For 2002 and 2003, TI ranged from 0.03 to 11 while u_{nose} ranged from 1 to 29 cm/s. Standard deviation increased with u_{nose}, with a value of 0.6 cm/s for u_{nose} of 1.6 cm/s for the three lowest u_{nose} values in 2002 and a value of 1.3 cm/s at u_{nose} of 24 cm/s for the top three values of u_{nose}. The TIs for these data were 0.41 and 0.06, respectively. Thus TI was relatively lower at higher current velocities; that is, the variation in current velocity increased at a slower rate than that of current velocity itself.

The TI was significantly related to u_{nose} ($P < 0.01$), the relationship for both 2002 and 2003 being best described (maximum R^2) by a negative power function. Thus TI decreased with u_{nose} according to the following equations (Figure 2.1a, b):

2002: $TI = (0.71 \pm 0.26)\, u_{nose}^{-0.64 \pm 0.24}$ $R^2 = 0.877$; N = 20, P<0.01 (2.2)

2003: $TI = (0.39 \pm 0.06)\, u_{nose}^{-0.15 \pm 0.08}$ $R^2 = 0.9827$; N = 14, P<0.01 (2.3)

No-Fish Locations (2002 and 2003 Observations)-By design, we selected no-fish locations that had physical features as similar as possible to those of the sites occupied by brown trout (i.e., sandy dips with occasionally some gravel that were shaded and had LWD cover but lacked *V. americana*).

For no-fish sites, the minimal values of TI declined with u_{local} (Figure 2.1a, b) in the same way as between u_{nose} and TI, that is,

2002: $TI = (0.65 \pm 0.14)\, u_{local}^{-0.43 \pm 0.12}$ $R^2 = 0.947$; N = 21, P<0.01 (2.4)

2003: $TI = (1.16 \pm 0.47)\, u_{local}^{-0.44 \pm 0.15}$ $R^2 = 0.982$, N = 12, P<0.01 (2.5)

Comparisons of Fish and No-Fish Locations (2002 and 2003 Observations)- Fish and no-fish sites were chosen to share the categorical features described above but were different in terms of current speeds and depth. The depths at fish and no-fish locations spanned the same range (Figure 2.2), and were not significantly different (unpaired t-tests, P±0.95). Current speeds spanned the same range (Figure 2.1).

The values of local current speed and TI were lower in 2002 than in 2003 for both fish and no-fish locations. This presumably reflects differences in discharge (0.47 m^3/s in 2002 and 0.67 m^3/s in 2003).

After taking into account the range of current speeds and depths typical of brown trout habitat for 2002 and 2003, the TI values for fish locations were significantly smaller than those in no-fish locations (ANCOVA; $P < 0.001$). Thus, brown trout chose lower turbulence locations over those meeting similar preferred physical habitat features.

TI Variation for Exemplary Stream Transects (2004)-The TI was measured for exemplary transects that were chosen to include typical habitat features as determined in the 2002 detailed survey of a 50- m reach. The first transect (Figure 2.3) included LWD upstream of and along the sampled cross-section (high LWD transect), creating a run area

Figure 2.1: Relationships between turbulence intensity (TI) and current speed (u) for various locations with brown trout and similar locations with no fish. The relationships between TI and the current speed at the fish's nose are shown by solid symbols for (A) 2002, (B) 2003, and (C) 2004; open symbols show the relationships between TI and average local current speed for the sites without fish in 2002 and 2003 as well as those for TI values within 5 cm of the bottom at sandy sites with large woody debris in 2004. The relationships were significantly lower for locations with fish than for those without fish (ANCOVA; $P < 0.001$). Panel (D) shows the relationship between TI and average local current speed more than 5 cm from the bottom at sandy sites with large woody debris in 2004.

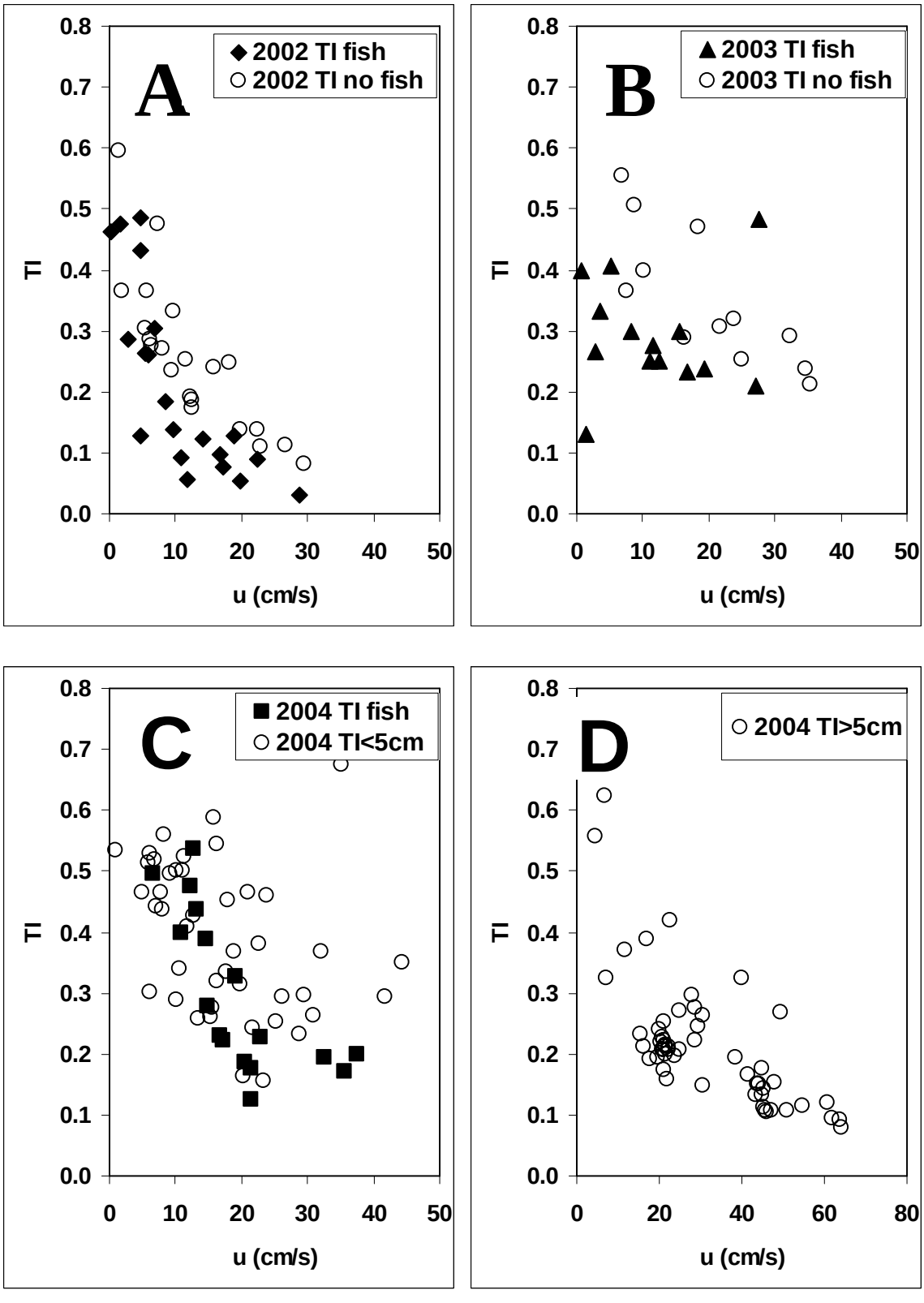
A
2002 TI fish
2002 TI no fish
TI
u (cm/s)
B
2003 TI fish
2003 TI no fish
TI
u (cm/s)
C
2004 TI fish
2004 TI<5cm
TI
u (cm/s)
D
2004 TI>5cm
TI
u (cm/s)

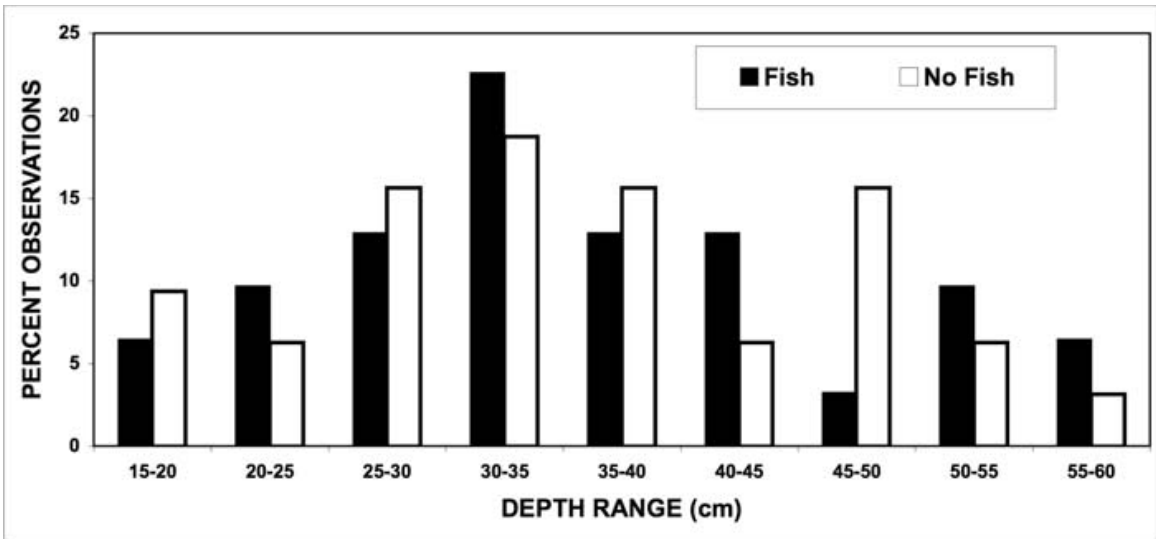

Figure 2.2: Depth distribution of the locations occupied by fish and the chosen locations without fish sampled in 2002 and 2003.

to the left, and a large central pool. The second transect (Figure 2.4) was characterized by a predominantly sandy-bottomed run (sandy transect) with an eroded dip, and a shallow sandbar with *V. americana*. Discharge was 0.80 m^3/s in 2004.

Current speeds in both the high LWD and sandy transects were typical of streams, the maximum u_{local} being found toward the center of the stream and the water surface and lower values being found near the boundaries (Figures 2.3, 2.4). In the high LWD density transect, u_{local} ranged from 0 to 60 cm/s. The highest u_{local} occurred at the center of the stream where LWD constricted and hence accelerated flow (a in Figure 2.3). In contrast, u_{local} was reduced by 20–30 cm/s downstream of LWD (b in Figure 2.3). The lowest u_{local} occurred at the streambed (c in Figure 2.3) and where LWD was dense (d in Figure 2.3). In contrast, in the sandy transect, the maximum u_{local} of 45 cm/s (e in Figure 2.3) was lower than in the high LWD transect because the sandy transect had a larger cross-sectional area (Figure 2.3) and few obstructions to channel the flow. Instead, u_{local} was reduced to about half the maximum as the depth gradually decreased towards the shoreline in an area with LWD oriented parallel to the current just upstream of the transect (f in Figure 2.3). However, the sandy transect differed from the high LWD transect in that there was a more extended velocity transition zone over the mid-stream region. Current speed was similarly reduced in a dip, a shallow depression towards the center of the transect (g in Figure 2.4). The lowest u_{local} occurred near the streambed, as

in the high LWD transect, and also in a patch of *V. americana* (h in Figure 2.4) in the sandy area.

The TI was lowest towards the high-velocity portions of the stream in both transects (o in Figures 2.3, 2.4). The TI was higher downstream of the LWD than upstream in the high LWD transect, taking values of 0.3–0.4 (p in Figure 2.3). However, the largest values of TI, around 0.6, occurred where stream edges combined with LWD (r in Figure 2.3). Where LWD was least prevalent in the high LWD transect, the TI value was about 0.35 at the streambed, higher than TI in the water column, but lower than TI in the presence of LWD (s in Figure 2.4).

In the sandy transect, TI values that occurred immediately downstream of the LWD (p in Figure 2.4) were somewhat higher than the midstream minimum. These values were similar to values resulting from the presence of LWD in the high LWD transect. Similarly, TI values increased near the streambed of the sandy transect (s in Figure 2.4), with elevated values near the streambed downstream of in-flow structures, such as *V. americana* (r in Figure 2.4). However, the largest TI in either transect occurred at the edge of the *V. Americana* patch (t in Figure 2.4).

Combining observations from both transects, TI varied from 0.08 to 0.73 over a range of u_{local} from 1 to 64 cm/s. As found for the fish and no-fish locations (equations 2.2 through 2.5), TI was inversely related to u_{local}, the relationship being best described by the power function

$$TI = (0.86\pm0.14)\, u_{local}^{-0.36\pm0.06}; \qquad R^2 = 0.899; \quad N = 118, P<0.001 \qquad (2.6)$$

As 85% of brown trout were located no more than 5 cm from the stream bed, the relationship between TI and u_{local} was determined for measurements at depths no more than 5 cm. For these data, $TI_{\leq 5\ cm}$ and $u_{\leq 5\ cm}$ were related as follows:

$$TI_{\leq 5\ cm} = (0.73\pm0.16)\, u_{\leq 5\ cm}^{-0.26\pm0.09}; \quad R^2 = 0.919; \quad N = 44\ P<0.001 \qquad (2.7)$$

The $TI_{\leq 5\ cm}$ was larger for a given u_{local} than TI for greater heights above the bottom (Figure 2.1D). This is not surprising as flow close to the bottom is within the shear zone where u_{local} changes rapidly with height, and hence where turbulence is likely to be high.

Figure 2.3: Sketch map (A) and flow characteristics (B, C) of a cross-stream transect with large accumulations of large woody debris (LWD). The cross-section faces upstream, into the flow. In panel (A), emergent LWD is indicated by shading and submerged LWD by diagonal shading. For clarity, only major pieces of LWD are shown, but these pieces will have created logjams of smaller items. Panel (B) presents contour plots showing the variation in current velocity (cm/s) over the cross-section, panel (C) contour plots showing the variation in turbulence intensity. The large cross-hatched sections represent areas of the water column that were too close to the surface for velocity to be measured.

A)

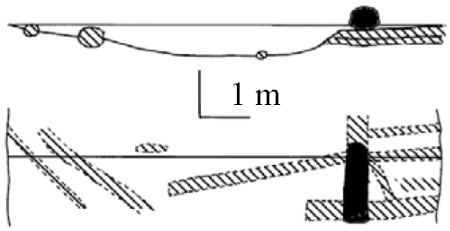
Cross section
1 m
Plane view

B)

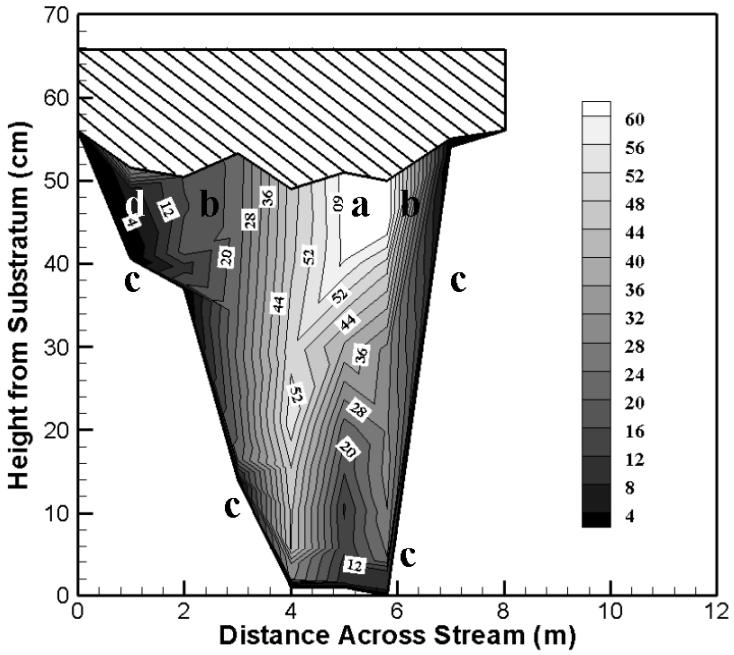
Height from Substratum (cm)
Distance Across Stream (m)
a
b
c
d

C)

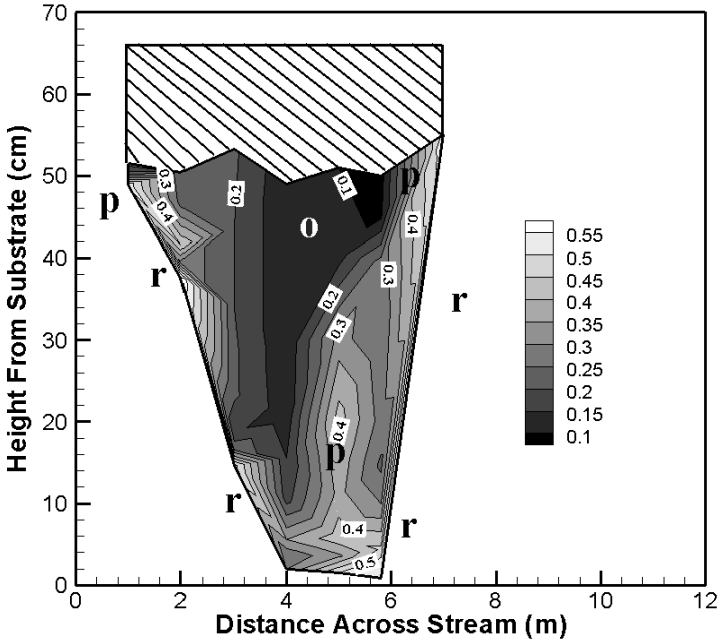
Height From Substrate (cm)
Distance Across Stream (m)
o
p
r

Figure 2.4: Sketch map (A) and flow characteristics (B, C) along a cross-stream transect over a sandy area of stream bed with little in-flow structures. In panel (A), irregular hatching denotes a macrophyte bed. Other features of the figure are as described in the caption to Figure 2.3.

A)

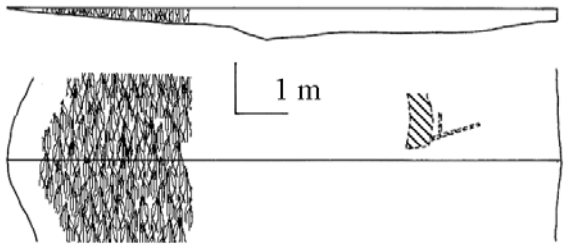

Cross section

Plane view

B)

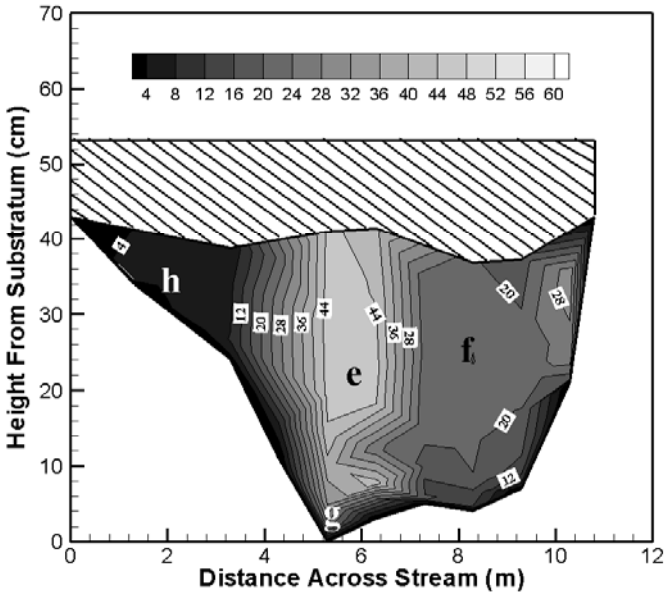

C)

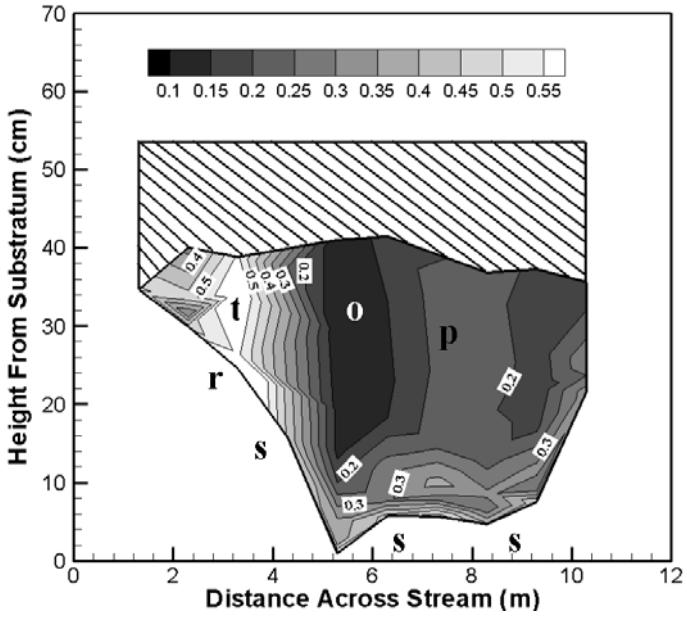

TI Variation and Fish Locations (2004 observations)-In addition to our systematic measurement of TI and u_{local}, we measured TI and u_{nose} for 17 brown trout using ADV in 2004 (Figure 2.1c). The TI in the fish locations varied from 0.18 to 0.53, covering much of the range of TI in the stream. However, for flow within 5 cm of the bottom where most brown trout were located, TI ranged from 0.16 to 0.73, so that brown trout occupied locations toward the lower end of the TI range.

As with the brown trout locations sampled in 2002 and 2003, TI was related to u_{nose} by a power function, namely,

$$TI = (0.39 \pm 0.26)\, u_{nose}^{-0.64 \pm 0.24}; \qquad R^2 = 0.877, \quad N = 14, P<0.01 \qquad (2.8)$$

Similarly, other physical habitat features were not correlated with TI in locations occupied by brown trout (multiple linear regression [$P > 0.5$] and Pearson correlation followed by Bonferroni test for significance [$P > 0.1$]). Finally, TI at u_{nose} for the brown trout was significantly lower than TI at $u_{\leq 5\ cm}$ (ANCOVA; $P < 0.028$).

Discussion

This study quantified turbulence in terms of the statistical variation in current speed relative to the average velocity at given locations and considers higher levels of TI to be associated with greater control challenges to stability (Webb 1998; Pavlov et al. 2000; Odeh et al. 2002; Enders et al. 2003). Turbulence intensity decreased as a power function with increasing speed, suggesting that stability challenges would rapidly decrease at higher current speeds. In contrast, Smith et al. (2005) suggested absolute values of standard deviation would be a better measure of the challenges of dealing with turbulence. In this view, if standard deviation were constant over all current speeds, TI would decrease linearly with current speed, but the stability challenges faced by a fish would be independent of current speed.

Stability, which involves the ability to control posture and location in the water column, is not a simple function of perturbation magnitude. Dynamic stability also depends on the momentum and kinetic energy of the system, these being functions of speed. Thus, the ability to achieve dynamic stability, such as for a fish exposed to turbulence, depends on both perturbations associated with velocity variation and the mean current speed faced by the fish. As speed increases, the momentum of a fish

increases. This promotes stability. As a result, dynamic stability can be sustained at a higher velocity in the face of larger perturbations (Webb 2006). This idea can be visualized from the experience of riding a bicycle. At very slow speeds, stability is difficult to achieve, and small perturbations can cause failure – i.e., loss of control. At high speeds, not only do such small perturbations become negligible, but stability can be achieved over a much larger range of perturbations.

Thus, we suggest that TI is an appropriate measure of turbulence effects in terms of the impact on fishes. The TI takes into account the speed-dependence of control and the ability to achieve stability over a larger range of turbulent velocity fluctuations as mean velocity increases. The physical analysis could directly consider momentum or even kinetic energy fluctuations rather than velocity fluctuations. However, the same numerical result as determined by equation (2.1) will be realized because the additional terms cancel out.

When choosing a location in their natural habitat fish make compromises among many interacting physical and biotic factors. Our observations were made during the day, and presumably reflect brown trout's choice of resting nonfeeding locations. At other times, factors, such as feeding and size-dependent choice of prey, also could affect location choices, that are associated with patterns of flow that are different from those that we studied. Nevertheless, in our study, brown trout were found in locations with lower TI than similar unoccupied sites, even though these fish in the West Maple River were found with cover, near the bottom, and at intermediate current velocities, factors that tend to promote turbulence. Brown trout were not found in the lowest TI because low values were found with the fastest currents in mid-stream and towards the water surface (Figures 2.3, 2.4). At the same time, the highest TI was avoided because this occurred in shallow water containing *V. americana* patches.

Turbulence arises as a result of shear owing to viscous effects in velocity gradients, which are largely created by interactions between the flow and instream structures of the stream bed or protuberances (Carling 1992; Atkinson 1999; Smith 2003; Roy et al. 2004; Smith et al. 2005). Fishes are found in currents where shear forces often tend to be high, so that it is especially noteworthy that brown trout choose lower TI locations from among those available. However, such turbulence-creating features are not

unique to trout streams. In other waters fish are typically found in the lower regions of the water column near the bottom or near or among protruding structures such as rocky materials, LWD, macrophytes and corals (Fausch and White 1981; Puckett and Dill 1985; Matthews and Heins 1987; Allan 1995; Matthews 1998; Enders et al. 2003; Standen et al. 2004; Fulton and Bellwood 2002). Additional research should focus on understanding the importance of turbulence in these nonstream habitats.

References

Allan, D. J. (1995). Stream ecology. Chapman and Hall, London.

Arnold, G. P., P. W. Webb, and B. H. Holford. (1991). The role of the pectoral fins in station-holding of Atlantic salmon (*Salmo salar L*). *Journal of Experimental Biology* **156**, 625–629.

Atkinson, M. J. (1999). Topographical relief as a proxy for the friction factors of reefs: estimates of nutrient uptake into coral reef benthos. Pages 99–103 in J. E. Maragos and R. Grober-Dunsmore, editors. Proceedings of the Hawaii Coral Reef Monitoring Workshop, Hawaii Division of Land and Natural Resources, Honolulu.

Bain, M. B., and N. J. Stevenson. (1999). Aquatic habitat assessment: common methods. American Fisheries Society, Bethesda, Maryland.

Baker, E. A., and T. G. Coon. (1995). Development and evaluation of alternative habitat suitability criteria for brook trout *Salvelinus fontinalis*. Michigan Department of Natural Resources, Fisheries Research Report 2017, Lansing.

Carling, P. A. (1992). The nature of the fluid boundary and the selection of parameters for benthic ecology. *Freshwater Biology* **28**:273–282.

Dolloff, A., J. Kershner, and R. Thurow. (1996). Underwater observation. Pages 533–554 in B. R. Murphy and D. W Willis, editors. Fisheries techniques. American Fisheries Society Bethesda, Maryland.

Eidietis, L., T. L. Forrester, and P. W. Webb. (2002). Relative abilities to correct rolling disturbances of three morphologically different fish. *Canadian Journal of Zoology* **80**, 2156–2163.

Enders, E. C., D. Boisclair, and A. G. Roy. (2003). The effect of turbulence on the cost of swimming for juvenile Atlantic salmon (*Salmo salar*). *Canadian Journal of Fisheries and Aquatic Sciences* **60**, 1149–1160.

Fausch, K. D., and R. J. White. (1981). Competition between brook trout (*Salvelinus fontinalis*) and brown trout (*Salmo trutta*) for positions in a Michigan stream. *Canadian Journal of Fisheries and Aquatic Sciences* **38**, 1220–1227.

Fulton, C. J., and D. R. Bellwood. (2002). Ontogenetic habitat use in labrid fishes: an ecomorphological perspective. *Marine Biology Progress Series* **236**, 255–262.

Girard, P., D. Boisclair, and M. Leclerc. (2003). The effect of cloud cover on the development of habitat quality indices for juvenile Atlantic salmon (*Salmo salar*). *Canadian Journal of Fisheries and Aquatic Sciences* **60**, 386–1397.

Goring, D. G., and V. I. Nikora. (2002). Despiking acoustic Doppler velocimeter data. *Journal of Hydraulic Engineering* **128**, 117–126.

Guay, J. C., D. Boisclair, M. Leclerc, and M. Lapointe. (2003). Assessment of the transferability of biological habitat models for Atlantic salmon parr (*Salmo salar*). *Canadian Journal of Fisheries and Aquatic Sciences* **60**, 1398–1408.

Hawkins, C. P., J. L. Kershner, P. A. Bisson, M. D. Bryant, L. M. Decker, S. V. Gregory, D. A. McCullough, C. K. Overton, G. H. Reeves, R. J. Steedman, and M. K. Young. (1993). A hierarchical approach to classifying stream habitat features. *Fisheries* **18(6)**, 3–12.

Kraus, N. C., A. Kohrmann, and R. Caberera. (1994). New acoustic meter for measuring 3D laboratory flow. *Journal of Hydraulic Engineering* **120**, 406–412.

Liao, J. C., D. N. Beal, G. V. Lauder, and M. S. Trianyafyllou. (2003). The Karman gait: novel body kinematics of rainbow trout swimming in a vortex street. *Journal of Experimental Biology* **206**, 1059–1073.

Matthews, W. J. (1998). Patterns in freshwater fish ecology. Chapman and Hall, New York.

Matthews, W. J., and D. C. Heins. (1987). Community and evolutionary ecology of North American stream fishes. University of Oklahoma Press, Norman.

McMahon, T. E., A. V. Zale, and D. J. Orth. (1996). Aquatic habitat measurements. Pages 83–120 in B. R. Murphy and D. W. Willis, editors. Fisheries techniques. American Fisheries Society, Bethesda, Maryland.

Nikora, V. I., and D. G. Goring. (1998). ADV turbulence measurements: can we improve their interpretation? *Journal of Hydraulic Engineering* **124**, 630–634.

Nikora, V. I., and D. G. Goring. (2000). Flow turbulence over fixed and weakly mobile gravel beds. *Journal of Hydraulic Engineering* **126**, 679–690.

Nikora, V. I., D. G. Goring, and B. J. F. Biggs. (2002a). Some observations of the effects of micro-organisms growing on the bed of an open channel on the turbulence properties. *Journal of Fluid Mechanics* **450**, 317–341.

Nikora, V. I., M. Green, S. Thrush, T. Hume, and D. G. Goring. (2002b). Structure of the internal boundary layer over a patch of horse mussels (*Atrina zelandica*) in the estuary. *Journal of Marine Research* **60**, 121–150.

Odeh, M., J. F. Noreika, A. Haro, A. Maynard, T. Castro-Santos, and G. F. Cada. (2002). Evaluation of the effects of turbulence on the behavior of migratory fish. Final

Report to the Bonneville Power Administration, Contract 00000022, Project 200005700, Portland, Oregon.

Pavlov, D. S., and S. N. Tyurukov. (1988). The role of hydrodynamic stimuli in the behavior and orientation of fishes near obstacles. *Voprosy Ikhtiologii* **28**, 303–314. (In Russian.)

Pavlov, D. S., A. I. Lupandin, and M. A. Skorobogatov. (2000). The effects of flow turbulence on the behavior and distribution of fish. *Journal of Ichthyology* **40(Supplement 2)**, S232–S261.

Pavlov, D. S., M. A. Skorobagatov, and L. G. Shtaf. (1982). The critical current velocity of fish and the degree of flow turbulence. *Reports of the USSR Academy of Sciences* **267**, 1019–1021. (In Russian.)

Pavlov, D. S., M. A. Skorobagatov, and L. G. Shtaf. (1983). Threshold speeds for rheoreaction of roach in flows with different degrees of turbulence. *Reports of the USSR Academy of Sciences* **268**, 510–512. (In Russian.)

Puckett, K. J., and L. M. Dill. (1985). The energetics of feeding territoriality in juvenile coho salmon (*Oncorhynchus kisutch*). *Behaviour* **92**, 97–111.

Raleigh, R. F. (1982). Habitat suitability index models: brook trout. U.S. Fish and Wildlife Service FWS/OBS-82/10.24.

Raleigh, R. F., L. D. Zuckerman, and P. C. Nelson. (1986). Habitat suitability index models and instream flow suitability curves: brown trout, revised. U.S. Fish and Wildlife Service Biological Report FWS/OBS-82/10.124.

Roy, A. G., T. Buffin-Be´langer, H. Lamarre, and A. D. Kirkbride. (2004). Size, shape, and dynamics of large-scale turbulent flow structures in a gravel-bed river. *Journal of Fluid Mechanics* **500**, 1–27.

Sanford, L. P. (1997). Turbulent mixing in experimental ecosystem studies. *Marine Biology Progress Series* **161**, 265–293.

Shtaf, L. G., D. S. Pavlov, M. A. Skorobogativ, and A. S. Baryekian. (1983). Fish behavior as affected by the degree of flow turbulence. *Voprosy Ikhtiologii.* **3**, 307–317. (In Russian.)

Smith, C. L. (1994). Fish watching. Cornell University Press, Ithaca, New York.

Smith, D. L. (2003). The shear flow environment of juvenile salmonids. Doctoral dissertation. University of Idaho, Moscow.

Smith, D. L., E. L. Brannon, and M. Odeh. (2005). Response of juvenile rainbow trout to turbulence produced by prismatoidal shapes. *Transactions of the American Fisheries Society* **134**, 741–753.

Standen, E. M., S. G. Hinch, and P. S. Rand. (2004). Influence of river speed on path selection by migrating adult sockeye salmon (*Oncorhynchus nerka*). *Canadian Journal of Fisheries and Aquatic Sciences* **61**, 905–912.

Wahl, T. L. (2000). Analyzing ADV data using WinADV. In Proceedings of the Joint Conference on Water Resources Engineering and Water Resources Planning and Management (CD-ROM). American Society of Civil Engineers, Reston, Virginia.

Webb, P. W. (1998). Entrainment by river chub, *Nocomis micropogon*, and smallmouth bass, *Micropterus dolomieu*, on cylinders. *Journal of Experimental Biology* **201**, 2403–2412.

Webb, P. W. (2002). Control of posture, depth, and swimming trajectories of fishes. *Integrative and Comparative Biology* **42**, 94–101.

Webb, P. W. (2004). Response latencies to postural disturbances in three species of teleostean fishes. *Journal of Experimental Biology* **207**, 955–961.

Webb, P. W. (2006). Stability and maneuverability. In R. E. Shadwick and G. V. Lauder, editors. Fish physiology. Elsevier, San Diego, California.

Wiley, M. J., P. W. Seelbach, K. Wehrly, and J. Martin. (2002). Regional ecological normalization using linear models: a meta-method for scaling stream assessment indicators. Pages 202–223 in T. P. Simon editor. Biological response signatures: indicator patterns using aquatic communities. CRC Press_Lewis Publishers, Boca Raton, Florida.

Williams, L. R., M. L. Warren, S. B. Adams, J. L. Arvai, and C. M. Taylor. (2004). Basin visual estimation technique (BVET) and representative reach approaches to wadeable stream surveys. *Fisheries* **29(8),** 12–22.

Zar, J. (1997). Biostatistical analysis. Prentice Hall, New York.

Zorn, T. G., P. W. Seelbach, and M. J. Wiley. (2002). Distributions of stream fishes and their relationships to stream size and hydrology in Michigan's lower peninsula. *Transactions of the American Fisheries Society* **131**, 70–85.

Chapter III

The Effects of Turbulent Eddies on Stability and the Critical Swimming Speed of Creek Chub (*Semotilus atromaculatus*)

Introduction

Turbulence is ubiquitous in natural flow environments and has been shown to affect gamete dispersal (Montgomery et al. 1996), food availability (Mackenzie et al. 1994, Mackenzie and Kiorboe 1995, 2000, Landry et al. 1995), individual energy budgets (Standen et al. 2002 and 2004, Enders et al. 2003), and habitat selection (Pavlov et al. 2000, Smith et al. 2005 and Cotel et al. 2006) of fishes. There is no consensus on a single definition of turbulence (Tennekes and Lumley 1972, Roshko 1976). A turbulent flow, for the purpose of this paper, is taken as flow which is composed of a continuum of eddies (Tennekes and Lumley 1972, Cimbala et al. 1988). This definition of turbulent flow acknowledges that the temporal unsteadiness commonly measured in rivers (Nikora and Goring 1998, Tritico and Hotchkiss 2005, Smith et al. 2005, Cotel et al. 2006) is primarily due to eddies (rotating packets of fluid). Further, it acknowledges that the most common flow experienced by fish in a fluvial environment is composed of a distribution of eddy sizes, vorticity, and orientations (Standen et al. 2002) which complicates the flow beyond current models which assume the flow to be rectilinear (most critical swimming speed studies such as Webb et al. 1984) or composed of a single eddy diameter (Lupandin 2005 and Liao et al. 2003).

Several researchers have proposed that eddy size and orientation relative to the fish should be important in understanding the effects of turbulence on fish swimming performance (Pavlov et al. 2000, Cada and Odeh 2001, Nikora et al. 2003, Biggs et al. 2005, Lupandin 2005, Tritico and Hotchkiss 2005, Liao 2007), with diameter, vorticity, and orientation of eddies being primary variables. This idea remains untested. Furthermore, understanding the effects of turbulent eddies on the swimming performance

of fish has the potential to aid in the design of fishways and stream restoration projects. The purposes of this paper are therefore to (1) describe the effects that turbulent eddy diameter, vorticity, and orientation have on the critical swimming speed and stability of creek chub, and to (2) explore a physical description of the fish-eddy interaction that accounts for the effects of turbulence on the fish-control system.

Materials and Methods

Changes in fish swimming performance were measured at several flow speeds and levels of turbulence induced by upstream cylinder arrays of differing diameters and orientations. The turbulent flow regimes were measured using particle image velocimetry (PIV) and were characterized according to eddy composition with eddies being characterized by eddy diameter (d_e), eddy vorticity (ω_e), and eddy orientation (vertical or horizontal). The spatial preference of fishes in the eddy field, speed at which fish first lost control of posture and location stability (first spill), spill location, spill frequencies, the method of recovery, and critical swimming were recorded on video and quantified.

Apparatus

Observations of fish swimming behavior were made during increasing velocity tests in an Engineering Laboratory Design Flow Visualization Water Tunnel (Figures 3.1 and 3.2) with an observation chamber 250 cm in length and 60 cm wide. The water depth was held at 55 cm for all tests. A 30-cm test section was delineated within the observation chamber by a downstream grid (12.5 mm egg-crate) and upstream by a similar grid or one of three cylinder arrays spanning the flume cross-section and oriented either vertically or horizontally. Arrays were comprised of cylinders with diameters 0.4 cm, 1.6 cm, and 8.9 cm, with gaps equal to cylinder diameter in each array. Therefore there were seven treatments: control, small horizontal (SH), small vertical (SV), medium horizontal (MH), medium vertical (MV), large horizontal (LH), and large vertical (LV) arrays. A 1.3 cm mesh of 0.04 cm diameter plastic thread was attached to the upstream side of the cylinders to prevent fish escaping. One wall of the observation chamber was papered with 2 cm x 2 cm black and white checkered paper to foster fish station holding. All edges of the test sections were electrified at 5 V DC to encourage swimming.

Figure 3,1: Flume and Test Section Configuration. Water is recirculated using a variable speed pump, the arrows showing the direction of flow. A 30 cm long test section, delineated by flow straightening restraining grids was located within the 60 cm wide x 55 cm water depth cross section viewing channel, 150 cm from the viewing channel entrance.

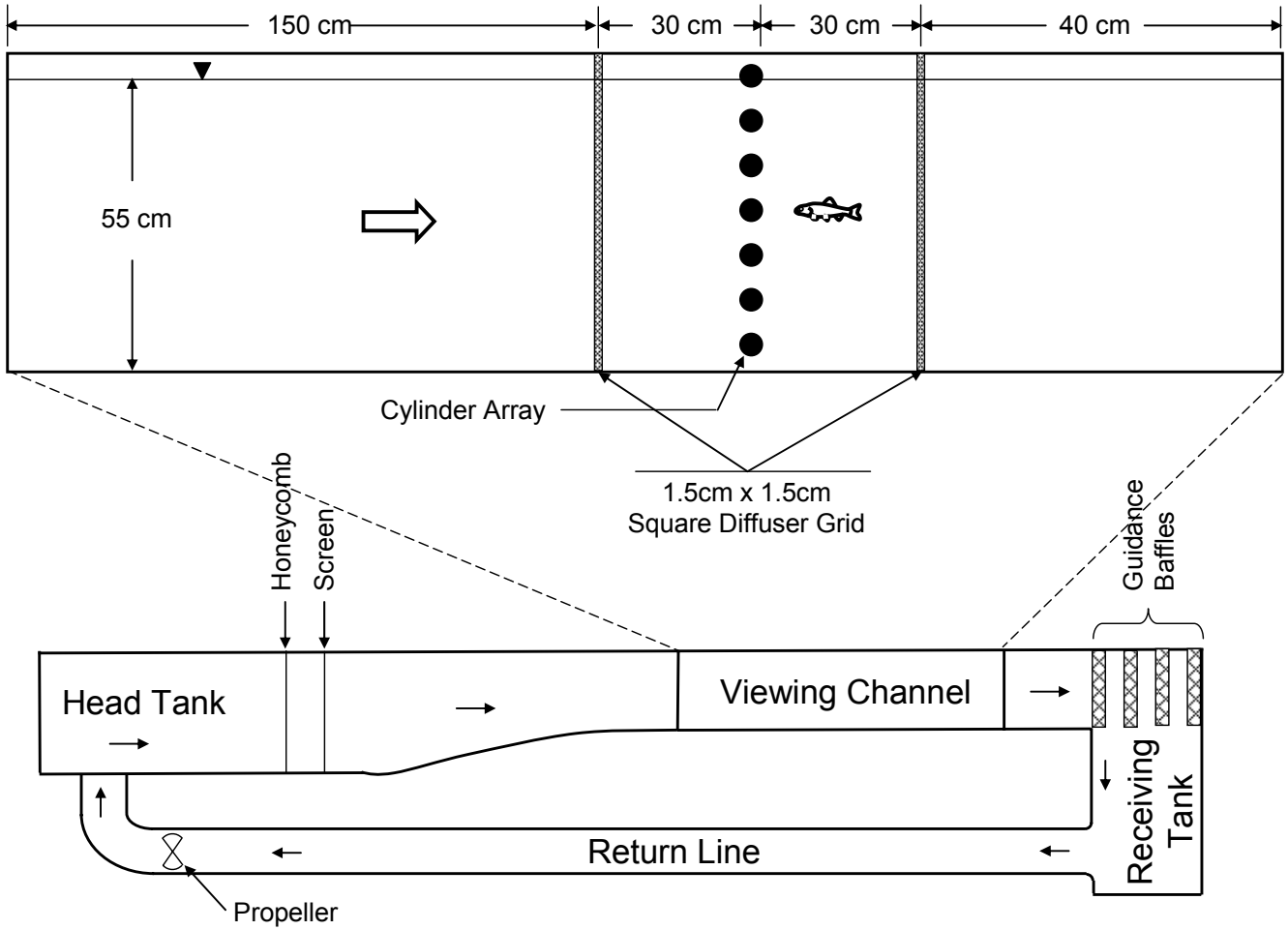
150 cm
30 cm
30 cm
40 cm
55 cm
Cylinder Array
1.5cm x 1.5cm
Square Diffuser Grid
Honeycomb
Screen
Guidance
Baffles
Head Tank
Viewing Channel
Receiving
Tank
Return Line
Propeller

Figure 3.2: Test Section Regions. a) The test section downstream from the control (1.5 cm mesh), small (0.4 cm diameter) and medium (1.6 cm diameter) cylinder arrays was subdivided into upstream (U), middle (M), and downstream (D) regions for flow visualization and spatial preference data collection. b) The test sections downstream from the large cylinder (8.9 cm diameter) arrays were further subdivided into regions directly downstream from the cylinder (C), regions directly downstream from a gap (G), and regions directly downstream from a cylinder edge (E). This classification resulted in nine regions in the test section in the large cylinder treatments: UC – upstream cylinder, UE – upstream edge, UG – upstream gap, MC – middle cylinder, ME – middle edge, MG – middle gap, DC – downstream cylinder, DE – downstream edge and DG – downstream gap. The gap between cylinders was equal to the cylinder diameter in each cylinder array. Observations of fish swimming within 2 cm of the wall and free surface were not used in the analysis.

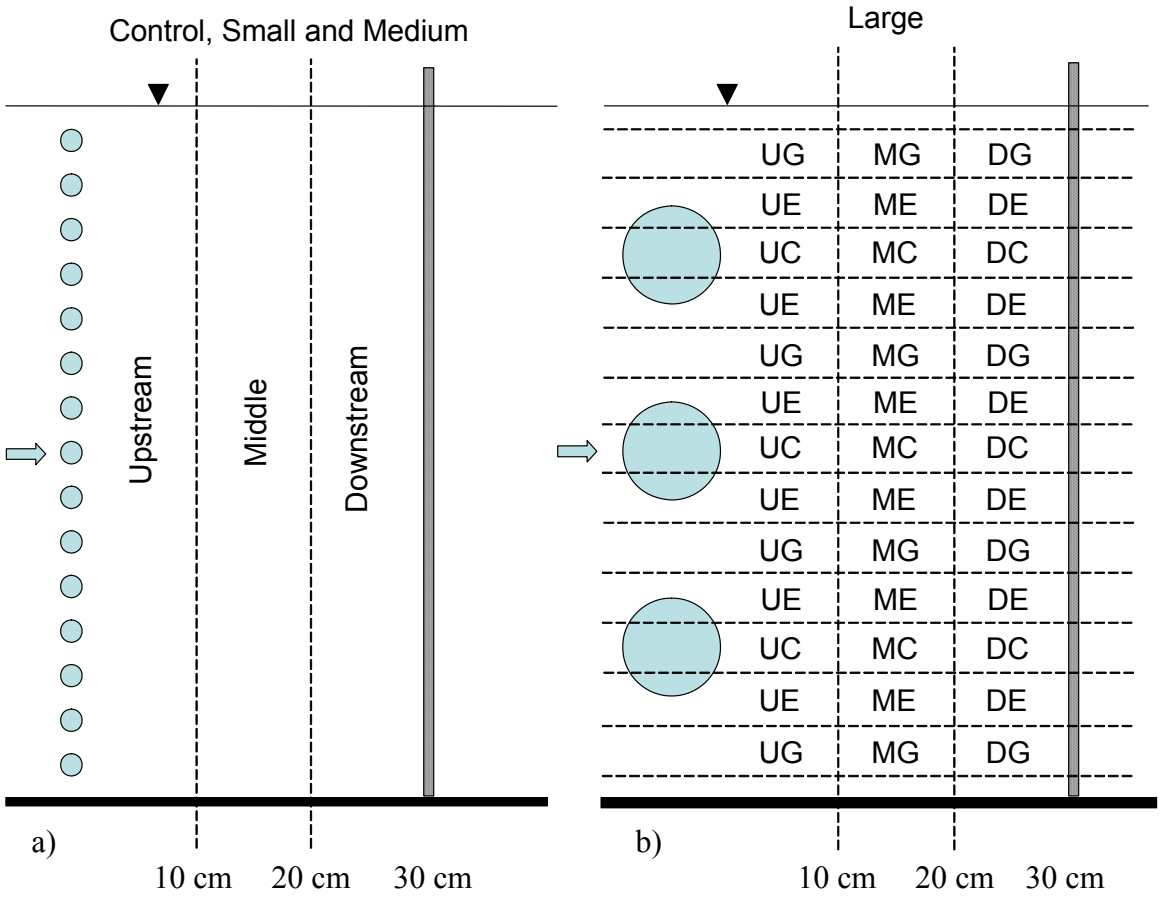
Control, Small and Medium
Large
Upstream
Middle
Downstream
UG MG DG
UE ME DE
UC MC DC
UE ME DE
UG MG DG
UE ME DE
UC MC DC
UE ME DE
UG MG DG
UE ME DE
UC MC DC
UE ME DE
UG MG DG
a)
b)
10 cm 20 cm 30 cm
10 cm 20 cm 30 cm

Flow analysis

Instantaneous flow patterns were recorded using two-dimensional PIV for velocities water-depth averaged over the test section cross section, $\bar{u}$, of 8.5, 17.1, 27.7, 38.7, and 50.2 $cm.s^{-1}$. The water was seeded with 1 μm diameter neutrally buoyant titanium dioxide particles, at a concentration of 1.2 ppm. Flow was illuminated using a 120 mJ NdYAG dual-head 532-nm pulsed laser (NewWave Gemini) with pulse duration of 100 μs, creating a laser sheet 0.75 mm thick spanning the test section either horizontally (for vertical cylinder arrays) or vertically (for horizontal cylinder arrays). Fifty image pairs were recorded for pulse separations of 8, 5, 3, 2, and 1 ms, at ū of 8.5, 17.1, 27.7, 38.7, and 50.2 cm/s respectively.

The vertical laser sheet was positioned along the flume centerline downstream from the horizontal cylinder arrays. Particle displacements were analyzed for an interrogation window within the laser sheet within the bottom 50% of the flume in order to avoid stray air bubbles in the upper part of the water column. These would have produced erroneous results due to cross-correlation analyses tracking bubble paths rather than the 1 μm diameter neutrally buoyant flow particles. Due to surface reflections and laser intensity requirements, the interrogation window was 26 cm sin the streamwise direction and 30 cm in the transverse direction, beginning 2 cm upstream from the downstream electrified restraining grid and 2 cm downstream from the upstream cylinder arrays or restraining grid. For vertical cylinder arrays, the interrogation window in the horizontal laser sheet was centered on the flume centerline, halfway between the bed and the free surface (Figure 3.3). A 0.9 mm thick black metal sheet was placed directly below the water surface to optically mask the surface waves created by the vertical cylinder arrays. The laser sheet was 25 cm below this sheet. The maximum boundary layer thickness was calculated to be 1.5 cm for the Reynolds numbers from 340 to 45,000 investigated (Schlichting 1979); therefore the boundary layer was outside the interrogation window. Eddy diameter, vorticity, and velocity were similar between horizontal and vertical configurations and differed by 0.0%, 1.7%, and 0.4%, respectively for the control, small-, and medium diameter cylinder arrays.

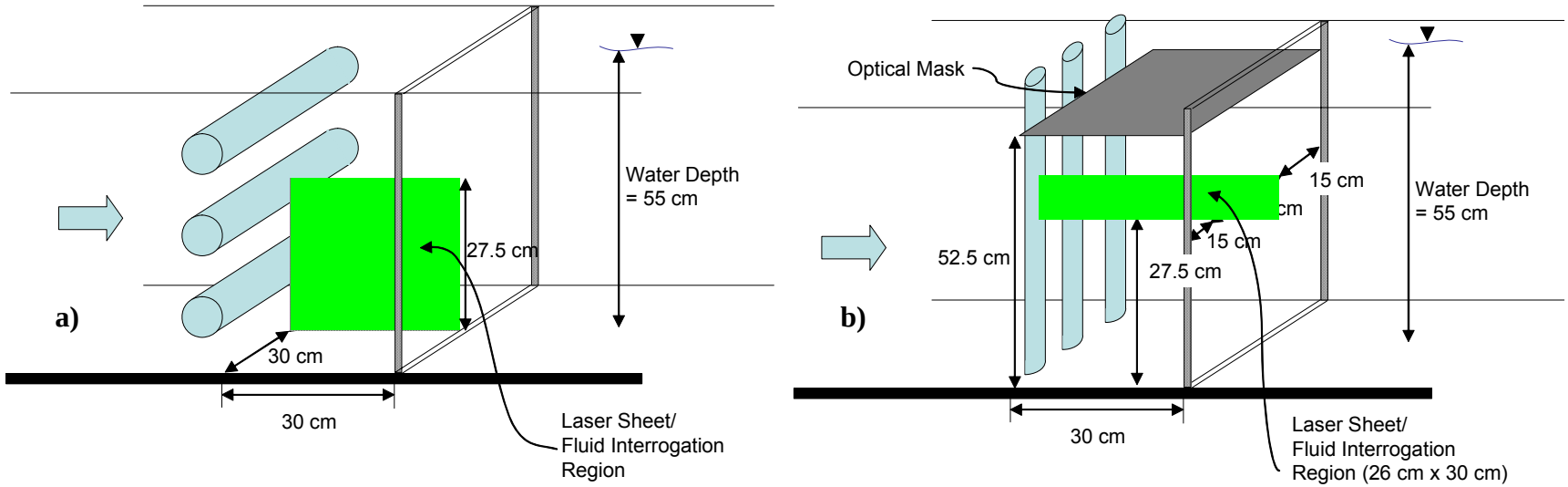

Figure 3.3: Location of PIV Interrogation Windows. a) Horizontal Cylinder – the green square indicates the laser sheet b) Vertical Cylinder – The laser sheet is now horizontal and a black sheet metal optical mask was placed 2.5 cm below the water surface to remove background surface refraction from the PIV images.

Flow was reconstructed from pairs of images of the particles as recorded by a 1 mega pixel 10-bit 30 fps UniqVision black and white CCD camera driven by PixelFlow software (General Pixels, Inc.; Huang et al. 1997, Gharib and Dabiri 2000, General Pixels 2000, Tritico et al. 2007). Fifty pairs of images were collected at 15 Hz at each $\bar{u}$, averaging 12 eddy shedding cycles from the cylinders.

Eddies were identified following the method described by Drucker and Lauder (1999). Cross-correlation techniques were used to convert consecutive images of particles into velocity vector fields. The vorticity (ω, twice the angular velocity) was calculated from the velocity vector field. Each local minimum and maximum vorticity within a vorticity field was taken as an eddy center following Drucker and Lauder (1999). The circulation about each eddy center was calculated in concentric circles until a maximum circulation (Γ_e – angular momentum per unit mass) was reached;

$$\Gamma_e=\omega_e*a_e \quad (3.1)$$

where a_e is the area circumscribed by the circle ($\pi d_e^2/4$) and ω_e is the spatially averaged vorticity within the circle. The diameter with maximum circulation was taken to be the eddy diameter (Drucker and Lauder 1999 and Wilga and Lauder 1999); each eddy's location, diameter, and average vorticity were recorded.

Because turbulent flows downstream of sources develop over space and time, the flow in the test section downstream from the control and the six cylinder treatments was subdivided into three streamwise regions (Figure 3.3a). Each streamwise region was approximately equal to the body length. These streamwise regions were termed upstream (0 – 10 cm downstream from the cylinders), middle (10 – 20 cm), and downstream (20 – 30 cm) regions (Figure 3.2a) and represent 0-1.1, 1.1-2.2, and 2.2-3.4 cylinder diameters downstream from the large cylinder arrays but 0-25, 25-50, and 50-75 cylinder diameters downstream from the small cylinder arrays.

Fish were observed swimming throughout the water column in the control, small- and medium-diameter cylinder array treatments without choosing locations relative to the cylinders. In contrast, fish regularly chose various swimming locations relative to the large cylinders. Therefore, flow was further analyzed for three cross-flow regions for the large cylinder array (Figure 3.3b).These locations were classified as a) the large cylinder (LC) area directly downstream from each large cylinder (cylinder centerline ± 2.3 cm), b)

the large edge (LE) area directly downstream from each cylinder edge (cylinder edge ± 2.3 cm), and c) the large gap area directly downstream from each gap between the cylinders (gap centerline ± 2.3 cm).

Fish

Creek chub were obtained from Fleming Creek, Michigan, USA at a water temperature of 21.1 °C. Fish were acclimated in the lab to room temperature (20.5 ±0.4 °C) for at least one week prior to the experiment and were fed to satiation daily. The experimental temperature was the same as the acclimation temperature. Seven creek chub with an average total length of 12.2±0.9 cm (mean±2SE) and mass of 16.8±3.5 grams were used in these experiments. Each fish was swum with every treatment. The order of the treatment for the fishes was randomized and fish were given a minimum of 3.5 days to recover between each test.

A single fish was placed in the observation section and acclimated to $\bar{u}$ of 8.5 cm/s. After 11 hours of acclimation, ū was increased by 3.5 $cm.s^{-1}$ increments at 2 minute intervals until the fish became entrained on the downstream grid for 3 seconds. The two-minute critical swimming speed was calculated as;

$$2\text{-min } u_{crit} = \overline{u_p} + \Delta \bar{u} * \Delta t/2 \qquad (3.1)$$

where $\overline{u_p}$ is the cross-sectionally averaged flow speed prior to fatigue and Δt is the time in minutes that the fish was able to sustain the highest cross-sectionally averaged flow speed (Brett 1963).

Fish were continuously videotaped at 30 frames per second simultaneously from the side and from below using two digital video cameras (Panasonic Model No. PV-DV601D). Fish moved about the test section, holding position for variable periods at various locations. Swimming kinematics were measured from video records when fish remained in a given location with no postural changes for >5 s, during which time fish velocity varied by <0.02 body-lengths.s^{-1} (Wilga and Lauder 2002).

In the presence of large cylinders fish suddenly lost the ability to control posture and hold position. The head rotated greater than 45° and the body was displaced downstream >0.5 of the stretched-straight body length. These events were described as

"spills" and indicated that control of posture and swimming trajectory was overwhelmed. Fish recovered from a spill by reorienting the body axis to the mean flow direction and holding position in the flow with no additional translation downstream. Each spill and recovery was analyzed frame-by-frame to determine the kinematics of the spill, the recovery, and the overall duration.

Additionally, the test section location in which each spill occurred was recorded and compared with the percent time spent at the location. The percent time spent at in a given flow region was determined by marking the fish's location in the test section at 5 second intervals for each treatment and speed.

Results

The presence of obstructions creates local flow variations. The local velocities, u_{local}, measured in the various test section regions (Figure 3.3) were equal to $\bar{u}$ (< ±3%) in all streamwise regions of the test section for the control, small, and medium cylinder arrays and in the LE region of the large cylinders. In the gap between cylinders (LG) u_{local} was on average 53% greater than $\bar{u}$ while directly behind the cylinders (LC) u_{local} was on average 38% less than $\bar{u}$ (Figure 3.4).

Turbulence Regimes

Biological flumes and low-turbulence flumes are not free from turbulence (Brett 1963, Farlinger and Beamish 1977, Enders et al. 2003), and the biological requirement of delimiting the upstream end of observation sections to avoid fish escape introduces additional turbulence. Hence the production of turbulent eddies was unavoidable in the control and all treatments but the range of eddy diameters was increased by the treatments.

Thus turbulent flow regimes are comprised of a range of turbulent eddy diameters (von Karman 1937, Taylor 1938, Batchelor and Townsend 1947). The distribution of eddy diameters tends to be positively skewed, with a large number of small eddies and relatively few large diameter eddies (Figure 3.5a and b). This positively skewed distribution pattern was found for all treatments in these experiments (Figure 3.5b). Cada and Odeh (2001), Nikora et al. (2003), Biggs et al. (2005), and Lupandin (2005) have

predicted that it is the relatively large/infrequent eddies in most flow distributions that have the greatest potential to perturb a fish when these are of similar size to the length of a fish. For this reason, the cylinder treatments were designed to increase the proportion of large eddies in the flow up to eddy diameters approaching the fish length (Figure 3.5b).

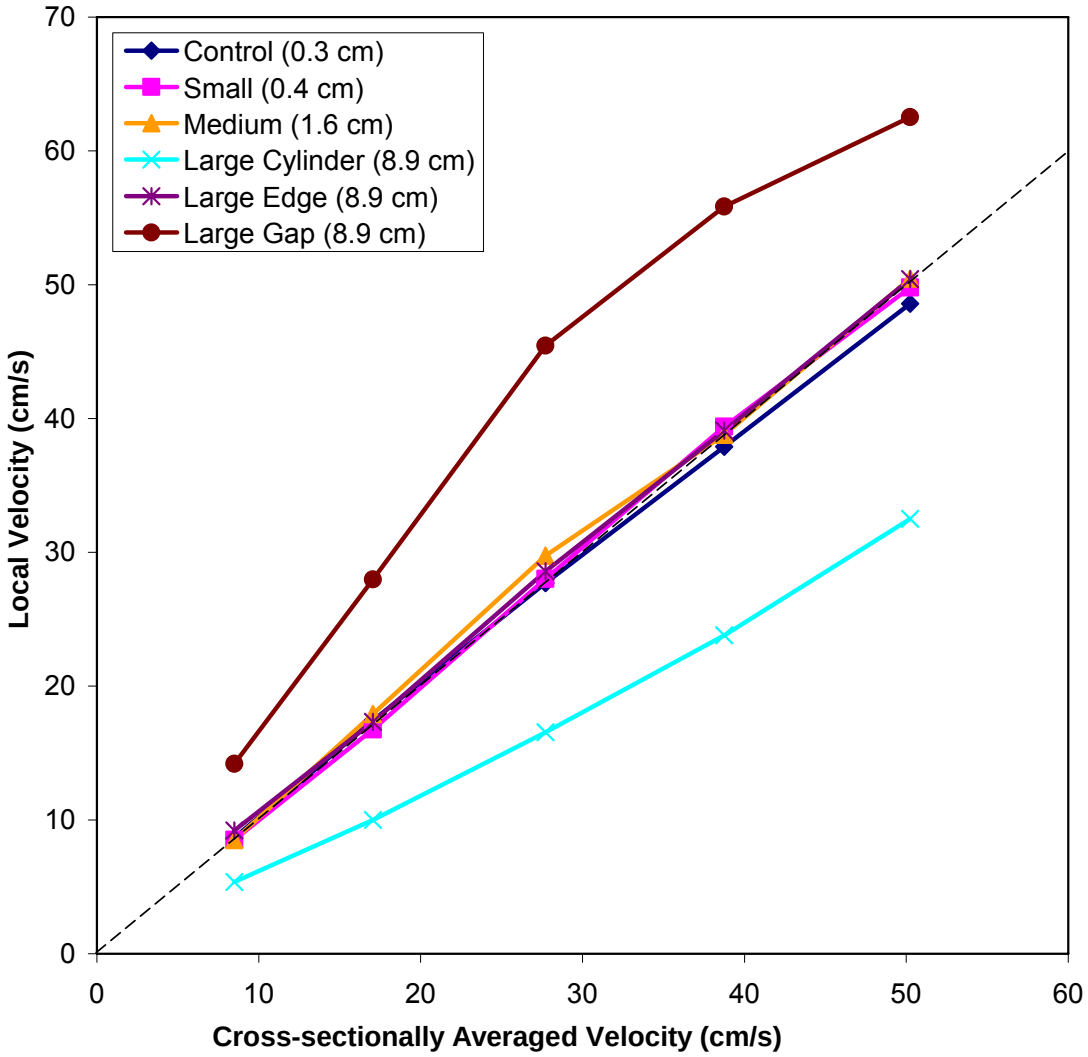

Figure 3.4: A comparison of local velocity to cross-sectionally averaged velocity for flow regions and treatment. The u_{local} within the middle streamwise region of the test section have been plotted and matched $\bar{u}$ for all control, small, and medium cylinder treatments. The u_{local} in the LC Region increased at a lesser rate than $\bar{u}$ while the u_{local} in the LG Region increased at a greater rate than the $\bar{u}$. The cylinder diameter is listed after each treatment in the figure legend.

Figure 3.5: The distribution of eddy diameters varied across cylinder treatment. The insert (a) is an example histogram for flow in the middle streamwise region of the medium horizontal cylinder treatment at $\bar{u}$ of 27.7 cm.s^{-1} showing the location of the 50th, 75th, and 95th percentile eddy. The primary figure (b) shows the eddy distributions across cylinder treatment. The proportion of large eddies (with respect to the 12.2 cm fish length) is increased with increasing cylinder diameter.

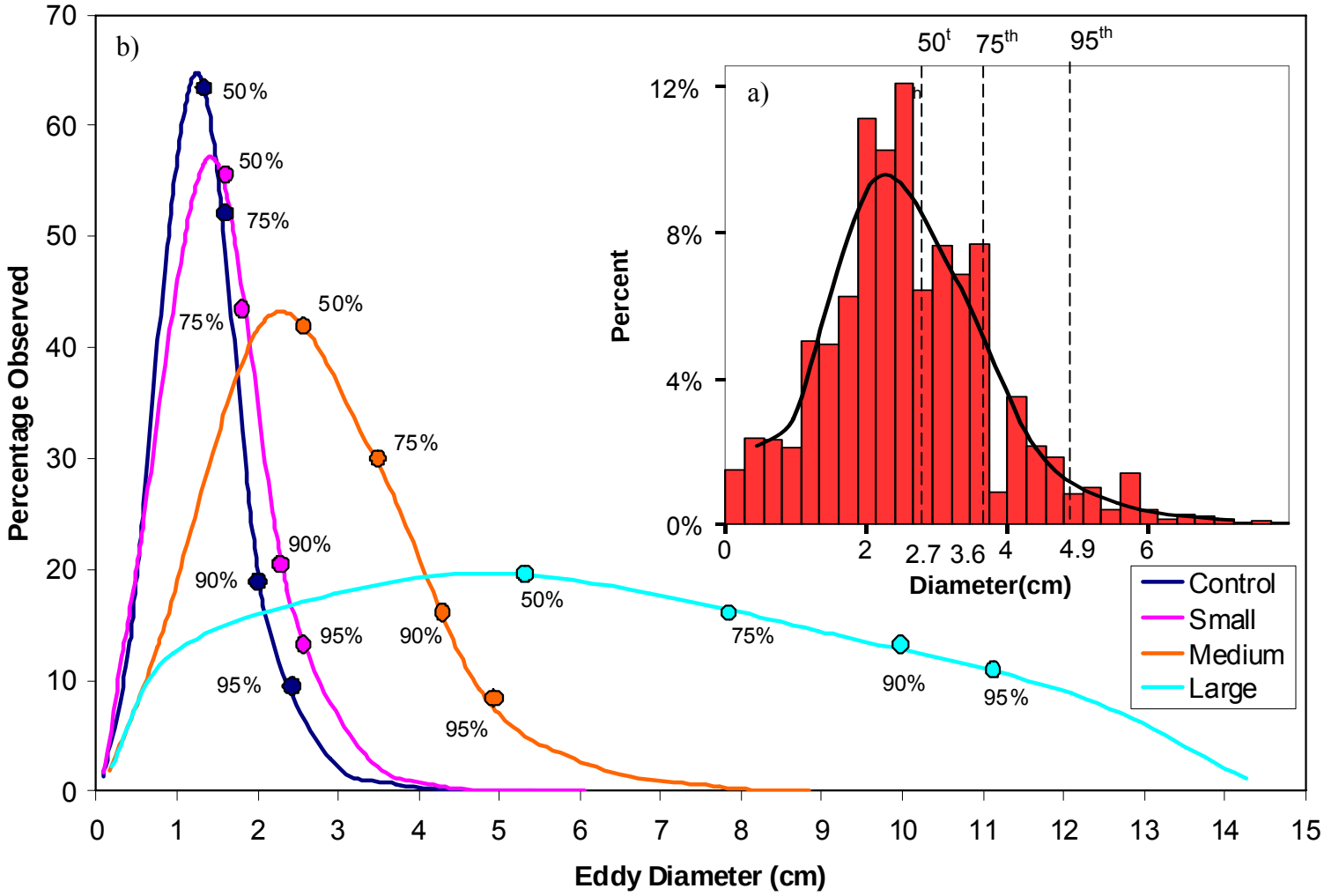
b)
a)
Percentage Observed
Eddy Diameter (cm)
Percent
Diameter(cm)
50t
75th
95th
50%
75%
90%
95%
Control
Small
Medium
Large

Spills, indicating loss of control over posture and location and downstream translation also occurred infrequently, suggesting that infrequent but large eddies in a flow indeed had the greatest impact on the fish. Spills occurred in treatments with eddy diameters above 9.3 cm (Figure 3.6), which occurred at the 95th percentile of eddies in the gap region of the test sections in the large cylinder treatments. Therefore, eddy characteristics for the 95th percentile eddies are reported for each treatment, as well as for the median (50th percentile) and the 75th percentile to give a more complete picture of the flow in each treatment. Thus, no spills were observed for fish swimming in the medium cylinder treatment where the 95th percentile eddy was 4.9 cm, while 8 spills were observed within the LG flow region where the 95th percentile eddy was 9.3 cm (Figure 3.6a).

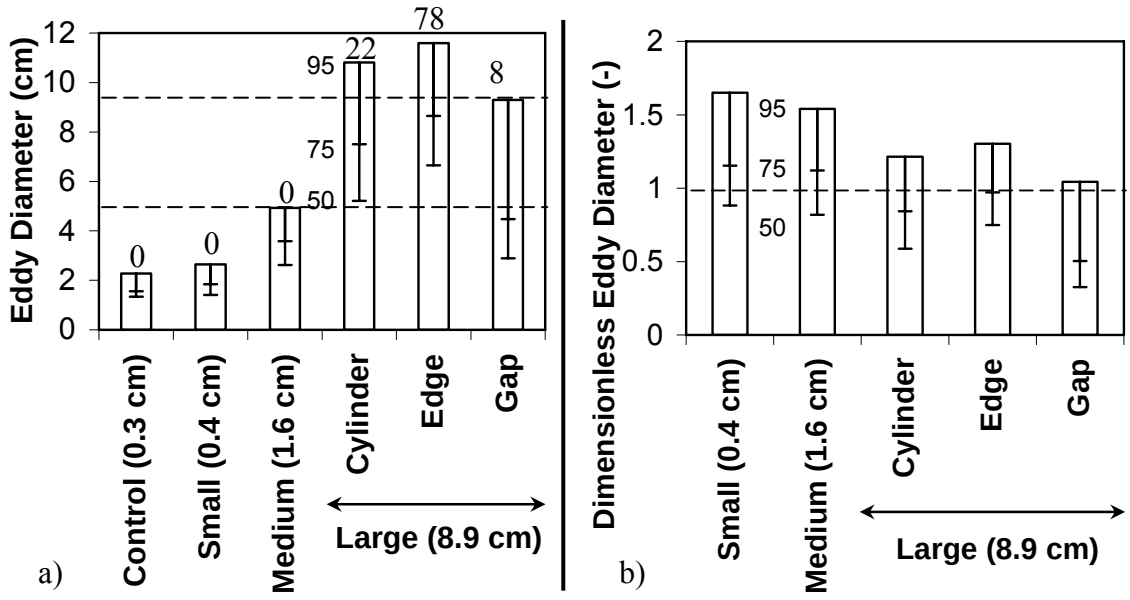

Figure 3.6: The 95th percentile eddy diameter varied across treatment and flow region. a) Eddy diameter increased with cylinder diameter (cylinder diameters are listed on the figures). For the large cylinders, eddy diameter was largest within the LE (edge) region and smallest within the LG (gap) region. The number of spills observed in each flow regime is listed above each bar. b) Dimensionless eddy diameter per cylinder half wake width at merging ($\frac{d_e}{d_{cyl} \cdot n}$), where n is the number of merged wakes, showing that eddy diameter scales with the cylinder and the number of merged wakes. The primary bar represents the 95th percentile eddy value while the whiskers represent the 50th and 75th percentiles. Data reported include all streamwise locations in the flow.

While the magnitudes of the eddy variables were different, the trends across flow regime and general conclusions were similar irrespective of whether the 50^{th}, 75^{th} or 95^{th} percentile eddy were analyzed.

The 95^{th} percentile eddy diameter increased with both cylinder diameter and the number (n) of adjacent wakes that merged within the test section, where a wake is defined as flow entrained by eddies shed from a cylinder (Tennekes and Lumley 1972) (Figure 3.6b). The number of wakes merging within the test section increased with the number of cylinders in the array as determined from the PIV data and verified using dye tracing, (Zdravkovich 2003). In the large cylinder arrays (consisting of three 8.9 cm diameter cylinders) wakes were not observed to merge within the test section, as has also been described by Zhang and Zhou (2001) and Akilli et al. (2004). In the medium cylinder arrays (consisting of 19-1.6 cm diameter cylinders) the number of wakes that merged within the test section ranged from 1 to 4 wakes. The average (and median) number of wakes merging was two. In the small cylinder arrays (consisting of 94-0.4 cm diameter cylinders) the number of wakes that merged within the test section ranged from 1 to 10 wakes. The average (and median) number of wakes merging was four.

The eddy diameter increased with cylinder diameter with the small, medium, and large cylinder arrays producing 95^{th} percentile eddy diameters of 2.6, 4.9, and 11.2 cm, respectively (Figure 3.6a). As expected, because the shear layer eddies are shed and convected through the edge regime of the flow, the largest eddies are found in the LE regime (95^{th} percentile eddy diameter = 11.6 cm).

Wakes have been observed to merge within three cylinder diameters when the gap to cylinder spacing is equal to one (Zdravkovich and Stonebanks 1990, Moretti 1993). Then eddies within the wake are approximately half the merged wake width in diameter and no longer grow ($d_e \propto x^0$) due to the fact that all fluid between cylinder wakes has been entrained into the resulting wakes (Okamoto and Takeuchi 1975, Blackburn 1994, Zdravkovich 2003). For this reason, variations in streamwise eddy diameter were small compared to treatment effects. Thus the 95^{th} percentile eddy vorticity increased linearly with $\bar{u}$ at all streamwise locations (Figure 3.7a) and increased with cylinder diameter

Figure 3.7: The 95th percentile eddy vorticity varied across treatment and flow region. a) Eddy vorticity by $\bar{u}$. Eddy vorticity increased linearly with $\bar{u}$. Data are from all streamwise locations. b) Eddy vorticity increased with cylinder diameter (diameters are shown in the parentheses), and for the large cylinders vorticity was greatest in the LE region and least within the LG region. c) by eddy diameters (95th percentile eddy in each region) downstream from the cylinders. Eddy vorticity was inversely proportional to the relative distance the eddy had traveled as measured in eddy diameters. The shedding vorticity was calculated as $\bar{u}$ divided by the wake half width ($\omega_0 = \frac{v_{avg}}{d_{cyl} \cdot n}$ where n is the number of merged wakes – wakes merged into groups of two, n=2, downstream from the medium cylinders and into groups of four, n=4, downstream from the small cylinders while wakes did not merge, n=1, downstream from the large cylinders). The solid bars and lines represent the rapidly rotating eddies (95th percentile) while the whiskers represent the 50th and 75th percentiles. Data from figures 3.7 b) and c) have been sliced along the transverse (for the large cylinder array treatments) and streamwise directions, respectively and therefore each bar or data point represent all data from that streamwise or transverse location, respectively. Data in figures b) and c) are for an exemplary speed of 27.7 cm.s^{-1}.

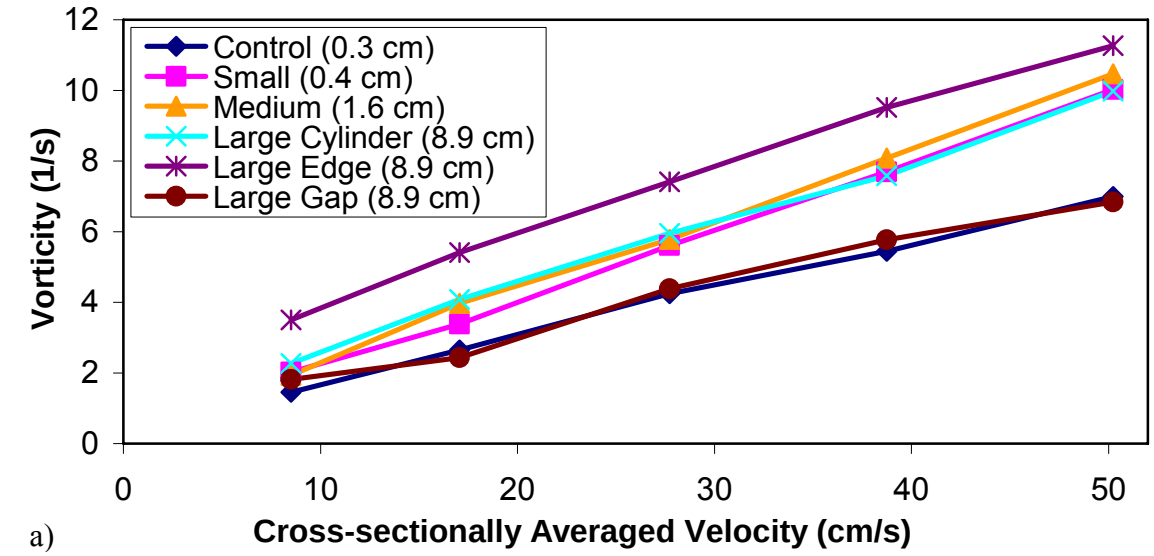
Control (0.3 cm)
Small (0.4 cm)
Medium (1.6 cm)
Large Cylinder (8.9 cm)
Large Edge (8.9 cm)
Large Gap (8.9 cm)
Vorticity (1/s)
Cross-sectionally Averaged Velocity (cm/s)
0
2
4
6
8
10
12
0
10
20
30
40
50

a)

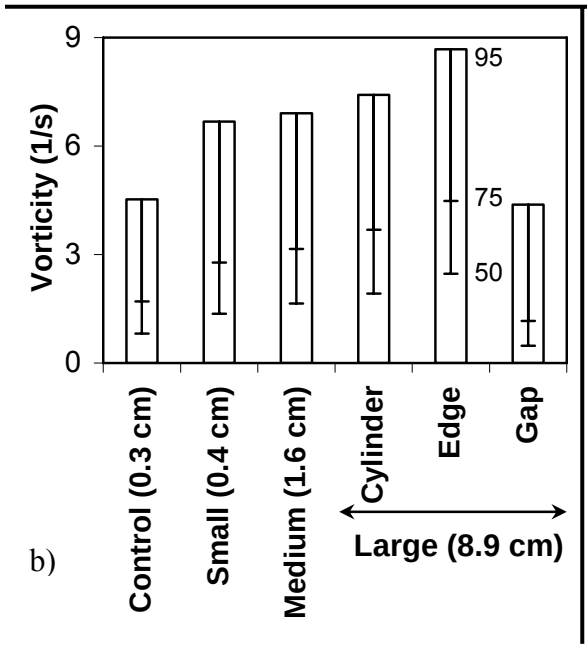
Vorticity (1/s)
0
3
6
9
95
75
50
Control (0.3 cm)
Small (0.4 cm)
Medium (1.6 cm)
Cylinder
Edge
Gap
Large (8.9 cm)

b)

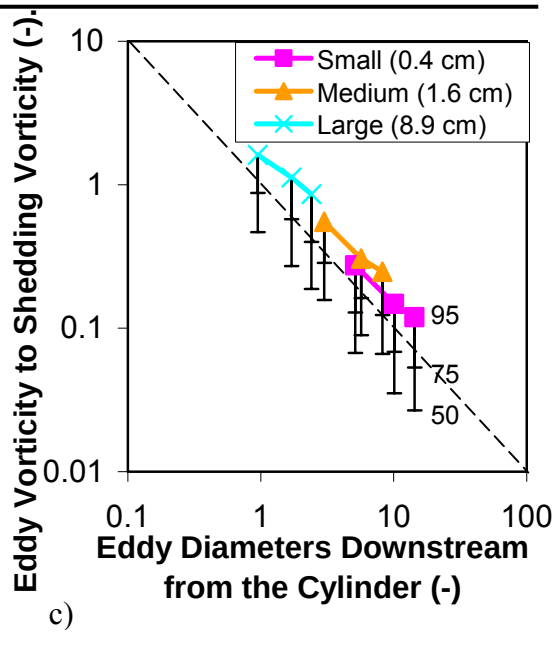
Small (0.4 cm)
Medium (1.6 cm)
Large (8.9 cm)
Eddy Vorticity to Shedding Vorticity (-)
0.01
0.1
1
10
95
75
50
0.1
1
10
100
Eddy Diameters Downstream
from the Cylinder (-)

c)

(Figure 3.7b). The LE regime is the location where the shear-layer eddies are shed and through which most shear-layer eddies are conveyed. As such, at an exemplary $\bar{u}$ of 27.7 cm.s^{-1} vorticity in the LE regime was 7.4 s^{-1} and greater than the vorticity of 4.2, 5.6, and 5.8 s^{-1} in the control, small, and medium cylinder treatments and also greater than the vorticity of 5.9 and 4.4 s^{-1} in the LC and LG regions. Conversely, the LG regime consists of relatively high speed rectilinear flow that was not entrained by wake eddies. This area, therefore, had similar vorticity to that of the control treatment. The 95th percentile eddy vorticity was 4.4 s^{-1} in the middle streamwise LG region at $\bar{u}$ of 27.7 cm.s^{-1} while the 95th percentile vorticity in the middle streamwise control was 4.5 s^{-1} at the same $\bar{u}$.

The turbulent flow develops in the upstream portion of the test section, just downstream from the cylinder arrays but changes with distance as eddies move downstream from the source. These changes scale with the number of eddy diameters flow moves downstream from the cylinder source. If the ratio of shedding eddy vorticity in the upstream zone is ω_0 and at a downstream location is ω_e then the ratio of eddy sizes varies with the streamwise distance, x from the cylinder array as (Figure 3.7c) (Tennekes and Lumley 1972, Williamson 1996):

$$\frac{\omega_e}{\omega_0} \propto \frac{x}{d_e}^{-1} \tag{3.2}$$

The shedding vorticity was calculated as (Huang et al. 2006);

$$\omega_0 = \frac{\bar{u}}{d_{cyl} \cdot n} \tag{3.3}$$

Thus eddy vorticity within wakes decays inversely with distance from the cylinder, so that $\omega_e \propto x^{-1}$ for a given shedding vorticity and eddy diameter. The net decay is due to the balance of viscous dissipation and production from vortex stretching. The latter occurs as different parts of an eddy length are convected downstream at different speeds, and increased eddy length reduces eddy diameter in order to conserve mass and through the conservation of angular momentum increases vorticity (Batchelor and Townsend 1947, see also Tennekes and Lumley 1972, Antonia et al. 1998).

Figure 3.8: Flow Region Preference. a) Preference within the control, small, and medium cylinder treatments. Preference did not change across treatment but fish were more commonly found in the downstream sections of the flow, a preference that became more pronounced with higher $\bar{u}$ (ANCOVA, $p<0.05$ for streamwise regions and $\bar{u}$). b) Preference within the LH test section. Fish moved from the downstream gap region into the middle cylinder region with increased $\bar{u}$ (ANCOVA, $p<0.05$ for streamwise and transverse regions and $\bar{u}$). c) Preference within the LV test section. Fish moved from the downstream gap region into the middle edge region with increased $\bar{u}$ (ANCOVA, $p<0.05$ for streamwise and transverse regions and $\bar{u}$). Preferences have been compiled for all flows less than 25 $cm.s^{-1}$ (left column) and for all flows greater than 25 $cm.s^{-1}$ (right column).

C, SH, SV, MH, and MV Treatments

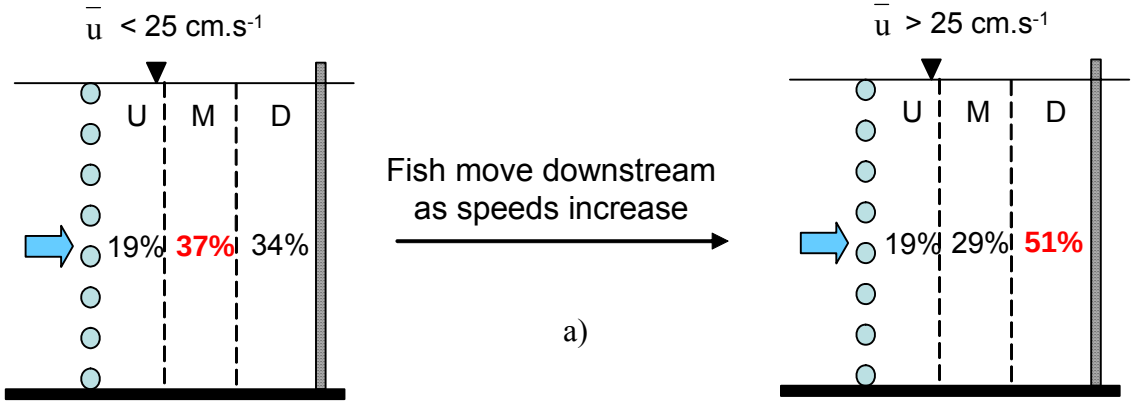

a)

LH Treatment

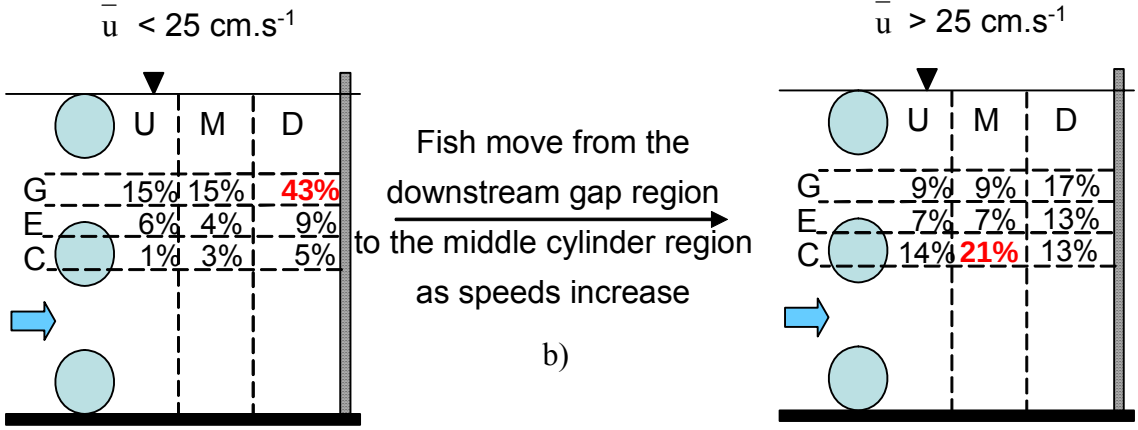

b)

LV Treatment

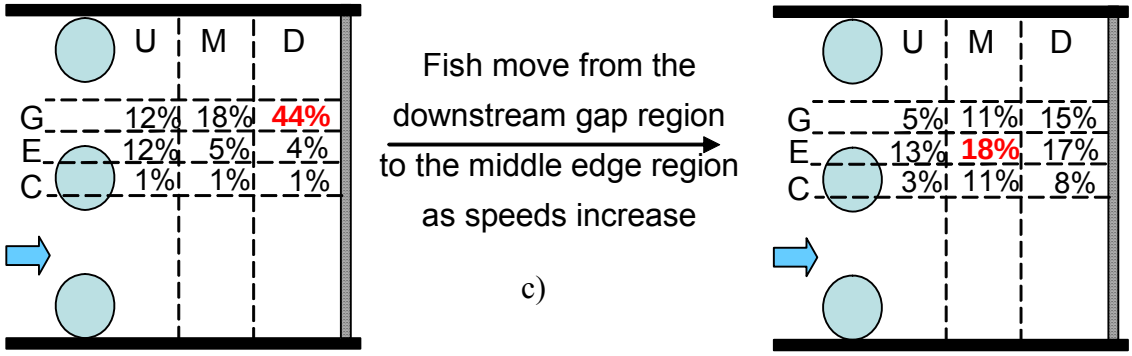

c)

Location Preference

While fish moved freely about the test section, they were found in some regions at a higher frequency than others (Figure 3.8). Location preference did not change across control, small and medium cylinder treatments (ANCOVA with streamwise location, treatment, $\bar{u}$, and interaction terms, $p>0.05$ for treatment and treatment interaction terms). Within these flows with smaller diameter eddies fish were more likely to found in the middle and downstream flow regions. As $\bar{u}$ increased, the likelihood that fish were observed in the downstream region increased (ANCOVA $p<0.05$, Figure 3.8a). The middle and downstream flow regions have turbulent eddies with less vorticity than the upstream region, consistent with previous studies showing increased avoidance of turbulent fluctuations with increasing speeds (Smith et al. 2005, Cotel et al. 2006).

For the large cylinder treatment fish were observed to hold station in specific regions relative to the cylinder, necessitating the dividing of flow across the stream into gap, edge, and cylinder regions. At low speeds fish spent most time, 43%, in the downstream gap flow region and spent the least amount of time, 1%, in the upstream cylinder flow region (ANCOVA with streamwise and transverse locations, treatment, $\bar{u}$, and interaction terms, $p<0.05$ for streamwise and transverse locations along with various interaction terms between all variables). As speed increased, fish in the LH treatment moved to the middle cylinder region while fish in the LV treatment moved to the middle edge region (Figure 3.8b and c). At the lowest speeds, where swimming required relatively little power, fish chose a regime with higher velocity but smaller diameter turbulent eddies with lower vorticity (Figures 3.4, 3.6a, 3.7b and c) than surrounding regions. As speed increased fish appeared to be using the turbulent wakes as time-averaged velocity shelters (Figure 3.4). However, station holding in the wake occurred less frequently indicating that these areas were not ideal refuges, as described by Webb (1998) for fishes holding station using single cylinders with diameters up to 0.3 fish-lengths. The observation that the fish used the edge regions of the LV cylinder array treatment more frequently than in the LH cylinder array treatment indicates that the fish were better able to control posture and location with the large, high vorticity vertical eddies found in the edge zone (Figure 3.6a and 3.7b) rather than the equivalent horizontal eddies.

Spills

A spill was defined as a rotation of the head, from the snout to the posterior edge of the operculum, of greater than 45° followed by downstream body translation of >0.5 body lengths and hence a displacement representing a loss of control of posture and location. Spills were not observed for fish swimming in the control, small-, or medium-cylinder treatments. In the LV treatment, sixteen smaller body rotations occurred followed by unidirectional tail flips that did not result in large downstream displacements. These were considered to be displacements that were within the re-stabilizing capability of the fishes and hence were not included among the spills.

Spills in turbulent flow created by the two orientations of large cylinders differed in their frequency, with 77 spills occurring in the LH treatment and 31 spills with the LV treatment. The probability of a spill occurring in the upstream edge regime of the LH treatment was 49% compared to 20% in the same region of the LV treatment. This was the region of flow which contained the largest eddies (Figure 3.7).

In addition, recovery behavior differed with orientation for the large cylinder treatments. For the LV cylinder array treatment, spills and recovery typically followed a sequence of (Figure 3.9):

1) Rapid body yawing rotation of the head and the start of downstream body translation
2) Bending of the body so that the caudal fin subtended an angle near perpendicular to the mean stream flow direction along with simultaneous deployment of the pectoral fin on the same side as the body bend.
3) Rapid lateral movement of the caudal fin, ending with the body aligned with the local flow
4) Retraction of the pectoral fins
5) Resumption of steady swimming

Spills and recoveries with the LV cylinder array lasted 410±40 ms.

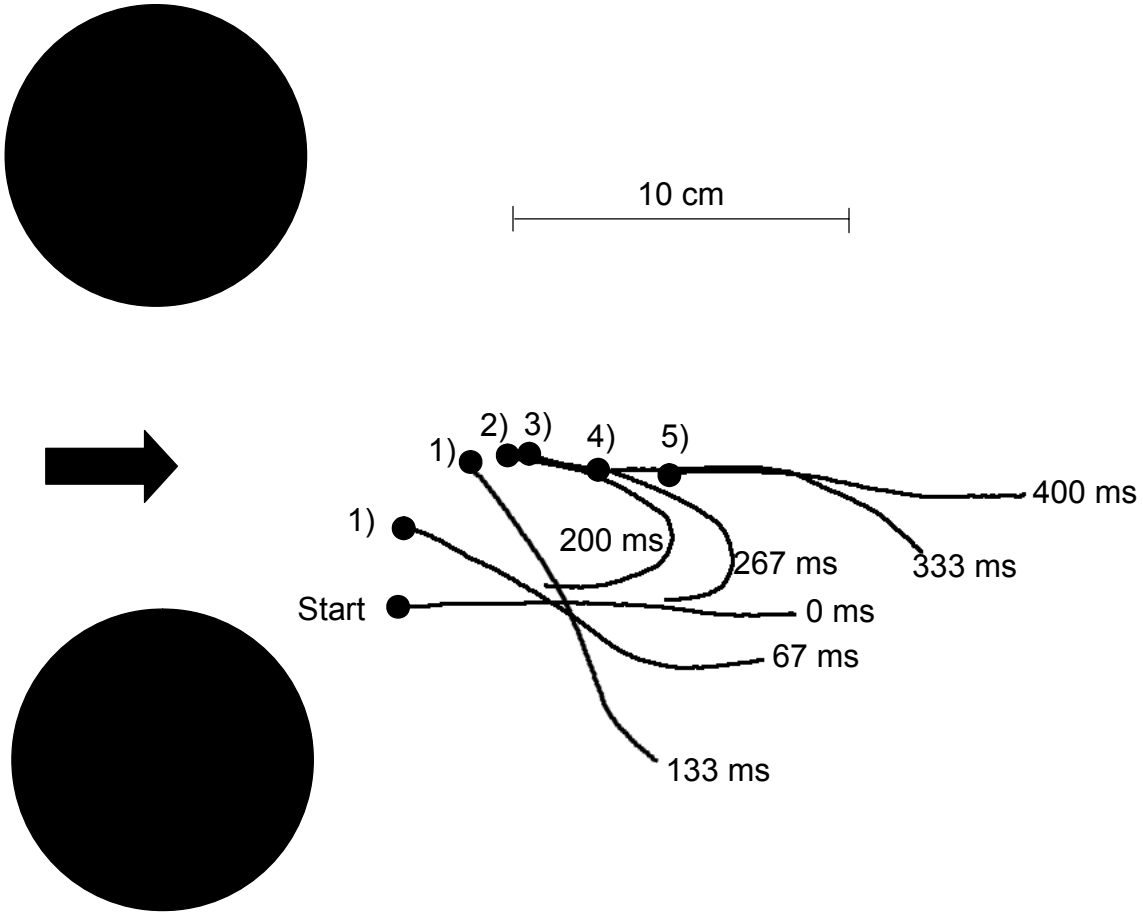

Figure 3.9: The body centerline is plotted across 67 ms time-steps for a representative spill and recovery. Each line represents the centerline of the fish at Δt = 67 ms intervals. Circles indicate the fish head, flow is from left to right on the page. Spills were defined as head rotations greater than 45 degrees (t = 133 ms) and downstream translation of at least half a body length (t=400 ms). This spill occurred behind the large vertical cylinders at $\bar{u} = 35.1$ cm.s^{-1} – spill patterns were similar in large horizontal cylinder cases with the addition of two rolls to allow for the tail to be used as a control surface in the appropriate plane.

Spills and recovery in the LH cylinder array treatment followed the same sequence as that of the LV cylinder but with the addition of two body rolls that oriented the caudal fin to counter the pitching moment of the flow perturbation:

1) Rapid body pitching rotation of the head and the start of downstream body translation
2) **90° body roll such that the fish dorsal-ventral axis was horizontal**

3) Bending of the body so that the caudal fin subtended an angle near perpendicular to the mean stream flow direction and simultaneous deployment of the pectoral fin on the same side as the body bend.
4) Rapid lateral (vertical) movement of the caudal fin, ending with the body aligned with the local flow.
5) Retraction of the pectoral fins
6) **90° body roll returning the dorso-ventral axis of the body to the horizontal plane**
7) Resumption of steady swimming

Spill and recovery in the LH cylinder array treatment lasted 510±40 ms, significantly longer than for the LV treatment (t-test, $p<0.05$).

Spills in the presence of large cylinders were observed at all $\bar{u}$ above 28 cm/s with the speed of first spill averaging 44±3 cm/s for fish swimming with the LV cylinder array, significantly higher than that of 37±1 cm/s with the LH treatment (t-test, $p<0.05$, Swanson et al. 1998, Maxwell and Delaney 2004) (Figure 3.10). Therefore the control system was overwhelmed at lower speeds in the presence of large horizontal eddies than in the presence of large vertical eddies.

Considering $\bar{u}$ at which spills occurred in the large cylinder treatments, fish spent the significantly largest percentage of their time in either the middle cylinder or middle edge regimes (ANOVA $p<0.05$, Figure 3.11a, b). However, fish frequently moved close to the cylinder, presumably to find a location where they could balance without swimming as Webb (1998) observed for fish station holding using small cylinders. As a result, fish spent 10% of their time in the upstream edge region of the flow but 60% of the spills occurred in the region (ANOVA, Figure 3.11c, d). Turbulent eddies in the upstream edge regime provided the greatest stability challenge for the fish.

Critical Swimming Speed

The mean 2-min u_{crit} of the creek chub swimming for the control treatment was 53.2±1.8 cm/s (mean ± 2 S.E.) (Figure 3.10). Values were significantly lower than the control for all cylinder treatments, the reduction in the 2-min u_{crit} being decreased by 5% within the SH treatment and 22% within the LH treatment (one-way ANOVA with

Figure 3.10: The critical swimming speed and speed of first spill varied across treatment. The bars represent the mean while the whiskers represent ± 2 standard errors about the mean. Spills (defined as head rotations followed by downstream body translation, see Figure 3.9) were not observed for fish swimming in the control, small-, or medium-cylinder array treatments. CSS = 2 minute critical swimming speed.

Critical Swimming Speed (cm/s).
55
53
51
49
47
45
43
41
39
37
35
Control
Small Vertical
Small Horizontal
Medium Vertical
Medium Horizontal
Large Vertical
Large Horizontal
CSS
CSS
CSS
CSS
CSS
CSS
1st Spill.
CSS
1st Spill.

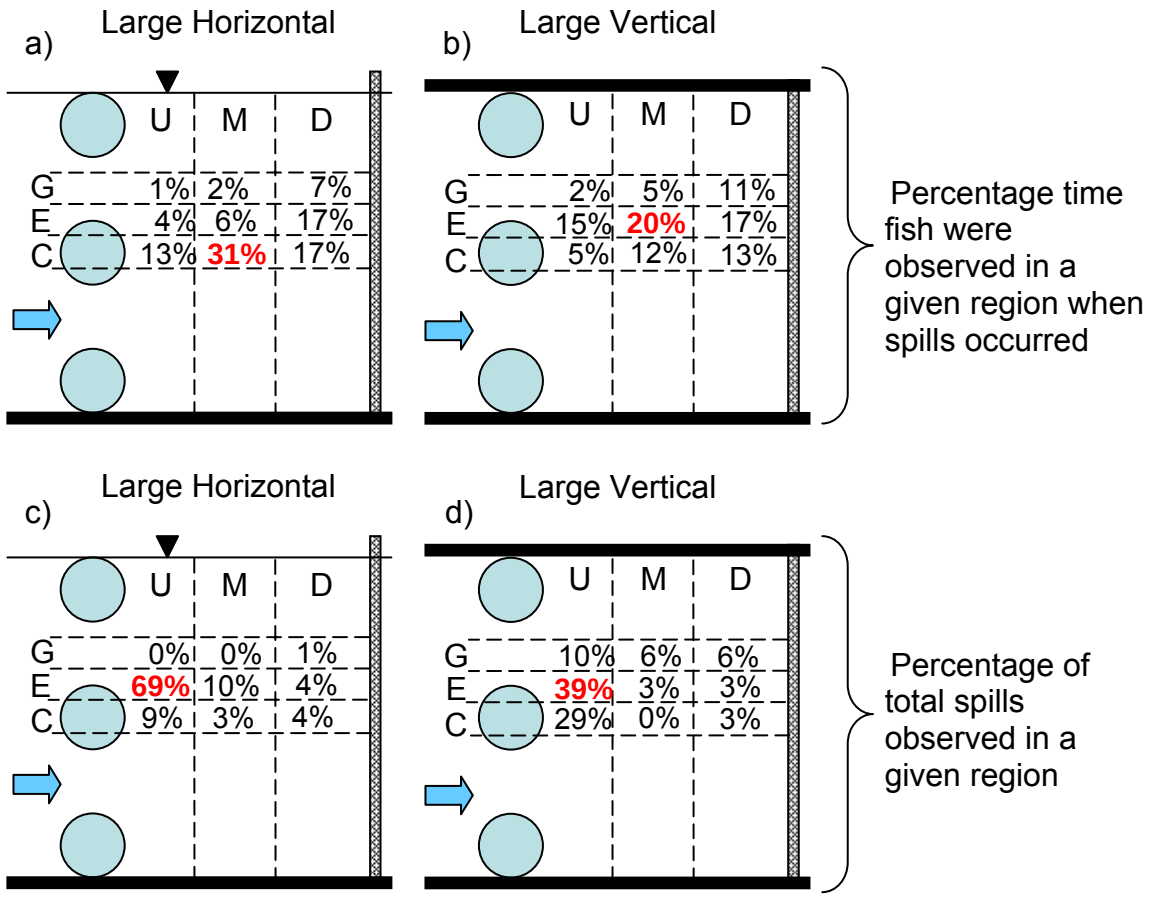

Figure 3.11: The percentage time fish were observed in a region for cross-sectionally averaged velocities that spills occurred and the percentage of total failures observed varied across flow region. a) Large Horizontal and b) Large Vertical values represent the mean percentage time spent in a section across all fish for $\bar{u}$ where spills were observed to occur (>28 cm/s). c) Large Horizontal and d) Large Vertical values represent the mean percentage of all spills that occurred in a section across all fish. The largest percentage in each figure has been highlighted in red.

repeated measures, $p < 0.05$ Swanson et al 1998, Maxwell and Delaney 2004). There was an exception for the SV treatment in which a 5% reduction in 2-min u_{crit} did not prove significant (ANOVA, $p = 0.063$). The 2-min u_{crit} for the SV, SH, MV, and MH treatments were not significantly different from each other (one-way ANOVA with repeated measures, $p > 0.05$) indicating that for the small and medium cylinder treatments there was no cylinder size or orientation effect. The 2-min u_{crit} for fish swimming directly downstream from the large cylinder vertical array was 10% lower than that for the control treatment and was significantly less than the 2-min u_{crit} for the small and medium

cylinder treatments (multiple matched pairs t-tests, $p<0.05$). The 2-min u_{crit} in the LV region was, however, significantly larger than the critical swimming speed for the LH treatment (total reduction in critical swimming speed from the control treatment of 22%, one-way ANOVA with repeated measures, $p < 0.05$). Thus both cylinder diameter and large cylinder orientation affected the critical swimming speed (Figure 3.11).

Discussion

The first purpose of these experiments was to describe the effects that turbulent eddy diameter, vorticity, and orientation had on the stability and critical swimming speed of creek chub. Failure of stability control in spills occurred in the large cylinder treatments associated with eddies with diameters at or above the 95th percentile in the d_e frequency distribution (Figure 3.6a). The small, medium, and large cylinder arrays produced 95th percentile eddies with diameters of approximately 0.2, 0.4, and 0.9 fish lengths, respectively. Spills started with a rapid head rotation followed by downstream translation. The initial displacement undoubtedly accelerates because once body rotation was initiated, the body became oriented at an increasingly large angle to the flow, which presumably rapidly increased drag on the head. This would be associated with a couple, increasing the yaw or pitch, depending upon the initial displacement as well as causing the body to be swept downstream. The primary axis of head and then body rotation during spills was consistent with the primary eddy orientation, with horizontal cylinders resulting in pitching displacements and vertical cylinders resulting in yawing displacements.

Spills occurred only in the presence of large cylinders, which created eddies with large diameters similar to fish length and with the highest vorticity. Fish that swam further from cylinders, where vorticity had decreased, rarely spilled (10% of all spills). Furthermore, spills occurred relatively rarely with 108 spills on average lasting 483 ms from initiation to recovery. This represented 0.5% of the total swimming time within the large cylinder treatments indicating that it was the relatively large infrequent eddies in the flow that resulted in body displacements. The 2-min u_{crit} was also reduced substantially in the large cylinder treatments; consistent with the spill results that showed spills were associated with eddies with a diameter similar to the fish length. Thus these observations

agree well with the idea of Pavlov et al. (2000), Cada and Odeh (2001) and Lupandin (2005) that eddies of a similar diameter to the fish length provide stability challenges to swimming fishes.

However, while large eddies of similar diameter to the fish length are considered to create the greatest stability challenges, the basis for such challenges cannot rest on diameter alone. I propose that the ratio of the momentum of the eddies relative to fish momentum, defined as the momentum ration, can explain the loss of stability. The relevant eddies are defined as causing significant perturbations in posture or location, shown to occur at and above the 95th percentile in the d_e- and ω_e distributions.

An eddy impinging on a fish is associated with a change in momentum (and hence a force) that may cause translational and/or rotational displacements of the fish. The exact displacement of the fish in an eddy-fish interaction will depend upon variables such as the location and duration of interaction, the path of the eddy and the fish during impact, and stabilizing behaviors by the fish. The maximum momentum of the eddy, Π_e, is given by;

$$\Pi_e = \tfrac{1}{4} m_e \omega_e d_e \tag{3.4}$$

where m_e is the eddy mass (Tennekes and Lumley 1972, Saffman 1992). The eddy mass is calculated as;

$$m_e = \rho_w \forall_e \tag{3.5}$$

where ρ_w is the water density and $\forall_e$ is the eddy volume. Following the "vortex string" conceptualization of eddies, that eddies are long rotating bodies of fluid (Pullin and Saffman 1998) the eddy volume can be calculated as;

$$\forall_e = a_e L_e \tag{3.6}$$

where a_e is the eddy area ($0.25\pi d_e^2$) and L_e is the eddy length. Eddies downstream from cylinder arrays span the flow cross-section hence determining the maximum overall eddy length, either from side to side (horizontal cylinder arrays) or bed to water surface (vertical cylinder arrays).

The entire length of an eddy does not interact with a fish. Rather, the length that impacts a fish will be equal to the fish width for horizontal eddies or equal to the fish depth for the vertical eddies. Fin deployment would increase the length of the eddy that

interacts with the fish. However, since the exact area of fin deployment is highly transient with time and speed only the fixed effects of body are included here. Therefore the fish width (L_w = 1.5±0.2 cm) was used for the eddy length in the horizontal cylinder treatments while the fish depth (L_d = 2.1±0.4 cm) was used for the eddy length in the vertical cylinder treatments.

Shed vortices destabilized along their length due to three-dimensional instabilities (Bernal and Roshko 1986). Williamson (1996) showed that for the Reynolds numbers found in these experiments, Re = 340 – 45,000, three-dimensional instabilities tend to break up vortex strings into lengths on the order of their diameter. It is unclear, however, whether the 1-3 eddy diameter downstream distance in the large cylinder array test section is of a sufficient length for the eddies to be broken up along their lengths. Even if eddies were broken up in this way, for the large eddies causing fish displacements, the eddy length $\cong d_e$ is >> L_w or L_d.

The minimum momentum of the fish, P_f, resisting displacement is;

$$\Pi_f = M_f V_f \tag{3.7}$$

where Π_f is the fish momentum, M_f is the fish mass and V_f is the fish velocity, which in the case of a fish holding station is equal to u_{local}.

The probability that an eddy-fish interaction will result in a displacement and a spill is expected to depend on the ratio of the eddy to the fish momentum (Π_r);

$$\Pi_r = \Pi_e / \Pi_f \tag{3.8}$$

Π_r is a conservative measure of the impact of an eddy on a swimming fish. First, the Π_e is maximized as it is calculated at the boundary of the eddy farthest from the core. Second, Π_f is a minimum momentum neglecting contributions from entrained water along the fish body as well as added mass effects that would occur with the acceleration of the fish in some new direction. The contribution of added mass will depend on the direction and magnitude of displacement accelerations, being largest for yawing and slip displacements and least for pitching and heave displacements because of the compression of the body cross-section in creek chub.

As an example, a creek chub (M_f = 16.8 g, L_f = 12.2 cm, L_w = 1.5 cm, L_d = 2.1 cm) traveling at three body-lengths per second (36.6 cm.s^{-1}) would have a momentum of Π_f = 615 g.cm.s^{-1}. If the fish impacts an eddy with a diameter equal to half the fish length

(d_e = 6.1 cm) with a vorticity of 5 s^{-1}, the calculated eddy momentum in the horizontal plane, $\Pi_{e\text{-}h}$, and in the vertical plane, $\Pi_{e\text{-}v}$, would be:

$$\Pi_{e\text{-}h} = \left(\frac{\pi\rho_w}{16}\right)\left(L_w\omega_e d_e^3\right) \tag{3.9a}$$

$$\Pi_{e\text{-}v} = \left(\frac{\pi\rho_w}{16}\right)\left(L_d\omega_e d_e^3\right) \tag{3.9b}$$

Based on the example values for eddy diameter, eddy vorticity, fish width or length, and assuming a water density of 1 $g.cm^{-3}$ the calculated eddy momentum would be $\Pi_{e\text{-}h}$ = 334 $g.cm.s^{-1}$ for a horizontal eddy and $\Pi_{e\text{-}v}$ = 468 $g.cm.s^{-1}$ for a vertical eddy, which corresponds to momentum ratios of $\Pi_{r\text{-}h}$ = 0.54 and $\Pi_{r\text{-}v}$ = 0.76, respectively.

The Π_r incorporates both the eddy diameter and the eddy vorticity. Π_e is related to the product of the eddy area and eddy diameter and using d_e as the characteristic length, Π_e is proportional to the eddy diameter^3. Fish mass is a function of fish volume, and using total length as the characteristic length, volume $\propto L_f^3$. Hence the momentum ratio is a function of the relative eddy diameter to the fish length $(d_e/L_f)^3$, which provides a physical explanation in terms of eddy momentum for the postulated relationship of the importance of the impact of eddy diameter with respect to the fish length causing instabilities. Including vorticity as a term is necessary as slowly spinning eddies are unlikely to produce the same stability challenges as rapidly spinning eddies.

The eddy momentum was substantially lower than the fish momentum for all cylinder treatments except the large cylinder arrays (Figure 3.12a). For the large cylinder treatments, eddy composition varied across streamwise and cross-stream regions (Figures 3.7 and 3.8) and consequently, Π_r also varied among these regions. The 95th percentile Π_r decreased from 1.6 in the large horizontal treatment and 2.3 in the large vertical treatment at the upstream third of the observation chamber to 0.9 in the large horizontal treatment and 1.3 in the large vertical treatment in the downstream third (Figure 3.12b). Across the flow (Figure 3.12c), Π_r was largest in the upstream LE flow region (Figure 3.12c) such that Π_r based on the 95th percentile eddy was 2.3 and decreased to 0.5 for the upstream LG flow region.

Figure 3.12: The ratio of the 95th percentile eddy to fish momentum varied across treatment and region. A horizontal dashed line has been included on the figures at the momentum ratio value of one to indicate where eddy momentum equals fish momentum. Values substantially less than one represent relatively weak eddies with respect to the fish and are unlikely to have the momentum to require control system response by the fish. The number of spills observed in each flow region has been included above each bar. The primary line or bar represents the 95th percentile eddy value while the whiskers represent the 50th and 75th percentiles. a) by cylinder diameter (cylinder diameters in parentheses within figure). Data from all flow regions are included in each bar. b) by eddy diameter downstream from the large cylinders. Data have been plotted for the large cylinder cases only since the other treatments did not have significant eddy momentum compared to the fish. c) by transverse location with respect to the large cylinders. d) by each of the nine flow regions. The momentum ratio is greatest in the upstream edge region (highlighted by the red primary boxes) and is also the location with the highest number of observed spills. Data from Figures 3.12 b) and c) have been sliced along the streamwise and transverse directions, respectively. Each data point in these graphs therefore represents all data from that streamwise or transverse location, respectively.

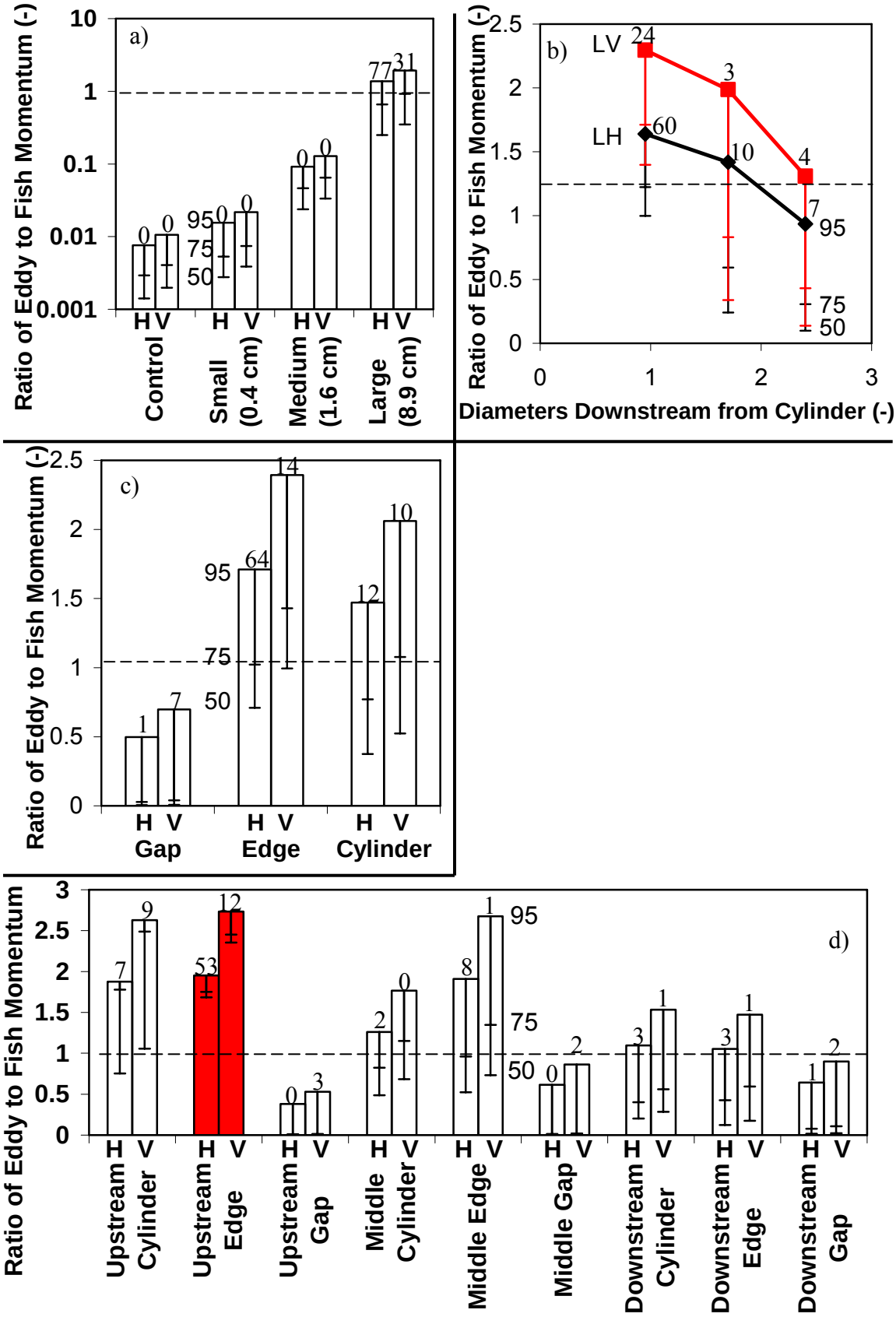
a)
Ratio of Eddy to Fish Momentum (-)
10
1
0.1
0.01
0.001
H V
Control
Small (0.4 cm)
Medium (1.6 cm)
Large (8.9 cm)
95
75
50
b)
LV
LH
Ratio of Eddy to Fish Momentum (-)
Diameters Downstream from Cylinder (-)
c)
Gap
Edge
Cylinder
d)
Upstream Cylinder
Upstream Edge
Upstream Gap
Middle Cylinder
Middle Edge
Middle Gap
Downstream Cylinder
Downstream Edge
Downstream Gap

Fish spent only 10% of their time in the LE zone of the flow. However, 60% of all spills occurred in this region. Thus the greatest probability of spills occurred in the flow region with the highest momentum ratio.

Spills occurred when the self-correcting and powered stabilizing capacity of the body and fins was exceeded (Webb and Weihs 1994, Lauder and Jayne 1996, Webb 2002 and 2004). The compressed creek chub body shape resulted in a given eddy having larger eddy length and hence greater Π_e creating yawing perturbations compared to pitching perturbations. However, there was a higher probability of a spill occurring in the upstream edge regime of the LH treatment (49%) compared for the same region of the LV treatment (20%). The effect of cylinder orientation on the entrainment rate of river chub (*Nocomis micropogon*) and smallmouth bass (*Micropterus dolomieu*) was tested by Webb (1998). While no significant effect of cylinder orientation on entrainment was found in that study it was argued that the typical fin orientations of fluvial fishes such as creek chub will make stabilization in the pitching direction more difficult than in the yawing direction. Therefore, the present observations provide additional support to earlier postulations that the stabilizing control system of fish such as creek chub would be better suited for countering yawing rather than pitching perturbations (Harris 1936 and 1938, Aleyev 1977, Fish and Shannahan 2000, Weihs 2002, Fish 2002, Webb 1998, and Webb 2006). In addition, similarities have been noted between functional morphological features and maneuverability in various directions depending upon body depth, body compression, and fin placement (Howland 1974, Webb et al. 1996, Schrank et al. 1999, Drucker and Lauder 2001).

Once spills occur, rapid recovery becomes important in order to both minimize the risk of injury and reduce energy requirements to regain location. The caudal fin, with fast-start types of body-fin motions was used to recover from both yawing and pitching displacements. These types of body motions are known to create the largest propulsive forces (Domenici and Blake 1997, Hale 1999) associated with the largest area, span, amplitude, and moment arm (Weihs 1972 and 1973, Webb et al. 1991). However, the caudal fin is oriented in the lateral plane for most fishes, and therefore can only create large torques to correct yawing displacements. In order to utilize this fin for recovery from pitching spills, the fin had to be rotated into the vertical plane. This was achieved by rolling the body 90°. Similar behavior has been reported by Webb et al. (1996) and Schrank et al. (1999) in goldfish (*Carassius auratus*), angelfish (*Pterophyllum scalare*), and silver dollars (*Metynnis hypsauchen*) maneuvering through horizontal slits and bent tubes.

Similarly, cetaceans combine rolling and rotation of the caudal peduncle to rotate the normally horizontal tail fluke into the vertical plane to execute yawing turns (Fish 2002, Rohr and Fish 2004). The addition of two rolls in recovery maneuvers by creek chub increased recovery time by 24% for vertical versus horizontal spills. The orientation of the large cylinder arrays also affected the 2-min u_{crit} with lower values for the horizontal arrays than the vertical arrays. Presumably there were energy costs associated with recovery maneuvers that contributed to lower critical swimming speeds.

The medium and small cylinder arrays resulted in a 5% reduction in the 2-min u_{crit} compared with the control. Tests of fish swimming in the LV and LH cylinder arrays resulted in a 10% and 22% reduction in the critical swimming speed, respectively, compared with the control. These values were both significantly different from the control and significantly different from each other (ANOVA, $p<0.05$). While the pattern of spills provides most insight into the limits of stability control in the presence of large eddies, the reduction in critical swimming speed when spills became more common attests to the general deleterious impacts of large eddies for overall swimming performance. The greater reduction in the 2-min u_{crit} for the large horizontal cylinder array further supports the observations on spill, showing that pitching perturbations in the flow present larger challenges than yawing perturbations.

Conclusions

A series of increasing velocity tests was conducted to determine the influence of turbulent eddies on the critical swimming speed of creek chub. Eddy vorticity, eddy diameter, and eddy orientation (spinning about horizontal or vertical axes of rotation) were varied using arrays of cylinders 0.4, 1.6, and 8.9 cm in diameter. As eddy momentum approached the fish momentum the occurrence of spills (defined as rapid head rotations followed by downstream translation) increased. Furthermore the greatest reduction in the two minute critical swimming speed (2-min u_{crit}) of fish occurred in the large cylinder flow treatments where the turbulent eddy momentum was greatest. Because eddy momentum is a function of the eddy mass and eddy vorticity, these results confirm the importance of turbulence scale (based on eddy diameter with respect to the fish length) and vorticity proposed by Pavlov et al. (2000) Cada and Odeh (2001), Lupandin (2005), and Liao (2007), among others.

The 2-min u_{crit} was affected by the orientation of cylinder arrays for the large cylinder treatment, being reduced 10 ± 4% compared to the control treatment with the vertical array and by 22 ± 3% for the horizontal array. This orientation effect for the large cylinders was investigated through video analysis of the fish spills. The probability of a spill occurring in the upstream edge regime of the LH treatment was 49% compared with a 20% probability for the same region of the LV treatment. Additionally, recovery from a spill took 24% more time for fish was in the horizontal turbulent eddy field compared to the vertical turbulent eddy field. The increased recovery time was due to two additional rolls which rotated the caudal fin into the plane of the displacement.

References

Akilli, H., Akar, A., and Karakus, C . (2004). Flow characteristics of circular cylinders arranged side-by-side in shallow water. *Flow Measurement and Instrum*. **15**, 187-197.

Aleyev. Y. G. (1977). *Nekton*. Junk, The Haque.

Antonia, R. A., Zhou, T., and Zhu, Y. (1998). Three-component vorticity measurements in a turbulent grid flow. *J of Fluid Mechanics*. **374**, 29-57.

Batchelor, G. K. and Townsend, A. A. (1947). Decay of vorticity in isotropic turbulence. *Proc. R. Soc. Lond. A* **190**, 534-550.

Bernal, L. P. and Roshko A. (1986). Streamwise vortex structure in plane mixing layers. *Journal of Fluid Mechanics*. **170**, 499.

Biggs, B. J. F., Nikora, V. I., and Snelder, T. H. (2005). Linking Scales of flow variability to lotic ecosystem structure and function. *River Res. and Applications*, **21**, 283-298.

Blackburn, H. M. (1994). Effect of blockage on spanwise correlation in a circular cylinder wake. *Exp. Fluids,* **13**, 134-136.

Brett, J. R. (1963). Energy required for swimming by young sockeye salmon with a comparison of drag force on a dead fish. *Transactions of the R. Soc. of Can.* **1**, 441.

Cada, G. F. and Odeh, M. (2001). Turbulence at hydroelectric power plants and its potential effects on fish. *Report to Bonneville Power Administration*, Contract No. 2000AI26531, Project No. 200005700: 1-37.

Cimbala, J. M., Nagib, H. M., and Roshko, A. (1988). Large structure in the far wakes of two-dimensional large bodies *J of Fluid Mech*anics **190**, 265-298.

Cotel, A. J., Webb, P. W., and Tritico, H. M. (2006). Do Brown Trout Choose Locations With Reduced Turbulence? *Transactions of the Am. Fisheries Soc.* **135**, 610-619.

Domenici, P. and Blake, R. W. (1997). The kinematics and performance of fish fast-start swimming. *J. Exp. Biol.* **200**, 1165-1178.

Drucker, E. G. and Lauder, G. V. (1999). Locomotor forces on a swimming fish: three-dimensional vortex wake dynamics quantified using digital particle image velocimetry. *J of Exp. Bio.* **202**, 2393-2412.

Drucker, E. G. and Lauder, G. V. (2001). Wake dynamics and fluid forces of turning maneuvers in sunfish. *J of Exp. Bio.* **204**, 431-442.

Enders, E. C., Boisclair, D., and Roy, A. G. (2003). The Effect of Turbulence on the Cost of Swimming for Juvenile Atlantic Salmon. *Canadian Journal of Fisheries and Aquatic Science*, **60**, 1149-1160.

Farlinger, S. and Beamish, F. W. H. (1977). Effects of time and velocity increments in the critical swimming speeds of largemouth bass (*Micropterus salmoides*). *Transactions of the American Fisheries Society* **106**, 436-439.

Fish, F. E. and L. D. Shannahan. (2000). The role of the pectoral fins in body trim of sharks. *J. Fish Biol.* **56**, 1062-1073.

Fish, F. E. (2002). Balancing requirements for stability and maneuverability in cetaceans. *Integrative and Comparative Biology*. **42**, 85-93.

General Pixels. (2000). *PixelFlow 2.1: Installation and User's Guide.*

Gharib, M. and Dabiri, D. (2000). An overview of digital particle image velocimetry in *Flow Visualization: Techniques and Examples* (ed Smits A and Lim T T) London: Imperial College Press.

Hale, M. E. (1999). Effects of size and ontogeny on the fast-start performance of several salmonid species. *J. Exp. Biol.* **202**, 1465-1479.

Harris, J. E. (1936). The role of fins in the equilibrium of swimming fish. I. Wind-tunnel tests on a model of *Mustelus canis* (Mitchell). *J. exp. Biol.* **13**, 476-493.

Harris, J. E. (1938). The role of the fins in the equilibrium of swimming fish II. The role of the pelvic fins. *J. exp. Biol.* **15**, 32-47.

Howland, H. C. (1974). Optimal strategies for predator avoidance: the relative importance of speed and manoeuverability. *J. Theor. Biol.* **47**, 333-350.

Huang, H., Dabiri, D., and Gharib, M. (1997). On errors of digital particle image velocimetry *Meas. Sci. Technol.* **8**, 1427-40.

Huang, Z. Olson, J. A., Kerekes, R. J., and Green, S. I. (2006). Numerical simulation of the flow around rows of cylinders. *Computers and Fluids*. **35**, 485-491.

Karman, T. von (1937). The fundamentals of the statistical theory of turbulence. *J. Aero. Sci.* **4**, 131-138.

Landry, F., Miller, T. J., and Leggett, W. C. (1995). The effects of small-scale turbulence on the ingestion rate of fathead minnow larvae. *Canadian Journal of Fisheries and Aquatic Sciences*, **52**, 1714-1719.

Lauder, G. V., and Jayne, B. C. (1996). Pectoral fin locomotion in fishes: Testing drag-based models using three-dimensional kinematics. *American Zoologist* **36,** 567-581.

Liao, J. C. (2007). A review of fish swimming mechanics and behavior in altered flows. *Philosophical Transactions of the Royal Society B.* **362**, 1973-1993.

Liao, J. C., Beal, D. N., Lauder, G. V. and Triantafyllou, M. S. (2003). The Karman gait: novel body kinematics of rainbow trout swimming in a vortex street. *Journal of Experimental Biology* **206**, 1059-1073.

Lupandin, A. I. (2005). Effect of Flow Turbulence on Swimming Speed of Fish. *Biology Bulletin*, **32,** 558-565.

Mackenzie, B. R. and Kiorboe, T. (1995). Encounter Rates and Swimming Behavior of Pause-Travel and Cruise Larval Fish Predators in Calm and Turbulent Laboratory Environments. *Limnology and Oceanography*, **40**, 1278-1289.

Mackenzie, B. R. and Kiorboe T. (2000). Larval Fish Feeding and Turbulence: A Case For the Downside. *Limnology and Oceanography*, **45**, 1-10.

Mackenzie, B. R., Miller, T. J., Cyr, S., and Leggett, W. C. (1994). Evidence for a Dome Shaped Relationship Between Turbulence and Larval Fish Ingestion Rates. *Limnology and Oceanography*, **39**, 1790-1799.

Maxwell, S. E. and Delaney, H. D. (2004). *Designing experiments and analyzing data*. 2nd Edition. Lawrence Erlbaum Associates, Inc. Mahwah NJ.

Montgomery, D. R., Buffington, J. M., Peterson, N. P., Schuett-Hames, D., and Quin, T. P. (1996). Stream-bed Scour, Egg Burial Depths, and the Influence of Salmonid Spawning on Bed Surface Mobility. *Canadian Journal of Fisheries and Aquatic Sciences*, **53**,1061-1070.

Moretti, P. M. (1993). Flow-induced vibrations in arrays of cylinders. *Annual Review of Fluid Mechanics*. **25**, 99-114.

Nikora, V. I., Aberlee, J., Biggs, B. J. F., Jowett, I. G., and Sykes, J. R. E. (2003). Effects of Fish Size, Time to Fatigue, and Turbulence on Swimming Performance: A Case Study of *Galaxias maculatus*. *Journal of Fish Biology*, **63**, 1365-1382.

Nikora, V. I., and Goring, D. G. (1998). Effects of Bed Mobility on Turbulence Structure. *NIWA Internal Report No 48.*

Okamoto, T. and Takeuchi, M. (1975). Effect of side walls of wind tunnel on flow around two-dimensional circular cylinder and its wake. *Bull. JSME,* **18**, 1011-1017.

Pavlov, D. S., Lupandin, A. I., and Skorobogatov, M. A. (2000). The Effects of Flow Turbulence on the Behaviour and Distribution of Fish. *Journal of Ichthyology*, **40**, S232-261.

Pullin, D. I. and Saffman, P. G. (1998). Vortex dynamics in turbulence. *Annual Review of Fluid Mechanics* **30**, 31-51.

Rohr, J. J. and Fish, F. E. (2004). Strouhal numbers and optimization of swimming by odontocete cetaceans. *The Journal of Experimental Biology* **207**, 1633-1642.

Roshko A. (1976). Structure of turbulent shear flows: A new look. *AIAA Journal*. **14(10)**, 1349-1357.

Saffman, P. G. (1992). *Vortex Dynamics*. Cambridge University Press

Schlichting, H. (1979). *Boundary-Layer Theory*. McGraw-Hill Publishing Co., New York, NY.

Schrank, A. J., Webb, P. W. and Mayberry, S. (1999). How do body and paired-fin positions affect the ability of three teleost fishes to maneuver around bends? *Can. J. Zool*. **77**, 203–210.

Smith, D. L., Brannon, E. L., and Odeh, M. (2005). Response of Juvenile Rainbow Trout to Turbulence Produced by Prismatoidal Shapes. *Transactions of the American Fisheries Society*, **134**, 741-753.

Standen, E. M., Hinch, S. G., Healey, M. C., and Farrell, A. P. (2002). Energetic Costs of Migration through the Fraser River Canon, British Columbia, in Adult Pink and Sockeye Salmon as Assessed by EMG Telemetry. *Canadian Journal of Fisheries and Aquatic Sciences*, **59**, 1809-1818.

Standen, E. M,, Hinch, S. G., and Rand, P. S. (2004). Influence of River Speed on Path Selection By Migrating Adult Sockeye Salmon. *Canadian Journal of Fisheries and Aquatic Science*, **61**, 905-912.

Swanson, C., Paciencia, S. Y, and Cech, J. J. (1998). Swimming performance of delta smelt: Maximum performance and behavioral kinematic limitations on swimming at submaximal velocities. *Journal of Experimental Biology*. **201**, 333-345.

Taylor, G. I. (1938). Production and dissipation of vorticity in a turbulent fluid. *Proc. R. Soc. Lond. A* **164**, 15-23.

Tennekes, H. and Lumley, J. L. (1972). *A First Course in Turbulence*. The MIT Press, Cambridge, MA.

Tritico, H. M. and Hotchkiss, R. H. (2005). Unobstructed and Obstructed Turbulent Flow in Gravel Bed Rivers. *Journal of Hydraulic Engineering*. **131**, 635-645.

Tritico, H. M., Cotel, A. J., and Clarke, J. N. (2007). Development, testing and demonstration of a portable submersible miniature particle imaging velocimetry device. *Measurement Science and Technology*. **18**, 2555-2562.

Webb, P. W. (1998). Entrainment by river chub Nocomis micropogon and smallmouth bass Micropterus dolomieu on cylinders. *J. Exp. Biol*. **201**, 2403–2412.

Webb, P. W. (2002). Control of Posture, Depth, and Swimming Trajectories of Fishes. *Integrative and Comparative Biology*, **42**, 94-101.

Webb, P. W. (2004). Maneuverability – General Issues. *IEEE Journal of Oceanic Engineering* **29,** 547-555.

Webb, P. W. (2006). Stability and maneuverability. In *Fish Physiology* (eds R. E. Shadwick and G.V. Lauder), pp. 281-332. Elsevier Press, San Diego.

Webb, P. W., Sims, D. and Schultz, W. W. (1991). The effect of an air/water interface on the faststart performance of rainbow trout (*Oncorhynchus mykiss*). *J. exp. Biol*. **155**, 219-226.

Webb P. W., Kostecki P. T., and Stevens E. D. (1984). The effect of size and swimming speed on locomotor kinematics of rainbow trout. *Journal of Experimental Biology* **109**, 77-95.

Webb, P. W., LaLiberte, G. D., and Schrank, A. J. (1996). Does body and fin form affect the maneuverability of fish traversing vertical and horizontal slits? *Environmental Biology of Fishes*. **46**, 7-14.

Webb, P. W. and Weihs, D. (1994). Hydrostatic stability of fish with swimbladders: Not all fish are unstable. *Can. J. Zool.* **72**, 1149–1154.

Weihs, D. (1972). A hydrodynamical analysis of fish turning manoeuvres. *Proc. R. Soc. Land. B.* **182**, 59-72.

Weihs, D. (1973). The mechanism of rapid starting of slender fish. *Biorheology* **10**, 343-350.

Weihs, D. (2002). Stability versus maneuverability in aquatic locomotion. *Integrative and Comparative Biology*. **42**, 127-134.

Wilga, C. D. and Lauder, G.V. (1999). Locomotion in sturgeon: function of the pectoral fins. *Journal of Experimental Biology* **202**, 2413-2432.

Wilga, C. D. and Lauder, G.V. (2002). Function of the heterocercal tail in sharks: quantitative wake dynamics during steady horizontal swimming and vertical maneuvering. *Journal of Experimental Biology* **205**, 2365-2374.

Williamson, C. H. K. (1996). Vortex dynamics in the cylinder wake. *Annual Review of Fluid Mechanics*. **28**, 477-539.

Zdravkovich, M. M. (2003). *Flow around Circular Cylinders Vol 2: Applications*. Oxford University Press. Oxford UK.

Zdravkovich, M. M. and Stonebanks, K. L. (1990). Intrinsically nonuniform and metastable flow in and behind tube arrays. *Journal of Fluids and Structures.* **4**, 305-319.

Zhang, H. J. and Zhou, Y. (2001). Effect of unequal cylinder spacing on vortex streets behind three side-by-side cylinders. *Physics of Fluids*. **13,** 3675-3686.

Chapter IV

Relationships between Body-Caudal Fin Swimming Kinematics and the Eddy Composition of Turbulent Flow

Introduction

Turbulence is ubiquitous in natural aquatic environments and has been postulated to be a substantial source of error in current bio-energetic models (Mackenzie et al. 1994, Landry et al. 1995, Cada and Odeh 2001). Most models of fish-like swimming are based on observations from fish swimming in low turbulence environments (Webb et al. 1984, discussed further in Standen et al. 2002 and Enders et al. 2005). Recent work by Enders et al. 2005 has shown that metabolic costs rise with increasing velocity fluctuations, but the physical mechanism for increased swimming costs in turbulent flow has not been proposed or confirmed. Recent results by Nikora et al. (2003), Liao et al. 2003, and Lupandin (2005) among others have indicated that the diameter and vorticity of turbulent eddies will play an important role in determining the kinematics of swimming fish. This paper reports the results of video-analysis of fish swimming kinematics during increasing velocity tests in order to understand the effects of turbulent eddy diameter (d_e) and vorticity (ω_e) on the kinematics of body-caudal fin propulsion.

Materials and Methods

Changes in body/caudal-fin kinematics were measured at several flow speeds and levels of turbulence induced by upstream cylinder arrays of differing diameters and orientations. The turbulent flow regimes were measured using particle image velocimetry (PIV) and were characterized according to d_e, ω_e, and the local velocity (u_{local}). The body and caudal fin swimming kinematics of tail beat frequency (F), amplitude (A), wavelength (λ), tail span (B), and tail angle of attack (θ) were measured (Lighthill 1971).

Creek chub were selected as a model fusiform-shaped soft-ray-fin species common to North America (Keast 1985, Webb 2004).

Apparatus

Observations of fish behavior were made during an increasing velocity test in a water tunnel with a test section 250 cm in length and 60 cm wide (Chapter III). The water depth was held at 55 cm for all tests. A 30-cm observation section was delineated within this test section by a downstream grid (12.5 mm egg-crate) and upstream by either a similar grid or by one of three cylinder arrays spanning the flume cross-section oriented vertically or horizontally. Arrays were comprised of cylinders with diameters 0.4 cm, 1.6 cm, and 8.9 cm, with gaps equal to cylinder diameter in each array. Thus there were seven treatments: control, small horizontal (SH), small vertical (SV), medium horizontal (MH), medium vertical (MV), large horizontal (LH), and large vertical (LV) arrays (Figure 3.2). A 1.3 cm mesh of 0.04 cm diameter plastic thread was attached to the upstream side of the cylinders to prevent fish escaping. One wall of the observation chamber was papered with 2 cm x 2 cm black and white checkered paper to foster fish station holding. All edges of the test sections were electrified at 5 V DC to encourage swimming.

Flow analysis

Data on instantaneous flow patterns were collected for velocities averaged over the observation cross-section, $\bar{u}$, of 8.5, 17.1, 27.7, 38.7, and 50.2 $cm.s^{-1}$ using two-dimensional PIV. The water was seeded with 1 μm diameter neutrally buoyant titanium dioxide particles, at a concentration of 1.2 ppm. Flow was illuminated using a 120 mJ NdYAG dual-head 532-nm pulsed laser (NewWave Gemini) with pulse duration of 100 μs, and creating a laser sheet 0.75 mm thick spanning the observation cross section either horizontally (for vertical cylinder arrays) or vertically (for horizontal cylinder arrays). Fifty image pairs were recorded at pulse separations of 8, 5, 3, 2, and 1 ms, at $\bar{u}$ of 8.5, 17.1, 27.7, 38.7, and 50.2 $cm.s^{-1}$ respectively.

Downstream from the horizontal cylinder arrays the vertical laser sheet was positioned along the flume centerline. The interrogation window was selected within the

bottom 50% of the flume in order to avoid stray air bubbles in the upper water column (Chapter III). Downstream from the vertical cylinder arrays, the horizontal laser sheet and interrogation window were centered on the flume centerline, halfway between the bed and the free surface.

Flow was reconstructed from pairs of images of the particles in the flow which were recorded on a 1 mega pixel 10-bit 30 fps UniqVision black and white CCD camera driven by PixelFlow software (General Pixels, Inc.; Huang et al. 1997, Gharib and Dabiri 2000, General Pixels 2000, Tritico et al. 2007). Fifty pairs of images were collected at 15 Hz at each $\bar{u}$, averaging 12 eddy shedding cycles from the cylinders. Due to surface reflections and laser intensity requirements, a smaller 26 cm streamwise by 30 cm transverse interrogation window was analyzed for each treatment beginning 2 cm upstream from the downstream grid and 2 cm downstream from the upstream cylinder array or grid.

Eddies were identified following the method described by Drucker and Lauder (1999). Cross-correlation techniques were used to convert consecutive images of particles into velocity vector fields. The vorticity (ω, twice the angular velocity) was calculated from the velocity vector field. Local minimum/maximum vorticity was taken as an eddy center. The circulation about each eddy center was calculated in concentric circles until a maximum circulation (Γ_e – angular momentum per unit mass) was reached

$$\Gamma_e=\omega_e*a_e \tag{4.1}$$

where a_e is the area circumscribed by the circle ($0.25\pi d_e^2$) and ω_e is the spatially averaged vorticity within the circle. The radius with maximum circulation was taken to be the eddy radius (Drucker and Lauder 1999 and Wilga and Lauder 1999); each eddy's location, diameter, and average vorticity were recorded.

Fish were observed swimming throughout the water column in the control, small- and medium-diameter cylinder array treatments without choosing locations relative to the cylinders. In contrast, fish regularly chose various swimming locations relative to the large cylinders. These locations were classified into three groups defined as follows: a) large cylinder (LC) area directly downstream from each large cylinder (cylinder centerline ± 2.3 cm), b) large edge (LE) area directly downstream from each cylinder edge (cylinder edge ± 2.3 cm), and c) large gap (LG) area directly downstream from each

gap between the cylinders (gap centerline ± 2.3 cm). Therefore, results have been described for flow structure through the water column for the control, small-diameter and medium-diameter cylinder arrays, and for the cylinder, edge and gap regions for large cylinders (Figure 4.1). The flow region had been further trisected into upstream, middle, and downstream regions in Chapter III. In Chapter III it was shown that while the 95th percentile eddy diameter did not change with streamwise location, the 95th percentile eddy vorticity did decay with streamwise distance. Further, it was shown that fish tended to swim in the downstream region of the tank (41, 37, 22% of time in the downstream, middle, and upstream flow regions, respectively) and tended to fail in the upstream region of the tank (19, 10, 71% of failures in the downstream, middle, and upstream flow regions, respectively). Conversely, the streamwise location in the tank was not a significant factor in predicting any of the BCF metrics reported here (one-way ANCOVA generalized linear model with streamwise location, gap/edge/cylinder, speed, and treatment as covariates along with interaction terms, $p>0.05$ for streamwise location and all interaction terms, Maxwell and Delaney 2004). This is likely due to the very low frequency of fish moving to the upstream region of the large cylinder treatments and holding station for >5 seconds. The streamwise data have therefore been grouped, and only the LG, LE, and LC flow regions distinction (same ANCOVA as previously reported with tail beat amplitude and frequency being dependent upon transverse location in the flow, $p<0.05$) are reported.

Fish

Creek chub were obtained from Fleming Creek, Michigan, USA at a water temperature of 21.1 °C. Fish were acclimated in the lab to room temperature (20.5 ±0.4 °C) for one week prior to the experiment and were fed to satiation daily (Chapter III). The experimental temperature was the same as the acclimation temperature. Seven creek chub with an average total length of 12.2±0.9 cm (mean±2SE) and mass of 16.8±3.5 grams were used in experiments. Each fish was swum with every treatment. The order of the treatment experienced was selected at random and fish were given a minimum of 3.5 days between each test.

A single fish was placed in the observation section and acclimated to $\bar{u}$ of 8.5 cm/s. After 11 hours acclimation, ū was increased by 3.5 cm.s^{-1} increments at 2 minute

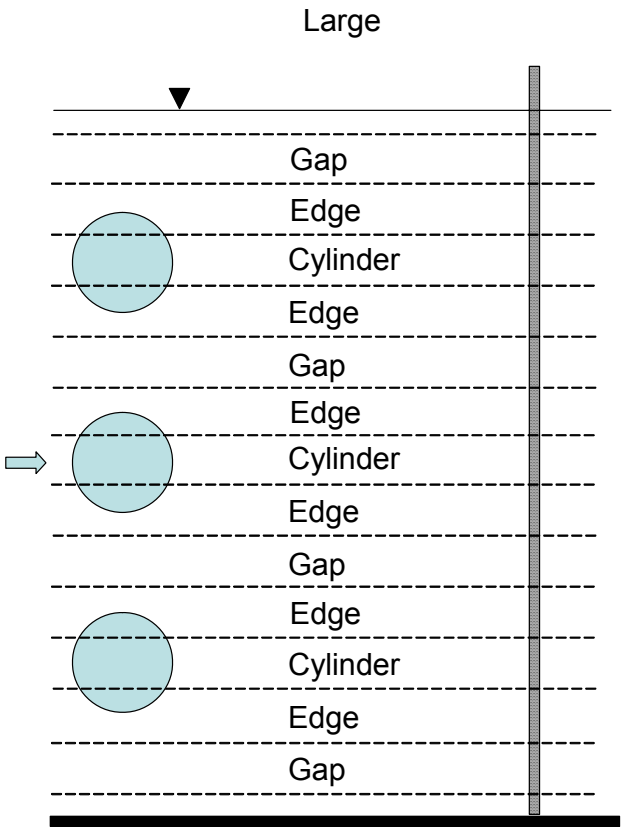

Figure 4.1: Large Cylinder Test Section Regions. The test sections downstream from the large cylinder arrays were subdivided into regions directly downstream from the cylinder (Cylinder region), regions directly downstream from a gap (Gap region), and regions directly downstream from a cylinder edge (Edge region). Data in regions next to the wall and free surface are not reported

intervals until the fish became entrained on the downstream grid for 3 seconds. The 2-min u_{crit} results are reported in Chapter III; in this paper we discuss the body/caudal fin kinematics at each of the $\bar{u}$ leading up to the critical swimming speed.

Fish were continuously videotaped at 30 frames per second simultaneously from the side and from below using two digital video cameras (Panasonic Model No. PV-DV601D). Fish moved about the test section, holding position for variable periods at various locations. Swimming kinematics were measured from video records when fish remained in a given location with no postural changes for >5 s during which fish velocities in the environmental frame of reference were <0.02 body-lengths.s^{-1} (Wilga and Lauder 2002). Station holding observations in which the fish used the pectoral fin for

propulsive purposes were excluded from analysis in order to focus on the effects of turbulent eddies on continuous body-caudal fin propulsion.

Various theoretical models describing the propulsive momentum transfers required for fish-like swimming have been proposed (Lighthill 1960 and 1971, Wu 1971, Schultz et al. 1991, Pedley and Hill 1999). The relevant parameters found in most reactive and resistance based models include: the tail beat frequency, the tail beat amplitude, the tail trailing edge depth, the body wavelength, and the cosine of the tail angle of attack.

Tail beat frequency was determined from the time required for the tail to move from one lateral maximum across the midline and return (Bainbridge 1958, Webb 1971, Webb et al. 1984, Liao et al. 2003). Tail beat amplitude was determined as the transverse distance the caudal fin moved from one lateral maximum to the opposite maximum (Bainbridge 1958). Body wavelength was determined by first fitting a cubic spline to the fish body outline (Muller et al. 1997). This method was checked against hand drawn midlines and resulted in a reasonable match along the entire body length. The fish midlines were then used to calculate half wavelengths as described by Webb et al. (1984) by recording the node distance between locations where the body midline crossed the global fish swimming midline (i.e. trajectory). The trailing edge angle of attack with respect to the mean body centerline was calculated during the wavelength analysis by determining the angle that the most posterior 5% of the fish body made with the centerline for each frame for twenty consecutive frames (Lighthill 1971). The trailing edge span was measured from the dorsal to the ventral tips of the caudal fin.

Results

The purpose of this analysis was to determine whether increasing levels of turbulence affected propulsive kinematics in swimming fish. While the 95th percentile eddy diameter and vorticity were each varied by 500% across the seven cylinder treatments (the 95th percentile diameter ranged from 1/6 to 1 fish body length) and the cylinder based Reynolds number ($Re_{cyl} = \frac{\bar{u}d_c}{\upsilon}$ where d_c is the cylinder diameter and ν is the kinematic viscosity of water) varied from 340 to 45,000, the only observed changes in

kinematics were decreased tail beat frequency and increased tail beat amplitude for fish swimming downstream from the large cylinders (Figure 4.2). Body wavelength (11.1±0.3 cm), tail span (2.7±0.0 cm), and tail angle of attack (20±1°) were not observed to vary across any of the treatments or with u_{local} (ANCOVA, $p>0.05$). The tail beat amplitude and frequency did not change across the control, small, or medium cylinder treatments while the tail beat amplitude also did not change with u_{local} (ANCOVA, $p<0.05$).

Similarly, none of the kinematic swimming variables measured during this study, including tail beat frequency, amplitude, wavelength, tail depth, or tail angle of attack varied significantly (ANCOVA of treatment, $\bar{u}$, location, $p>0.05$ for all treatment and interaction terms when only the control, small, and medium cylinder treatments were included) from the control treatment for fish swimming in the small and medium cylinder treatments (Figure 4.3). The lack of change in swimming kinematics for the small and medium cylinder treatments was not wholly unexpected given the small eddy momentum compared to the fish momentum. Chapter III showed that the momentum of the 95th percentile eddies in these two treatments was less than 1/10th the momentum of the fish and did not affect the spill rates (rapid head rotation about the center of mass followed by downstream translation) or the critical swimming speed. Further, Chapter III found that location preference within the test section did not change across the control, small, or medium cylinder treatments.

The momentum of the eddy was calculated as;

$$\Pi_e = \tfrac{1}{4} m_e \omega_e d_e \tag{4.2}$$

where m_e is the eddy mass. See equations 3.5 and 3.6 for the equations to calculate eddy mass. The momentum of the fish was calculated as;

$$\Pi_f = M_f V_f \tag{4.3}$$

where M_f is the fish mass and V_f is the fish velocity (Figure 3.12a). The momentum ratio is;

$$\Pi_r = \Pi_e / \Pi_f \tag{4.4}$$

The momentum ratio is a function of eddy vorticity to the first power and the relative magnitude of the eddy diameter to the fish length to the 3rd power $(d_e/L_f)^3$ (Chapter III).

Figure 4.2: Variation of local velocity, vorticity, and eddy diameter with cross-sectionally averaged velocity and flow region. The left-hand panels show relationships for a) u_{local}, b) the 95th percentile vorticity, the slope of the vorticity with respect to u_{local} (divided by 4π) is the fish-based persistence parameter, and c) the 95th percentile eddy diameter for all cylinder arrays. The u_{local} and eddy parameters differed for the large cylinders (right-hand panels) depending on location across the flow defined in Figure 4.1.

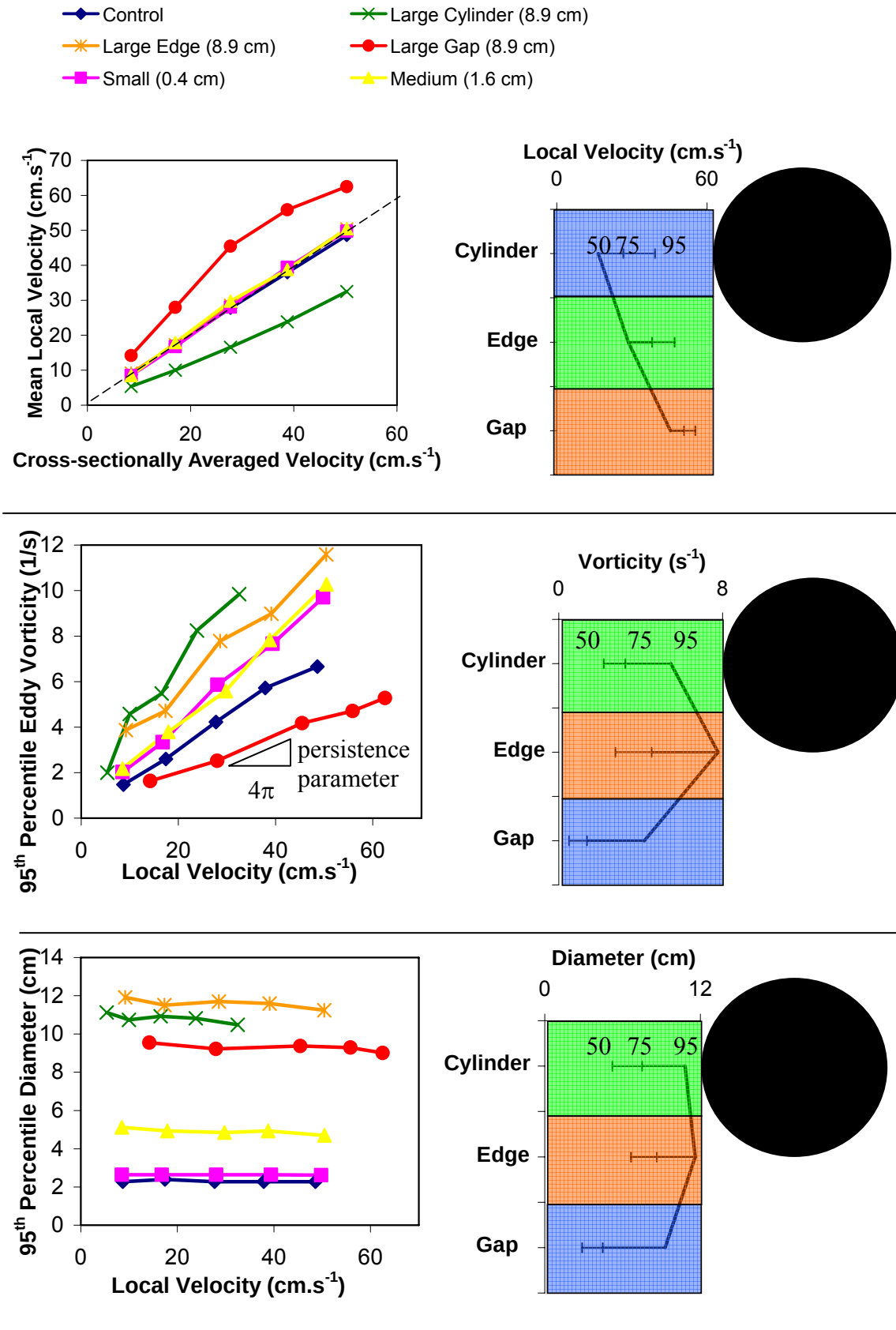
Control
Large Cylinder (8.9 cm)
Large Edge (8.9 cm)
Large Gap (8.9 cm)
Small (0.4 cm)
Medium (1.6 cm)
Mean Local Velocity (cm.s-1)
Cross-sectionally Averaged Velocity (cm.s-1)
Local Velocity (cm.s-1)
Cylinder
Edge
Gap
50 75 95
a)
95th Percentile Eddy Vorticity (1/s)
Local Velocity (cm.s-1)
persistence parameter
4π
Vorticity (s-1)
b)
95th Percentile Diameter (cm)
Diameter (cm)
c)

Figure 4.3: Tail beat frequency and amplitude across speed and turbulent regime. a) Tail beat amplitude did not vary with speed but was greater than the C, SH, SV, MH, and MV treatments (A = 2.9±0.1 cm) in the LC (A = 6.5±1.2 cm) and LE (A = 4.4±0.8) regions (ANCOVA of treatment and $\bar{u}$ such that $p>0.05$ for speed and interaction term while $p<0.05$ for treatments as displayed) b) The tail beat frequency in the C, SH, SV, MH, and MV treatments was $F=0.05\pm0.01u_{local} + 1.2\pm0.1\ s^{-1}$, $r^2=1.0$. The tail beat frequency in the LG ($F=0.03\pm0.01u_{local} + 1.3\pm0.3\ s^{-1}$, $r^2=0.93$), LC ($F=0.07\pm0.01u_{local}\ s^{-1}$, $r^2=0.96$), and LE ($F=0.06\pm0.01u_{local}\ s^{-1}$, $r^2=0.89$) was less than the tail beat frequency in the other treatments (ANCOVA, $p<0.05$). The two dashed lines represent the range of eddy shedding frequencies previously reported by various investigators and summarized by Sumner et al. (1999) for flow downstream from a three cylinder array (large cylinder array for this study). The slope of the frequency-amplitude product (c) with speed is the fish based Strouhal number which is a measure of the total work required to swim at a given speed. The Strouhal number is significantly greater (ANOVA, $p<0.05$) for fish swimming in the LC region (0.39 ± 0.05, $r^2 = 0.98$) than for fish swimming in the control, small, medium, and large edge regimes (0.27 ± 0.02, $r^2 = 0.98$). Conversely, the fish based Strouhal number was significantly less for fish swimming in the LG regime (0.23 ± 0.02, $r^2 = 0.96$) where fluid was highly rectilinear (t-test, $p<0.05$). The lines represent the linear regression of the mean while the data points represent the mean and the error bars represent ± 2 standard errors of the mean.

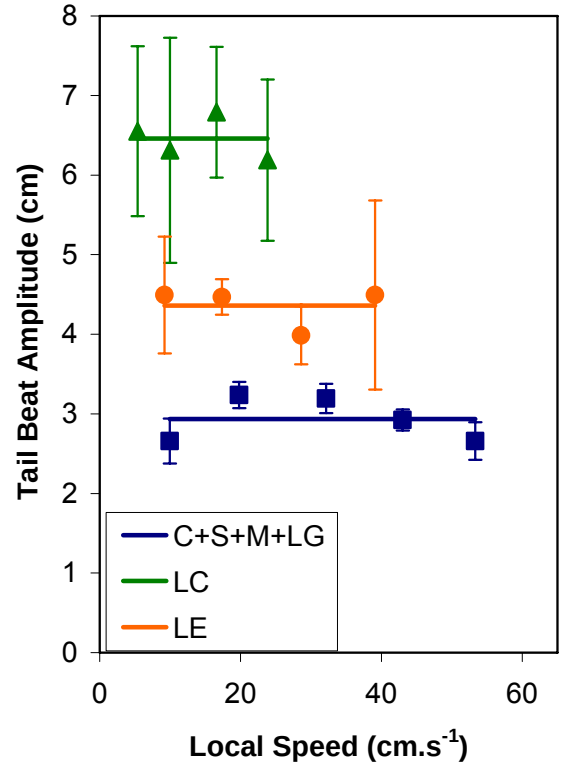
Tail Beat Amplitude (cm)
Local Speed (cm.s-1)
C+S+M+LG
LC
LE

a)

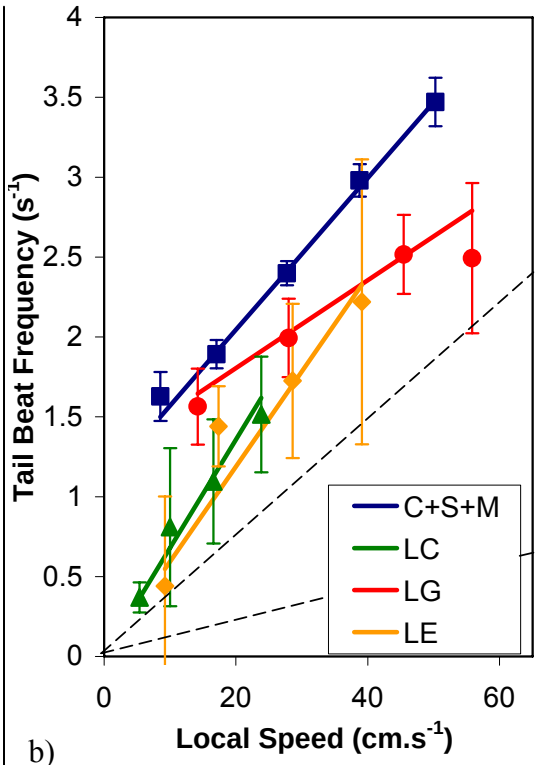
Tail Beat Frequency (s-1)
Local Speed (cm.s-1)
C+S+M
LC
LG
LE

b)

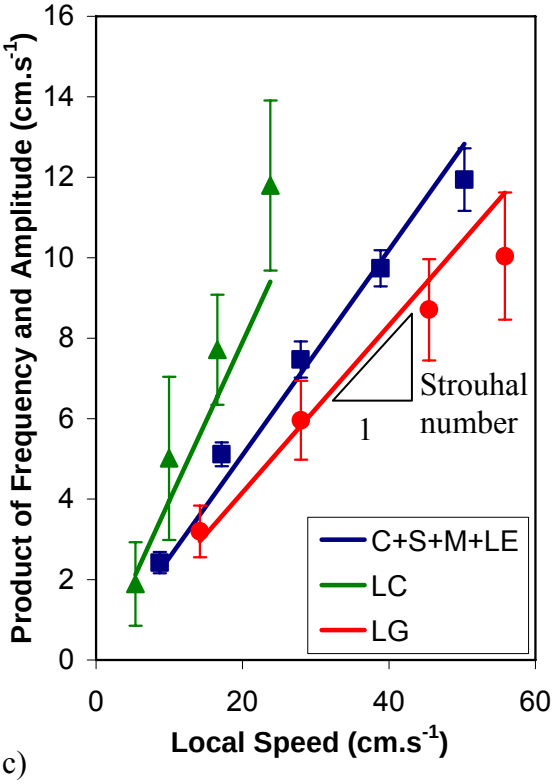
Product of Frequency and Amplitude (cm.s-1)
Local Speed (cm.s-1)
Strouhal number
1
C+S+M+LE
LC
LG

c)

Large cylinder treatments: Flow description and kinematics

Eddy diameter, vorticity, and velocity were similar between horizontal and vertical configurations (differences of 0.0%, 1.7%, 0.4%, respectively) and no significant difference ($p<0.05$) in body/caudal fin kinematics were observed between orientations. The horizontal and vertical data have therefore been combined.

The 95th percentile eddies downstream from the large cylinders had momentum on the same order of magnitude as that of the fish (Figure 3.12a). Under these conditions tail beat frequencies were reduced and tail beat amplitudes were increased compared to those found in the control. The magnitude of change in tail beat frequency and amplitude depended on fish location with respect to the cylinders.

The tail beat amplitude was larger than the control, small, and medium cylinder treatments in the LC and LE flow regimes, but the tail beat amplitude was not significantly different (ANOVA, $p<0.05$) in the LG flow regime (Figure 4.3a). The LG flow regime was composed of relatively small eddies (95th percentile = 9.2 cm) compared to the LC (95th percentile = 10.8 cm) and the LE (95th percentile = 11.6 cm) flow regimes (Figure 4.3c). While eddy diameter correlated with changes in tail beat amplitude, the tail beat amplitudes in the LG, LC, and LE regions were 3.0±0.2 cm, 6.5±1.2 cm, and 4.4±0.8 cm, respectively; each was significantly smaller than the 95th percentile eddy diameter (multiple t-tests comparing tail beat amplitude to 95th percentile eddy diameter, $p<0.05$). Tail beat amplitude for each region did not change with $\bar{u}$ (ANOVA, $p<0.05$).

The tail beat frequencies were less than the control, small, and medium cylinder treatments in all large cylinder array flow regimes (ANOVA $p<0.05$). The tail beat frequency increased with u_{local} at the greatest rate in the LC region and increased at the slowest rate in the LG region (Figure 4.3b), matching the trend in 95th percentile eddy vorticity (Figure 4.3b).

As the tail beat frequency and tail beat amplitude were the only parameters adjusted by creek chub, their product was used as an indicator of changes in swimming kinematics across various turbulent conditions (Lighthill 1971, Figure 4.3c). The ratio (or slope) of this product with the u_{local} is the fish based Strouhal number, St_f (Triantafyllou et al. 1991);

$$St_f = \frac{FA}{u_{local}} \quad (4.5)$$

The fish based Strouhal number "defines the maximum aerodynamic angle of attack and the time scales associated with growth and shedding of vortices which are the source of aerodynamic force production" (Taylor et al. 2003, see also Anderson et al. 1998, Wang 2000) Anderson et al. (1998) showed that the thrust produced by an oscillating foil in the flow was related to the creation, growth, and shedding of an eddy along the foil body. It has further been shown by Drucker and Lauder (1999) that the eddies shed from swimming fishes are often initiated and propagated along the body. From this perspective, the growth of eddies along a fish body will depend upon the tail beat frequency, amplitude, and velocity of the fluid as captured by St_f. The St_f for creek chub swimming in the control, small, and medium turbulent flow regimes was 0.25±0.01 (Table 4.1) which is similar to those found in other investigations of fish and cetacean swimming in the free stream (Triantafyllou et al. 1993, Liao et al. 2003, Rohr and Fish 2004). The St_f in the LE flow regime was not significantly different from the St_f in the control, small, and medium flow regimes (ANOVA, $p<0.05$). The St_f greatest in the LC flow regime (0.38±0.06) and least in the LE flow regime (0.21±0.02) (Figure 4.3c) indicating that fish were adjusting their kinematics such that in flows where the large eddies were relatively stationary, represented by the LC region, the St_f was increased, conversely in flows where large turbulent eddies pass in the streamwise direction rapidly, represented by the LG region, the St_f was decreased.

Discussion

The small, medium, and large cylinder arrays produced 95th percentile eddies with diameters of approximately 0.2, 0.4, and 0.9 fish lengths, respectively. Further, the vorticity ranged from a minimum of 1.5 s^{-1} in the control at 8.5 $cm.s^{-1}$ to a maximum of 11.3 s^{-1} in the LE treatment at 50.2 $cm.s^{-1}$. Body wavelength, tail depth, and tail angle attack did not vary across these treatments or speeds. Tail beat amplitude was larger in the large cylinder array treatments than the other treatments and did not vary with u_{local}. Tail beat frequency was lower in the large cylinder treatments and increased with u_{local} in all treatments. The rate that the tail beat frequency increased with u_{local} varied across large

cylinder treatment flow region such that the greatest rate of increase occurred in the LC region and the least occurred in the LG region. This variation resulted in the St_f being largest, 0.39, in the LC region and least, 0.23, in the LG region. The flow region directly downstream from the large cylinders, LC region, was characterized by slower u_{local}, on average 38% < $\bar{u}$, than neighboring regions along with moderately large 95th percentile eddy diameter, 10.8 cm, and vorticity, 5.9 s^{-1} at a representative $\bar{u}$ of 27.7 $cm.s^{-1}$. Conversely, the flow region between the large cylinders, LG, was characterized by faster u_{local}, on average 53% > $\bar{u}$, than neighboring regions along with smaller 95th percentile eddy diameter, 9.3 cm, and vorticity, 4.4 s^{-1} at a representative $\bar{u}$ of 27.7 $cm.s^{-1}$. Therefore in the LC flow region, where the St_f is largest, the turbulent flow is relatively stationary while in the LG flow region, where the St_f is least, the turbulent flow moves through the region rapidly. A turbulent flow parameter which captures the stationarity of turbulent eddies with respect to an interface (in this case a fish) is the persistence parameter.

Persistence Parameter

The persistence parameter, first defined by Cotel (1995) and Cotel and Breidenthal (1997) ($\frac{\omega_e \cdot L}{4\pi \cdot u_{local}}$ where π is the constant ~3.142 and L is an appropriate length scale) measures the number of times an eddy rotates while traveling a distance L. It is therefore a measure of the rotational to translational components of a flow and captures the rotational time scale associated with an eddy traveling along an interface of length L. The parameter was originally proposed by Cotel (1995) to explain turbulent entrainment in stratified flow; as such the appropriate length scale was the dominant eddy diameter for entrainment. In the case of fish/eddy impacts the appropriate length scale is the fish length (L_f). The fish based persistence parameter, T_f, is therefore defined as;

$$T_f = \frac{\omega_e \cdot L_f}{4\pi \cdot u_{local}} \qquad (4.6)$$

The fish based persistence parameter is equal to the number of revolutions an eddy makes while traveling along the fish body length and provides a metric for the rotational time

scale of an eddy while traveling along a fish body length. As such it is a measure of the stationarity of turbulent eddies with respect to the fish. The fish based persistence parameter varied by flow region downstream from the large cylinder treatments (Figure 4.2b) with the maximum value occurring in the LC regime ($T_f = 0.66$) and the least value occurring in the LG regime ($T_f = 0.12$). The persistence parameter value of 0.66 in the LC regime implies that the 95th percentile eddy rotated 66% of a full rotation, or 240°, while traveling down the fish body as compared with a rotation of 12% (40°) in the LG regime.

Strouhal Number – Persistence Parameter Relationship

The fish based Strouhal number reflects the dominant propulsive movements with respect to the u_{local} and increases linearly with the fish based persistence parameter which is a measure of the time scale of eddy rotation along the fish length (Figure 4.4, $St_f = (0.99\pm0.27)*T_f + (0.21\pm0.02)$, $r^2=0.95$) for these tests. The tail beat amplitude remained constant for a given turbulence regime (Figure 4.3a). In free stream flow, the tail beat amplitude is often reported as a function of body length (e.g. an often cited value is that $A \sim 0.2\ L_f$ Bainbridge 1958, Webb et al. 1984, and Liao et al. 2003). The Strouhal-persistence relationship implies that $F*A \sim \omega_e*L_f$. Since A is proportional to L_f, for a given flow regime, the length scales in this dimensional analysis drop out and the tail beat frequency is proportional to the eddy vorticity ($F \sim \omega_e$). In terms of time scales this dimensional analysis implies that the tail beat duration is proportional to the rotational time of the 95th percentile turbulent eddy. This finding is similar to the findings reported by Liao et al. (2003) which found that tail beat frequency was proportional to the shedding frequency for fish swimming downstream from a single cylinder – since shedding frequency and eddy vorticity are proportional to each other. Liao et al. (2003) showed that fish swimming using the Karman gait for cylinder based Reynolds numbers of 5,600 to 20,000 matched the tail beat frequency to the shedding frequency of a single upstream cylinder. Zdravkovich and Stonebanks (1990) and Sumner et al. (1999) summarize the shedding frequencies reported downstream from cylinder arrays like the arrays used in the current experiments. For cylinder arrays with equal gap to cylinder spacing, the cylinder based Strouhal number ranged from 0.1 to 0.325. The cylinder

Figure 4.4: Fish based Strouhal number increased linearly with 95th percentile fish based persistence parameter. The fish based Strouhal number is defined as the product of the tail beat frequency (F) and the tail beat amplitude (A) divided by u_{local} which in station holding fish is equal to the fish speed ($St_f = \frac{F \cdot A}{u_{local}}$). The fish based persistence parameter is defined as the product of the eddy vorticity (ω_e) and the length of the fish (L_f) divided by the constant 4π and u_{local} ($T_f = \frac{\omega_e \cdot L_f}{4\pi \cdot u_{local}}$). C = control, S = small, M = medium, LG = large gap, LE = large edge, and LC = large cylinder flow regimes. The linear relationship between St_f and the fish-based persistence parameter indicates that as the number of rotations that a turbulent eddy made while traveling along the fish body increased, the time scales associated with the growth and shedding of force producing vortices also increased.

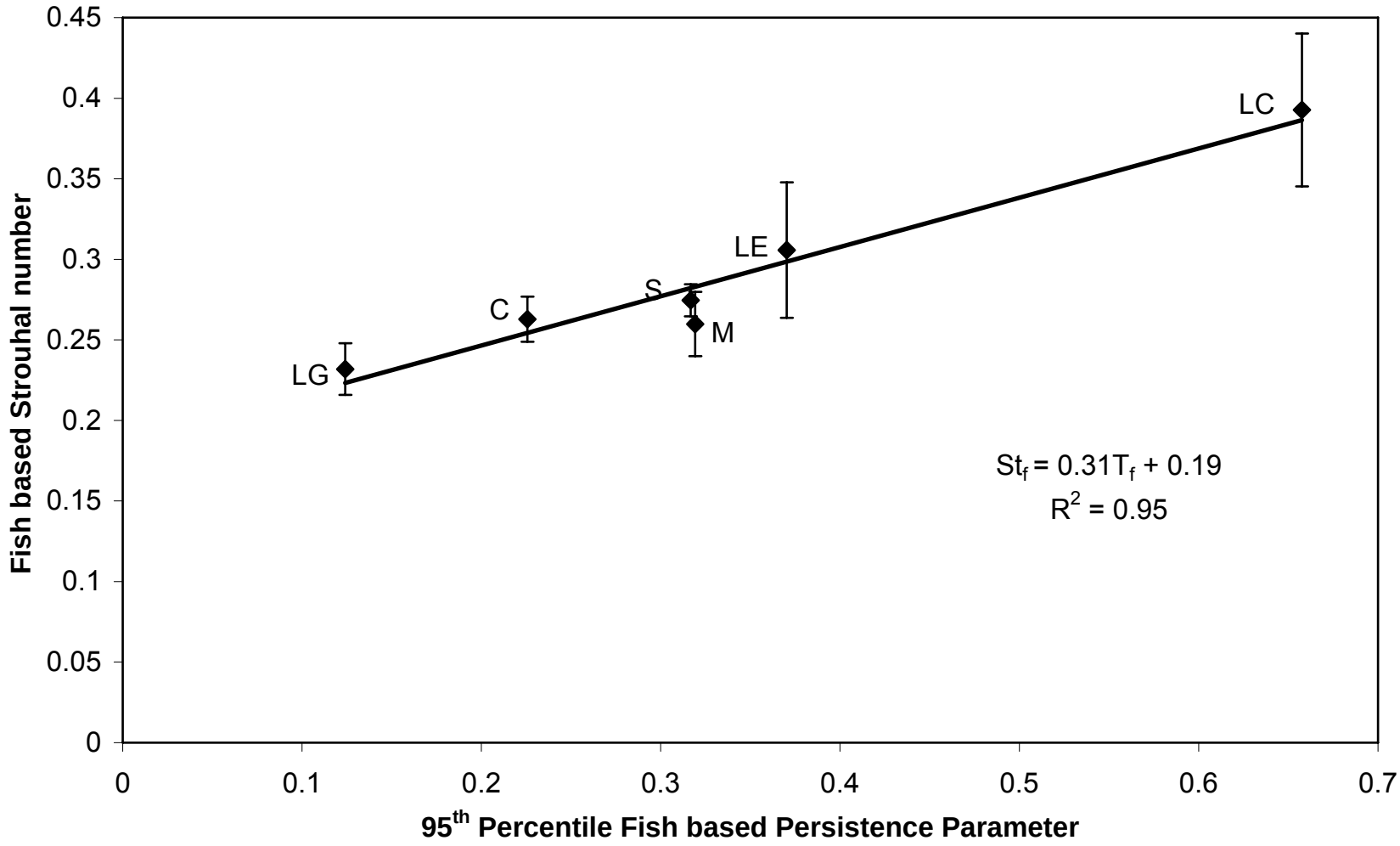
0.45
0.4
0.35
0.3
0.25
0.2
0.15
0.1
0.05
0
0
0.1
0.2
0.3
0.4
0.5
0.6
0.7
Fish based Strouhal number
95th Percentile Fish based Persistence Parameter
LG
C
S
M
LE
LC
St_f = 0.31T_f + 0.19
R^2 = 0.95

based Strouhal number, St_c, was defined as:

$$St_c = \frac{f_c d_c}{\bar{u}} \quad (4.7)$$

where f_c is the frequency that eddies are shed from a cylinder and d_c is the cylinder diameter. In these experiments the tail beat frequencies for fish swimming downstream from an array of large cylinders fell between the tail beat frequency for free-stream continuous swimming and the range of cylinder frequencies for the large cylinder diameter array (Figure 4.3b). Due to the more complex turbulent flows associated with cylinder arrays, matching of tail beat to shedding frequency was not exhibited. Instead, the time scales of tail beat frequency and eddy vorticity were shown to be connected. These results imply an interaction between eddies produced during fish-like swimming (Triantafyllou et al. 1993, Drucker and Lauder 1999) and turbulent eddies in the flow.

Conclusions

A series of increasing velocity tests (L_f = 12.2 cm) produced turbulence regimes with varying eddy diameter (95th percentiles from 1/6 to 1 fish length), eddy vorticity (95th percentile vorticity ranged from 1.5 to 11.3 s^{-1}) and u_{local} (0.4 to 5.1 body lengths per second). Body-caudal fin kinematics (tail beat frequency, tail beat amplitude, body wavelength, tail depth, and tail angle of attack) were video analyzed for changes across turbulent regime. The body wavelength, tail depth, and tail angle of attack were not observed to change across treatment or speed ($p<0.05$). Furthermore, the tail beat amplitude and frequency were not observed to change from the control treatment to the small (cylinder diameter = 0.4 cm) or medium (cylinder diameter = 1.6 cm) cylinder treatments. In the small and medium cylinder treatments the momentum of the 95th percentile eddies ($0.25 m_e \omega_e d_e$) was more than an order of magnitude less than the momentum of the fish ($M_f V_f$). In the large cylinder treatments (cylinder diameter = 8.9 cm) the eddy momentum was slightly greater than the fish momentum (95th percentile momentum ratio = 1.6). In the presence of eddies with significant momentum compared to the fish, the tail beat frequency was reduced while the tail beat amplitude increased. This reduced tail beat frequency and increased tail beat amplitude is reminiscent of the Karman gait reported by Liao et al. (2003) but differs in two ways. First, an increase in

body wavelength was not observed. Second, matching of tail beat frequency with the cylinder shedding frequency was not observed. A linear relation between the fish based Strouhal number ($St_f = \frac{F \cdot A}{u_{local}}$) and the fish based persistence parameter ($T_f = \frac{\omega_e \cdot L_f}{4\pi \cdot u_{local}}$) indicated, however, that as the number of rotations a turbulent eddy made while traveling along the fish body increased, the time scales associated with fish-like swimming also increased. For a given turbulent flow regime the tail beat amplitude did not change with local velocity and it was shown, through dimensional analysis, that for a given turbulent regime the tail beat duration was proportional to the rotational time scale of the turbulent eddies. These results imply that turbulent eddies with sufficient momentum interact with eddies produced during fish like swimming. In order to validate the hypothesized interactions between turbulent eddies and force generating eddies, simultaneous PIV and video analysis should be conducted on fish swimming in highly rotational turbulent flows.

References

Anderson, J. M., Streitlien, K., Barrett, D. S. and Triantafyllou, M. S. (1998). Oscillating foils of high propulsive efficiency. *Journal of Fluid Mechanics* **360**, 41-72.

Bainbridge, R. (1958). The speed of swimming of fish as related to size and to the frequency and amplitude of the tail beat. *Journal of Experimental Biology* **35**, 109-133.

Cada, G. F. and Odeh, M. (2001). Turbulence at hydroelectric power plants and its potential effects on fish. *Report to Bonneville Power Administration*, Contract No. 2000AI26531, Project No. 200005700: 1-37.

Cotel, A. J. (1995). Entrainment and detrainment of a jet impinging on a stratified interface. Ph.D. Thesis, University of Washington.

Cotel, A. J. and Breidenthal, R. E. (1997). A model of stratified entrainment using vortex persistence. *Applied Scientific Research* **57**, 349-366.

Drucker, E. G. and Lauder, G. V. (1999). Locomotor forces on a swimming fish: three-dimensional vortex wake dynamics quantified using digital particle image velocimetry. *Journal of Experimental Biology* **202**, 2393-2412.

Enders, E. C., Boisclair, D. and Roy, A. G. (2005). A model of the total swimming costs in turbulent flow for Atlantic salmon (*Salmo salar*). *Canadian Journal of Fisheries and Aquatic Sciences* **62**, 1079-1089.

General Pixels. (2000). *PixelFlow 2.1: Installation and User's Guide.*

Gharib, M. and Dabiri, D. (2000). An overview of digital particle image velocimetry in *Flow Visualization: Techniques and Examples* (ed Smits A and Lim T T) London: Imperial College Press.

Huang, H., Dabiri, D., and Gharib, M. (1997). On errors of digital particle image velocimetry *Meas. Sci. Technol.* **8**, 1427-40.

Keast, A. (1985). The piscivore feeding guild of fishes in small freshwater ecosystems. *Environmental Biology of Fishes* **12**, 119-129.

Landry, F., Miller, T. J., and Leggett, W. C. (1995). The effects of small-scale turbulence on the ingestion rate of fathead minnow larvae. *Canadian Journal of Fisheries and Aquatic Sciences* **52**, 1714-1719.

Lauder, G. V., and Jayne, B. C. (1996). Pectoral fin locomotion in fishes: Testing drag-based models using three-dimensional kinematics. *American Zoologist* **36,** 567-581.

Liao, J. C., Beal, D. N., Lauder, G. V. and Triantafyllou, M. S. (2003). The Karman gait: novel body kinematics of rainbow trout swimming in a vortex street. *Journal of Experimental Biology* **206**, 1059-1073.

Lighthill, M. J. (1960). Note on the swimming of slender fish. *Journal of Fluid Mechanics* **9**, 305-317.

Lighthill, M. J. (1971). Large-Amplitude Elongated-Body Theory of Fish Locomotion. *Proceedings of the Royal Society of London. Series B, Biological Sciences* **179**, 125-138.

Lupandin, A. I. (2005). Effect of Flow Turbulence on Swimming Speed of Fish. *Biology Bulletin* **32**, 558-565.

Mackenzie, B. R., Miller, T. J., Cyr, S., and Leggett, W. C. (1994). Evidence for a Dome Shaped Relationship Between Turbulence and Larval Fish Ingestion Rates. *Limnology and Oceanography* **39**, 1790-1799.

Maxwell, S. E. and Delaney, H. D. (2004). *Designing experiments and analyzing data*. 2nd Edition. Lawrence Erlbaum Associates, Inc. Mahwah NJ.

Muller, U. K., Van Den Heuvel B. L. E., Stamhuis E. J., and Videler J. J. (1997). Fish footprints: Morphology and energetics of the wake behind a continuously swimming mullet (*Chelon labrosus*). *Journal of Experimental Biology* **200**, 2893-2906.

Nikora, V. I., Aberlee, J, Biggs B J F, Jowett I G, and Sykes J R E. (2003). Effects of Fish Size, Time to Fatigue, and Turbulence on Swimming Performance: A Case Study of Galaxias maculatus. *Journal of Fish Biology* **63**, 1365-1382.

Pedley TJ and Hill SJ. (1999). Large-Amplitude Undulatory Fish Swimming: Fluid Mechanics Coupled to Internal Mechanics. *The Journal of Experimental Biology* **202**, 3431-3438.

Rohr JJ and Fish FE. (2004). Strouhal numbers and optimization of swimming by odontocete cetaceans. *The Journal of Experimental Biology* **207**, 1633-1642.

Schultz, W. W., Zhou Q.-N., and Webb P. W. (1991). A Two-dimensional Model of Fish Swimming. Mechanics and Physiology of Animal Swimming Meeting, Marine Biological Association, Plymouth, U.K., April, 1991.

Smith D L, Brannon EL, and Odeh M. (2005). Response of Juvenile Rainbow Trout to Turbulence Produced by Prismatoidal Shapes. *Transactions of the American Fisheries Society* **134**, 741-753.

Standen, E M, Hinch S G, Healey M C, and Farrell A P. (2002). Energetic Costs of Migration through the Fraser River Canon, British Columbia, in Adult Pink and Sockeye

Salmon as Assessed by EMG Telemetry. *Canadian Journal of Fisheries and Aquatic Sciences* **59**, 1809-1818.

Sumner, D., Wong, S. S. T., Price, S. J. and Paidoussis, M. P. (1999). Fluid behaviour of side-by-side circular cylinders in steady cross-flow. *Journal of Fluids and Structures* **13,** 309-338.

Taylor, G. K., Nudds, R. L. and Thomas, A. L. R. (2003). Flying and swimming animals cruise at a Strouhal number tuned for high power efficiency. *Nature* **425**, 707-711.

Triantafyllou, MS, Triantafyllou GS, and Gopalkrishnan R. (1991). Wake mechanics for thrust generation in oscillating foils. *Physics of Fluids* **3**, 2835-2837.

Triantafyllou GS, Triantafyllou MS, and Grosenbaugh MA. (1993). Optimal thrust development in oscillating foils with applications to fish propulsion*. Journal of Fluid Structures* **7**, 205-224.

Tritico, H. M., Cotel, A. J., and Clarke, J. N. (2007). Development, testing and demonstration of a portable submersible miniature particle imaging velocimetry device. *Measurement Science and Technology* **18**, 2555-2562.

Wang ZJ. (2000). Vortex shedding and frequency selection in flapping flight. *Journal of Fluid Mechanics* **410**, 323-341.

Webb PW. (1971). The swimming energetics of trout I: thrust and power output at cruising speeds. *Journal of Experimental Biology* **55**, 489-520.

Webb PW. (2004). Response latencies to postural disturbances in three species of teleostean fishes. *The Journal of Experimental Biology* **207**, 955-961.

Webb PW, Kostecki PT and Stevens ED. (1984). The effect of size and swimming speed on locomotor kinematics of rainbow trout. *Journal of Experimental Biology* **109**, 77-95.

Wilga C.D. and Lauder G.V. (1999). Locomotion in sturgeon: function of the pectoral fins. *Journal of Experimental Biology* **202**, 2413-2432.

Wilga C.D. and Lauder G.V. (2002). Function of the heterocercal tail in sharks: quantitative wake dynamics during steady horizontal swimming and vertical maneuvering. *Journal of Experimental Biology* **205**, 2365-2374.

Wu TY. (1971). Hydrodynamics of Swimming Propulsion 1: Swimming and Optimum Movements of Slender Fish with Side Fins. *Journal of Fluid Mechanics* **46**, 546-568.

Zdravkovich, M. M. and Stonebanks, K. L. (1990). Intrinsically nonuniform and metastable flow in and behind tube arrays. *Journal of Fluids and Structures* **4**, 305-319.

Chapter V

The Effects of Turbulent Flow Eddy Composition on Median and Paired-Fin Use

Introduction

Turbulence has previously been shown to affect metabolic rate (Enders et al. 2003), habitat selection (Pavlov et al. 2000, Smith et al. 2005 and Cotel et al. 2006), propulsive costs (Chapter IV), and critical swimming speed (Chapter III) for fishes. Turbulence is presumed to act by destabilizing fish through the creation of forces that are asymmetrical along the body, thereby tending to cause rotational and/or translational displacements on the fish (Odeh et al. 2002, Chapter III). The magnitude of the perturbing force is expected to depend on the momentum of eddies in the turbulent flow relative to the momentum of the fish. Webb (2006) argued that in order to maintain trajectory and postural orientation in a turbulent flow, stabilization through fin deployment similar to that of maneuvering is required. There are currently no observations showing changes in fin deployment with increased eddy momentum, or that fin use deployment patterns are consistent with countering expected body perturbations from eddies (Webb 2006, Liao 2007).

Chapter IV found that caudal fin beat amplitude and frequency increased during steady swimming with eddy diameter (d_e) and vorticity (ω_e), respectively. The caudal fin represents the control surface with the greatest area with respect to the flow and the largest moment arm from the center of mass for countering flow perturbations, especially for yawing moments. In many fluvial fish species, such as the creek chub used in this study, the remaining median/paired fins are used regularly during swimming, but contribute little to momentum transfers that drive propulsion. Therefore, non-caudal fin deployment provides an opportunity for a clearer understanding of their use as control surfaces in turbulent flow (McLaughlin and Noakes 1998, Webb 1998). The purposes of this paper are to determine whether increased turbulent eddy momentum results in

increased median and paired-fin deployment and to develop an understanding of the patterns of fin deployment with turbulent eddy orientation and size.

Materials and methods

Changes in median and paired-fin use were measured at several flow speeds and turbulent eddy compositions induced by upstream cylinder arrays of differing diameters and orientations. The turbulent flow regimes were measured using particle image velocimetry (PIV) and were characterized according to eddy diameter (d_e), eddy vorticity (ω_e), and the local velocity (u_{local}). The use of dorsal, anal, pelvic, and pectoral fin control surfaces was recorded on video and quantified in terms of the percentage of time and area deployed. Creek chub were selected as a model fusiform-shaped soft-ray-fin species common to North America (Keast 1985, Webb 2004).

Apparatus

Observations of fish behavior were made during an increasing velocity test in a water tunnel with a test section 250 cm in length and 60 cm wide (Chapter III). The water depth was held at 55 cm for all tests. A 30-cm observation section was delineated within this test section by a downstream grid (12.5 mm egg-crate) and upstream by either a similar grid or by one of three cylinder arrays spanning the flume cross-section oriented vertically or horizontally. Arrays were comprised of cylinders with diameters 0.4 cm, 1.6 cm, and 8.9 cm, with gaps equal to cylinder diameter in each array. Thus there were seven treatments: control (C), small horizontal (SH), small vertical (SV), medium horizontal (MH), medium vertical (MV), large horizontal (LH), and large vertical (LV) arrays (Chapter III). A 1.3 cm mesh of 0.04 cm diameter plastic thread was attached to the upstream side of the cylinders to prevent fish escaping. One wall of the observation chamber was papered with 2 cm x 2 cm black and white checkered paper to foster fish station holding. All edges of the test sections were electrified at 5 V DC to encourage swimming.

Flow analysis

Data on instantaneous flow patterns were collected for velocities averaged over the observation cross-section, $\bar{u}$, of 8.5, 17.1, 27.7, 38.7, and 50.2 $cm.s^{-1}$ using two-dimensional PIV. The water was seeded with 1 μm diameter neutrally buoyant titanium dioxide particles at a concentration of 1.2 ppm. Flow was illuminated using a 120 mJ NdYAG dual-head 532-nm pulsed laser (NewWave Gemini) with pulse duration of 100 μs, and creating a laser sheet 0.75 mm thick spanning the observation cross section either horizontally (for vertical cylinder arrays) or vertically (for horizontal cylinder arrays). Fifty image pairs were recorded at pulse separations of 8, 5, 3, 2, and 1 ms, at $\bar{u}$ of 8.5, 17.1, 27.7, 38.7, and 50.2 $cm.s^{-1}$ respectively.

The vertical laser sheet downstream from the horizontal cylinder arrays was positioned along the flume centerline. The interrogation window (region over which particle displacements were tracked) was selected within the bottom 50% of the flume in order to avoid stray air bubbles in the upper water column (Chapter III). The horizontal laser sheet and interrogation window downstream from the vertical cylinder arrays were centered on the flume centerline, halfway between the bed and the free surface.

Flow was reconstructed from image pairs of the particles in the flow which were recorded on a 1 mega pixel 10-bit 30 fps UniqVision black and white CCD camera driven by PixelFlow software (General Pixels, Inc.; Huang et al. 1997, Gharib and Dabiri 2000, General Pixels 2000, Tritico et al. 2007). Fifty image pairs were collected at 15 Hz at each ū, averaging 12 eddy shedding cycles from the cylinders. Due to surface reflections and laser intensity requirements, a smaller 26 cm streamwise by 30 cm transverse interrogation window was analyzed for each treatment beginning 2 cm upstream from the downstream grid and 2 cm downstream from the upstream cylinder arrays or grid.

Eddies were identified following the method described by Drucker and Lauder (1999). Cross-correlation techniques were used to convert consecutive images of particles into velocity vector fields. The vorticity (ω, twice the angular velocity) was calculated from the velocity vector field. Each local minimum and maximum vorticity within a vorticity field was taken as an eddy center following Drucker and Lauder (1999). The circulation about each eddy center was calculated in concentric circles until a maximum circulation (Γ_e) was reached ($\Gamma_e=\omega_e*a_e$ where a_e is the area circumscribed by the circle

and ω_e is the spatially averaged vorticity within the circle). The radius with maximum circulation was taken to be the eddy radius (Drucker and Lauder 1999 and Wilga and Lauder 1999); each eddy's location, diameter, and average vorticity were recorded.

Previous observations showed that fish swam throughout the water column in the control, small- and medium-diameter cylinder array treatments without choosing locations relative to the cylinder. In contrast, fish regularly chose swimming locations relative to the large cylinders. These locations were classified into three groups defined as follows: a) large cylinder (LC) area directly downstream from each large cylinder (cylinder centerline ± 2.3 cm), b) large edge (LE) area directly downstream from each cylinder edge (cylinder edge ± 2.3 cm), and c) large gap (LG) area directly downstream from each gap between the cylinders (gap centerline ± 2.3 cm). Therefore, results have been described for flow structure through the water column for the control, small-diameter and medium-diameter cylinder arrays, and for the cylinder, edge and gap regions for large cylinders (Chapter III).

The flow region had been further trisected into upstream, middle, and downstream regions in Chapter III. In Chapter III it was shown that while the 95th percentile eddy diameter did not change with streamwise location the 95th percentile eddy vorticity did decay with streamwise distance. Further, it was shown that fish tended to swim in the downstream region of the tank (41, 37, 22% of time in the downstream, middle, and upstream flow regions, respectively) and tended to fail in the upstream region of the tank (19, 10, 71% of failures in the downstream, middle, and upstream flow regions, respectively). Conversely, the streamwise location in the tank was not a significant factor in predicting any of the MPF metrics reported here (one-way ANCOVA generalized linear model with streamwise location, gap/edge/cylinder, speed, and treatment as covariates along with interaction terms, $p>0.05$ for streamwise location and all interaction terms, Maxwell and Delaney 2004). The streamwise data have therefore been grouped and only the LG, LE, and LC flow regions distinction as reported (same ANCOVA as previously reported with percentage time and percentage area deployed for all fins being dependent upon transverse location in the flow, $p<0.05$).

Fish

Creek chub were obtained from Fleming Creek, Michigan, USA at a water temperature of 21.1 °C. Fish were acclimated in the lab to room temperature (20.5 ±0.4 °C) for one week prior to the experiment and were fed to satiation daily (Chapter III). The experimental temperature was the same as the acclimation temperature. Seven creek chub with an average total length of 12.2±0.9 cm (mean±2SE) and mass of 16.8±3.5 grams were used in experiments. Each fish was swum with every treatment. The order of the treatment experienced was selected at random and fish were given a minimum of 3.5 days between each test.

A single fish was placed in the observation section and acclimated to $\bar{u}$ of 8.5 cm/s. After 11 hours acclimation, ū was increased by 3.5 $cm.s^{-1}$ increments at 2 minute intervals until the fish became entrained on the downstream grid for 3 seconds. The 2-min u_{crit} results are reported in Chapter III; in this paper we discuss the median/paired fin kinematics at each of the $\bar{u}$ leading up to the critical swimming speed.

Fish were continuously videotaped at 30 frames per second simultaneously from the side and from below using two digital video cameras (Panasonic Model No. PV-DV601D). Fish moved about the test section, holding position for variable periods at various locations. Swimming kinematics were measured from video records when fish remained in a given location with no postural changes for >5 s during which fish velocities in the environmental frame of reference were <0.02 $body\text{-}lengths.s^{-1}$ (Wilga and Lauder 2002).

In addition, video records were analyzed to record anal, dorsal, and paired fin usage. Fin deployment was quantified in terms of the percentage of time each fin was extended and the projected area of the fin at each speed increment. The latter were normalized by the maximum projected area observed for each fish. A fin was considered deployed if greater than 10% of this maximum area was extended from the body. Observations were restricted to swimming with the body and caudal fin (BCF swimming), excluding mixed BCF swimming and rowing with the pectoral fins (Drucker and Lauder 2001, Webb 2002).

Results

Flow regimes

The presence of structures in a flow creates local variations in flow. Biological flumes and low turbulence flumes are not free from turbulence (Farlinger and Beamish 1977, Enders et al. 2003). Additionally, the biological requirement of delimiting the upstream end of observation sections to avoid fish escape introduces further sources of turbulence. Hence there were turbulent eddies in the control and all treatments. As noted above, fish swam throughout the water column in the control treatment and with the small– and medium– diameter cylinder arrays but swam in cylinder, edge, and gap regions for large cylinders, where the structures had large effects on the flow as perceived by these fish.

Seven unique turbulent flow regimes were created in these experiments. The u_{local} in each flow regime was equivalent to the cross-sectionally averaged flow velocity, $\bar{u}$, except for the LC flow regime, which provided a time averaged velocity refuge (on average u_{local} 38% less than $\bar{u}$) and the LG flow regime where velocity was on average 53% greater than $\bar{u}$ (Figure 4.2a). The 95th percentile eddy diameter varied from 1/6 to 1 fish length in the control and LE regimes, respectively (Figure 4.4c). The experimental treatments successfully created a range of eddy diameters less than or equal to the fish length in order to explicitly test the role of turbulence scale on median and paired-fin use (Chapter III). Eddy diameters did not vary with u_{local}. The 95th percentile eddy vorticity increased with u_{local} and varied across flow regime from a low of 1.5 s^{-1} at 8.5 $cm.s^{-1}$ in the control treatment to 11.3 s^{-1} at 50 $cm.s^{-1}$ in the LE flow regime, nearly an order of magnitude variation in vorticity was induced (Figure 4.2b).

Non-Caudal Fin Deployment

Fin use generally decreased as u_{local} increased, as has been described previously in many fishes (Alexander 1965, Archer and Johnston 1989, Drucker 1996, Korsmeyer et al. 2002). The pectoral fins have been the most commonly studied non-caudal fin system, due to their role in labriform swimming (Blake 1979 and 1980, Gibb et al. 1994, Thorson and Westneat 2005). More recently, decreases in pectoral fin use which are not associated with a transition from labriform to body/caudal fin swimming have been described in

bluegill sunfish (*Lepomis macrochyrus*) and Atlantic needlefish (*Strongylura marina*) by Standen and Lauder (2005) and Liao (2002), respectively. While dorsal- and anal-fin use did not change across treatment or region (see next section, Non-Caudal Fin Deployment Percentiles), paired fin use increased with increasing cylinder diameter and was larger in the edge and control regions than in the gap region (ANCOVA, $p<0.05$). Three distinct patterns of pectoral fin deployment based on control surface deployment angles with respect to the fish center of mass and flow direction (see Pectoral-Fin Deployment Pattern section) were noted, and the number of observations of these patterns varied across cylinder orientation and flow speed.

Non-Caudal Fin Deployment Percentiles

A regression analysis was performed comparing either percentage time deployed or percentage area deployed with u_{local} for each of the flow regimes. The trend lines for flow regimes that were not significantly different from each other (one-way ANCOVA generalized linear model with $\bar{u}$, and treatment as covariates along with interaction terms, $p>0.05$ for treatment and all interaction terms, Maxwell and Delaney 2004) were combined and reanalyzed. Slopes in the trend lines that were not significantly different from zero (ANOVA, $p<0.05$) indicate that no change in usage occurred with increasing velocity.

The deployment of the anal fin did not vary across treatments (ANCOVA with treatment and $\bar{u}$, $p<0.05$) (Figure 5.1a, b). The anal fin was deployed 100% of the time at all swimming speeds, while the area used decreased linearly from 76% at u_{local} of 5 $cm.s^{-1}$ to 50% at u_{local} of 63 $cm.s^{-1}$. A similar pattern was seen for the dorsal fin in that treatment had no significant effects on usage (ANCOVA, $p<0.05$) (Figure 5.1c, d). The combined data across treatments also showed that deployment time was independent of u_{local}, here averaging 85% of the time. The area decreased linearly with speed in a similar manner to the anal fins from 67% of the maximum observed area at 5 $cm.s^{-1}$ to 40% at 63 $cm.s^{-1}$ (ANOVA, $p<0.05$).

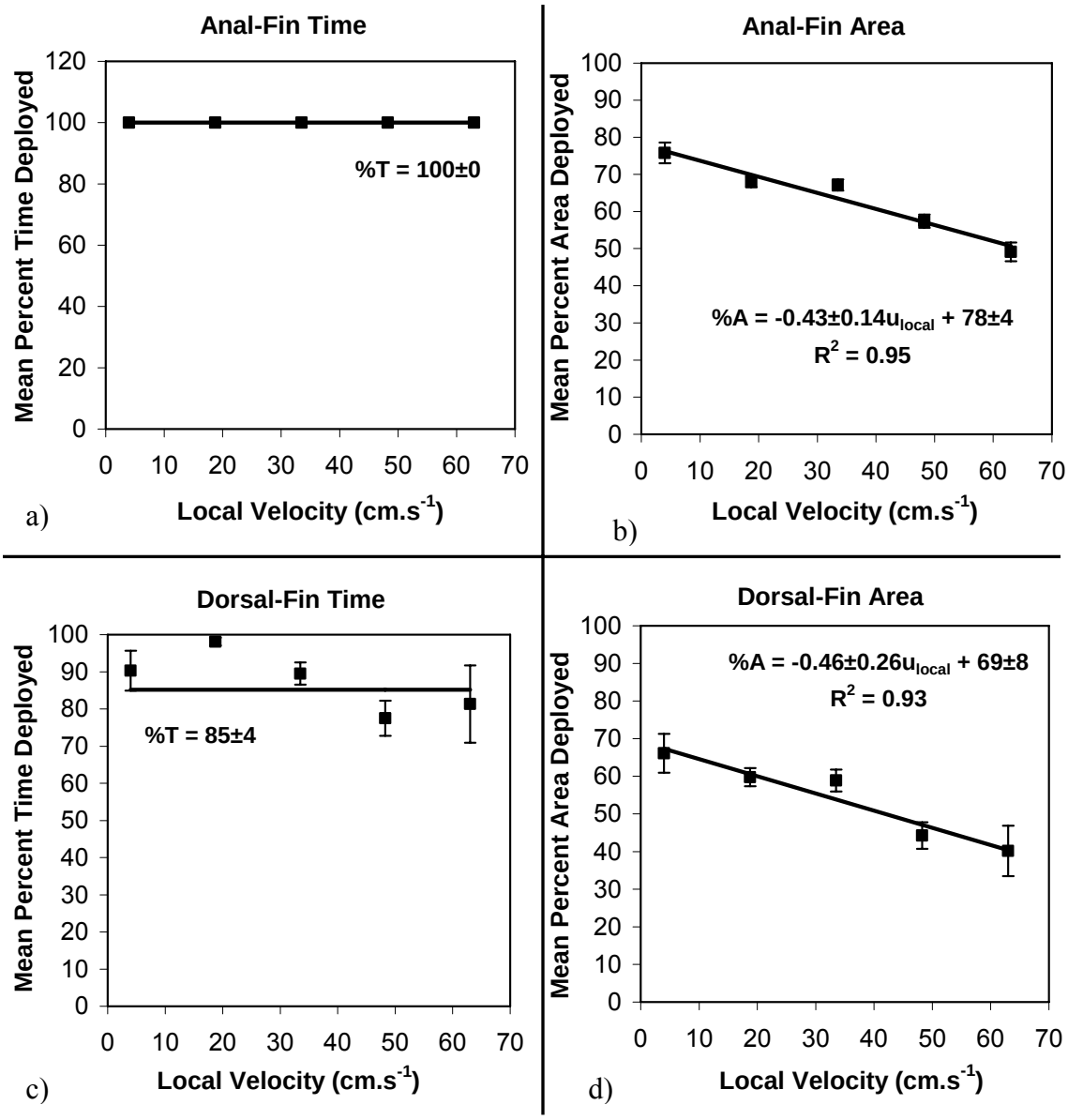

Figure 5.1: Median-Fin Usage. Dorsal- and anal-fin use did not change across treatment or flow region (ANCOVA with speed and treatment, where $p>0.05$ for both the treatment and the interaction terms) therefore data have been combined. a) The anal-fin percentage time deployed. b) The anal-fin percentage area deployed. c) The dorsal-fin percentage time deployed. d) The dorsal-fin percentage area deployed. The lines represent the linear regression of the mean while the data points represent the mean and the error bars represent ± 2 standard errors of the mean.

Paired-fin use changed across both speed and flow regime (ANCOVA, $p<0.05$) (Figure 5.2). Pelvic-fin usage was significantly greater in the LC and LE flow regimes than it was in the other flow regimes (ANCOVA $p<0.05$, Figure 5.2a, b). Fish swimming in the LC and LE flow regimes deployed their pelvic fins 96% of the time (Figure 5.2a) and at 88% of the maximum area (Figure 9.2b) independent of u_{local}. In the remaining flow regimes (C, S, M, LG), the time that the pelvic fins were deployed decreased linearly from 58% at u_{local} of 8 $cm.s^{-1}$ to 23% at u_{local} of 63 $cm.s^{-1}$ (ANOVA, $p<0.05$ Figure 5.2a). The pelvic area that was deployed within the C, S, M, and LG flow regimes decreased in a similar manner to the time of deployment such that 68% of the fin area was deployed at 8 $cm.s^{-1}$ and reduced to 13% at 63 $cm.s^{-1}$ (ANOVA, $p<0.05$ Figure 5.2b).

A further differentiation in fin usage across flow regimes was exhibited in the pectoral fins such that three unique fin use groups were apparent (Figure 5.2 c and d). Similar to the pelvic-fin usage in the LC and LE regimes, the pectoral-fin was deployed 92% of the time (Figure 5.2c) at 88% of the maximum area (Figure 5.2d) and did not change with swimming speed (ANOVA $p>0.05$). Pectoral-fin usage in the S, M, and LG flow regimes was greater than the control yet less than the LE/LC regimes (ANCOVA, $p<0.05$). The time the pectoral fins in the S, M, and LG flow regimes were deployed decreased from 52% at 8 $cm.s^{-1}$ to 19% at 63 $cm.s^{-1}$ (ANOVA, $p<0.05$ Figure 5.2c). The percentage area that the pectoral fins in the S, M, and LG flow regimes were deployed compared to the maximum decreased in a similar fashion to the percentage time deployed such that 74% of the area was deployed at 8 $cm.s^{-1}$ to 19% at 63 $cm.s^{-1}$ (ANOVA, $p<0.05$ Figure 5.2d). Fish swimming in the control regime deployed pectoral fins less than in any of the other flow regimes, such that the percentage time the pectoral fins were deployed decreased linearly from 12% at 17 $cm.s^{-1}$ to 0% at 33 $cm.s^{-1}$ (ANCOVA, $p<0.05$ Figure 5.2c). Similarly, the percentage area deployed decreased linearly from 38% at 17 $cm.s^{-1}$ to 0% at 33 $cm.s^{-1}$ in the control regime (ANOVA, $p<0.05$ Figure 5.2d).

From the results of the regression analysis, it is apparent that as turbulent eddy diameter and vorticity increased, paired fin use increased. Turbulence can act on a fish to produce either rotational or translational displacements. Turbulent eddies of the same size as the fish length have been proposed to have the greatest rotational impact on fish due to the maximization of moment about the fish center of mass (Cada and Odeh 2001,

Figure 5.2: Paired-Fin Usage. Pelvic- and pectoral-fin use changed across u_{local}, treatment, and region (ANCOVA, $p<0.05$). a) The pelvic fins percentage time deployed. b) The pelvic fins percentage area deployed. c) The pectoral fins percentage time deployed. d) The pelvic fin percentage area deployed. The lines represent the regression of the mean, the symbols represent the mean values at a given $\bar{u}$, and error bars represent ± 2 standard errors of the mean. C = control, S = small cylinder treatment, M = medium cylinder treatment, LC = large cylinder treatment directly downstream from the cylinders, LE = large cylinder treatment downstream from the cylinder edge, LG = large cylinder treatment in the gap between cylinders.

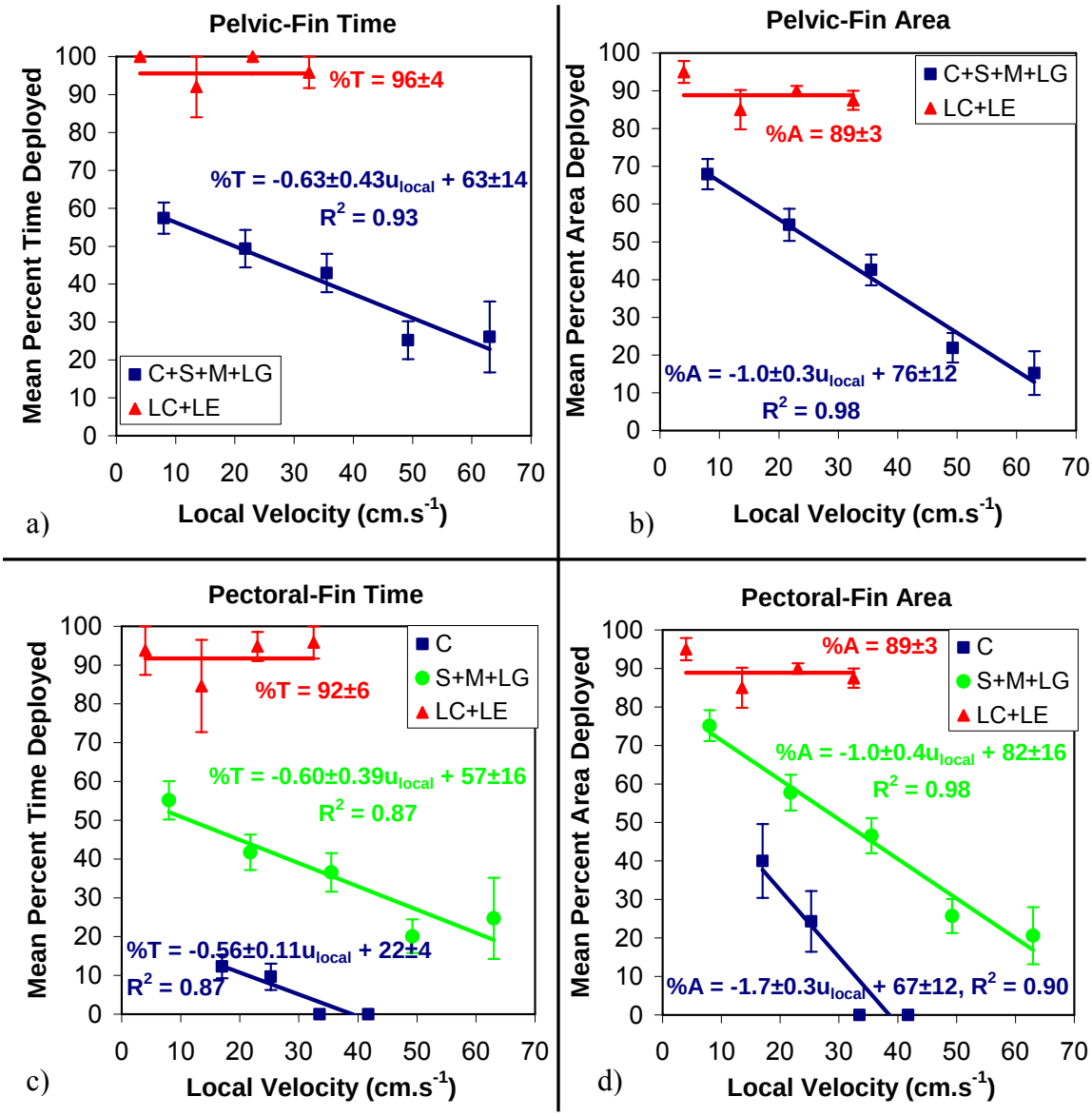
Pelvic-Fin Time
Mean Percent Time Deployed
%T = 96±4
%T = -0.63±0.43u_local + 63±14
R² = 0.93
C+S+M+LG
LC+LE
Local Velocity (cm.s⁻¹)
a)
Pelvic-Fin Area
Mean Percent Area Deployed
C+S+M+LG
LC+LE
%A = 89±3
%A = -1.0±0.3u_local + 76±12
R² = 0.98
Local Velocity (cm.s⁻¹)
b)
Pectoral-Fin Time
Mean Percent Time Deployed
C
S+M+LG
LC+LE
%T = 92±6
%T = -0.60±0.39u_local + 57±16
R² = 0.87
%T = -0.56±0.11u_local + 22±4
R² = 0.87
Local Velocity (cm.s⁻¹)
c)
Pectoral-Fin Area
Mean Percent Area Deployed
%A = 89±3
C
S+M+LG
LC+LE
%A = -1.0±0.4u_local + 82±16
R² = 0.98
%A = -1.7±0.3u_local + 67±12, R² = 0.90
Local Velocity (cm.s⁻¹)
d)

Lupandin 2005). Chapter III argues that the impact of an eddy on the stability of a fish is related to the momentum ratio, Π_r, (the relative momentum of the eddy, Π_e, to that of the fish, Π_f);

$$\Pi_r = \frac{\Pi_e}{\Pi_f} = \frac{\frac{m_e \omega_e d_e}{4}}{M_f V_f} \quad (5.1)$$

where m_e is the eddy mass (see Chapter III for a discussion of the eddy mass calculation), M_f is the fish mass, and V_f is the fish velocity (since the fish were analyzed during station holding $V_f = u_{local}$). Chapter III further showed that when the momentum of the 95th eddy approached the fish momentum, the spill rate (defined as rapid head rotation followed by downstream translation) increased dramatically. Similarly, the percentage time the pectoral fins are deployed is shown to increase with the momentum ratio (Figure 5.3). In addition to the pectoral-fin deployment rate shown in Figure 5.3, the increase with momentum ratio exists for both pectoral and pelvic fins along with both the deployment time and the area metrics. The semi-log relationship indicates that pectoral fin usage increases rapidly across low levels of momentum ratio while usage levels off as the percentage time and area approached 100%.

Pectoral-fin deployment pattern

In order to further investigate the manner in which the pectoral fins were deployed across flow regimes, the fish's pectoral fin orientation and flapping direction were recorded. Pectoral fins were deployed rapidly and were most often immediately retracted, the occurrence of deployment was not temporally periodic or synchronized with any given phase of the tail beat, indicating that deployments were used reactively to aperiodic disturbances.

The deployment of paired fins is variable among fishes and with speed (Brett and Sutherland 1965, Wilga and Lauder 1999, Fish and Shannahan 2000, Drucker and Lauder 2003). In these experiments, pectoral fin deployment could be classified into three patterns. The first pattern was the extension of one or both fins in the longitudinal (horizontal) plane, with vertical beating, here called lateral horizontal pectoral fin deployment (Figure 5.4a). This was primarily observed at the lowest $\bar{u}$ (8.5 cm.s^{-1})

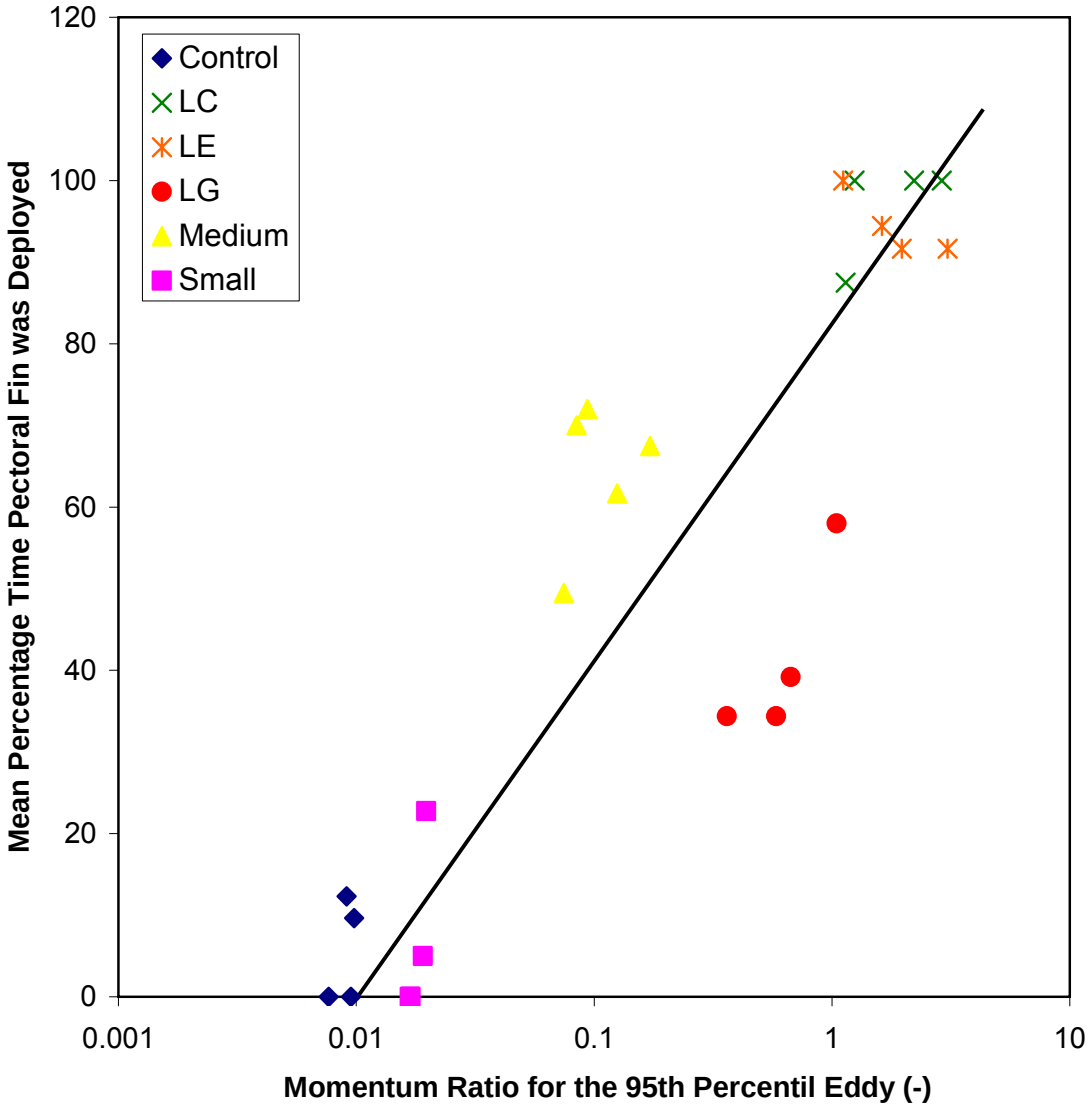

Figure 5.3: Mean Pectoral-fin % Time Deployed vs 95th Percentile Eddy Momentum Ratio. The eddy momentum ratio (P) is the ratio of the momentum of the 95th percentile turbulent eddy ($0.25m_e\omega_e d_e$) to the momentum of the fish ($M_f V_f$). The percentage time the pectoral fins were deployed increased with the momentum ratio.

Figure 5.4: Pectoral-Fin Deployment Pattern: Three distinct patterns of pectoral-fin deployment were observed. Descriptions of each of the three patterns are included in the text. The first pattern, a) light blue fin and bar color, has been termed lateral horizontal pectoral fin deployment. The second pattern, b) dark blue fin and bar color, has been termed lateral perpendicular pectoral fin deployment. The final pattern, c) red fin and bar color, has been termed dorso-ventral perpendicular pectoral fin deployment. Observations of both lateral-perpendicular and dorso-ventral perpendicular fin deployment patterns were sometimes observed during a single station holding event and have been labeled using a red/blue stripe.

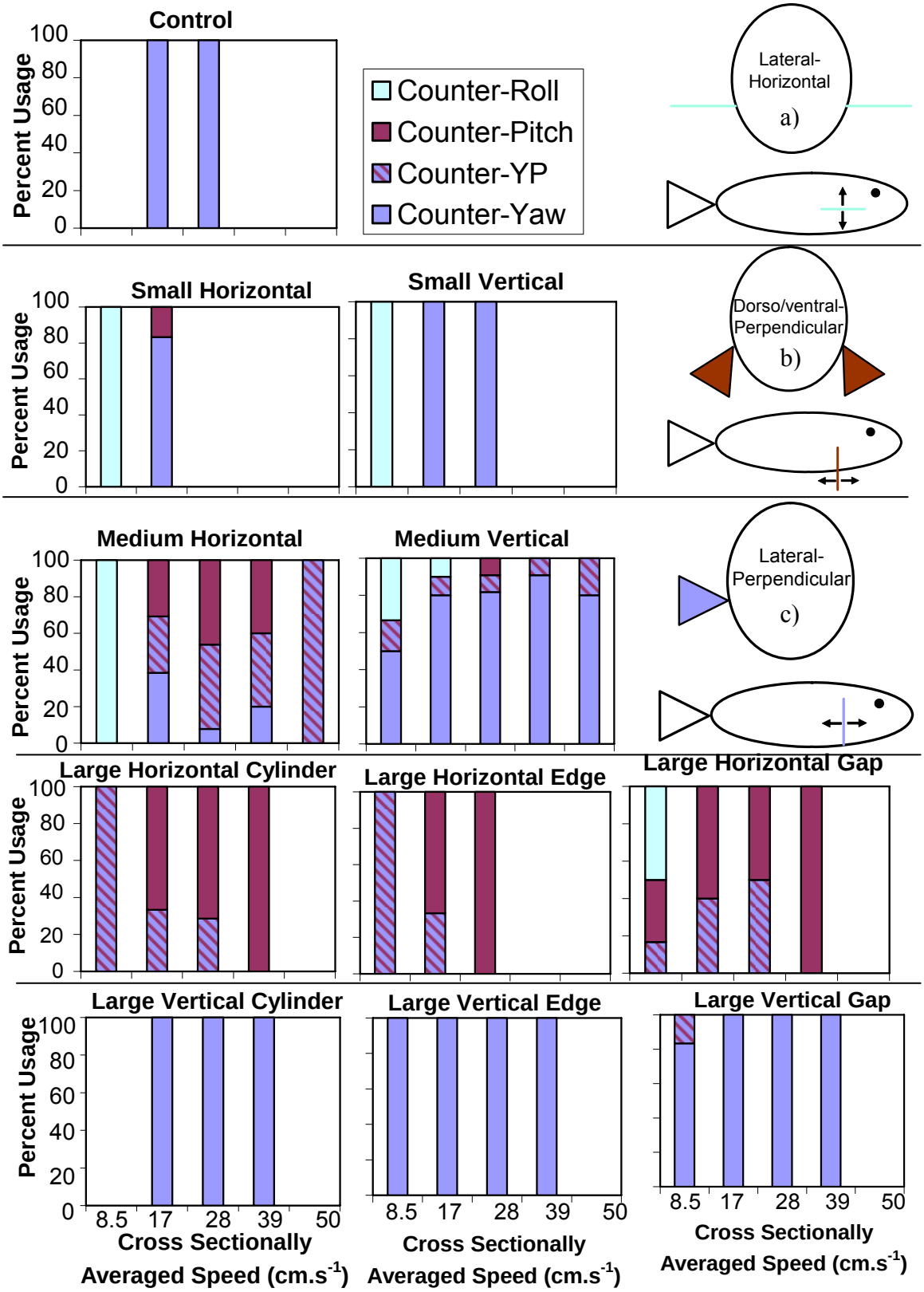
Control
Percent Usage
100
80
60
40
20
0
Counter-Roll
Counter-Pitch
Counter-YP
Counter-Yaw
Lateral-Horizontal
a)
Small Horizontal
Small Vertical
Dorso/ventral-Perpendicular
b)
Medium Horizontal
Medium Vertical
Lateral-Perpendicular
c)
Large Horizontal Cylinder
Large Horizontal Edge
Large Horizontal Gap
Large Vertical Cylinder
Large Vertical Edge
Large Vertical Gap
8.5
17
28
39
50
Cross Sectionally Averaged Speed (cm.s-1)

downstream of the small and medium diameter cylinder arrays and in the LG region. The second pattern of pectoral-fin use observed involved a single pectoral fin extended laterally with the fin surface perpendicular to the body with or without some fore-aft beating, here called lateral perpendicular pectoral fin deployment (Figure 5.4c). This pattern is consistent with the "low speed turning" pattern described by Drucker and Lauder (2003) for fish maneuvering about the vertical axis (yawing). This was the most widely used pattern, being employed for 100% of the time in the control and 91% of the time for all vertical cylinder arrays. The final pattern of pectoral-fin use was the extension of both pectoral fins, again perpendicular to the body with or without some fore-aft beating (Figure 5.4b). In this situation, the fins were deployed either dorsally or ventrally. This pattern is defined as dorso-ventral perpendicular pectoral fin deployment and was the primary pattern exhibited downstream of the LH cylinders, being used 67% of the time. A combination of this pattern and lateral perpendicular pectoral fin deployment was also prevalent in the MH and LH flow regimes.

Discussion

These experiments sought to evaluate patterns of control-surface deployment during rectilinear swimming in different levels of flow turbulence while station holding. Turbulence was induced by three cylinder arrays with cylinder diameters of 0.4, 1.6, and 8.9 cm with gaps equal to the cylinder diameter. In typical biological laboratory and field situations, there is turbulence in the flow, comprised of a range of eddy sizes. The eddy distribution is comprised of many small eddies and few large eddies. The cylinder arrays were chosen to increase the range of eddy sizes with increasingly large eddies. Furthermore, it has been postulated that eddies with similar diameters to the fish length will pose the greatest challenges to stability. The cylinder diameters were chosen to create such eddies (95^{th} percentile eddy diameters ranged from 1/6 to 1 total fish length). The momentum ratio spanned four orders of magnitude, ranging from eddies which were extremely weak compared to the fish, to eddies which had slightly greater momentum than the fish.

In spite of a four order magnitude change in momentum ratio, no significant difference in dorsal or anal-fin use was discernable across flow regimes (ANCOVA,

$p<0.05$). Both of these fins were deployed nearly all the time across all u_{local} (85% and 100% for the dorsal and anal fins, respectively) while the area that was deployed decreased with u_{local}. Lighthill (1977) showed that the dorsal fin plays an important role in damping body recoil during undulatory swimming. Deployment of the dorsal fin increases the effective body depth of the anterior portion of the fish in order to counter recoil forces due to the caudal fin. The decrease in dorsal fin deployment with increasing swimming speed, also seen by Standen and Lauder (2005) and Liao (2002) not associated with transition from labriform to body/caudal fin propulsion, is postulated to be the result of a greater ability to dampen recoil forces with increasing speed (therefore less body depth is required). The anal fin was always deployed, and while its location and alignment in the lateral plane would provide an appropriate moment arm for countering yawing moments, it is likely that the anal fin was primarily being used as a propulsive extension of the caudal fin, given its continuous deployment across all experiments (Standen and Lauder 2005 and 2007).

The pectoral fins represent the largest control surfaces anterior to the center of mass. Their anterior location makes them important control features for rapid response to turbulent flow due to the positive feedback of forces that occur with the deployment of fins anterior the center of mass. The rapid and appropriate deployment of anterior fins can counter rotational perturbations prior to the onset of rotational displacements (Harris 1936, Weihs 1972, 1993, 2002, Aleyev 1977, Drucker and Lauder 2003, Webb 2006, Higham 2007). While the anterior position of the pectoral fins results in rapid body response (thereby maintaining appropriate postural alignment to the flow), the unstable nature of anterior control systems leads to the possibility of over-correction, against which the self-corrective trimming forces from the posterior paired fins are likely used (Harris 1936, 1938, Fish and Shannahan 2000, Fish 2002, Higham 2007). In these experiments it was consistently observed that when the pectoral fins were deployed, the pelvic fins were also deployed.

While posterior fin surfaces are “self correcting” in rectilinear flow, in the sense that forces on the fins act to realign the body with the local flow direction, the realignment force is a function of the body angle of attack meaning that for a corrective force to exist the body must first be misaligned to the flow (Robinson and Laurmann

1956, Weihs 1993). This downstream self-correction, while stable in the time-averaged sense, results in a wobbling pattern in the presence of flow perturbations (Robinson and Laurmann 1956, Cotel and Webb 2004). This wobbling is presumed to increase drag on the system (Pedley and Hill 1999, Wang 2000); therefore, rapid correction to flow perturbations before the onset of displacement, followed by minor corrective trimming, is expected to reduce energy requirements for the fish system. While pectoral-fin use is shown to increase with increasing eddy momentum, the usage statistics do not differentiate between horizontal and vertical eddy orientation (e.g., the percentage time the pectoral fins are deployed in the LH flow regimes is the same as the percentage time the pectoral fins are deployed in the LV flow regimes).

The pectoral and pelvic fins tended to be used simultaneously as anterior (rapid-response) and posterior (self correcting) control surfaces with respect to center of mass. When the pectoral fins were deployed, the pelvic fins were also deployed. As the turbulent eddy momentum ratio increased, the percentage time and percentage area of pelvic and pectoral fin deployment increased. The time and area deployed were taken as indicators of the relative effort required to maintain stability. In the flow regimes with the largest eddy momentum (LC and LE), pectoral and pelvic fins were deployed nearly continuously implying that these flow regimes were providing significant destabilizing forces against which the paired-fin system was maximized. Eddies with a diameter similar to that of a fish are expected to produce large moments on the fish body. Chapter III predicted that the simplest way for a fish to counter these moments was through its own momentum which would act to counter perturbation accelerations from the eddy. Another way to counter the eddy moments is through the deployment of control surfaces. The control surfaces on a fish are positioned orthogonally across the fish body (Webb 1998) with respect to the center of mass. Therefore, when the fins are deployed, the force acting on the fin from the water will result in a moment about the fish center of mass. It is therefore expected that as the perturbing moments on the fish from eddies increases, the percentage time and area that the fins are deployed should increase.

Chapter III showed that it was in flow regimes with large eddy momentum (LC and LE) where postural spills (rapid head rotation followed by downstream translation) occurred frequently (Figure 3.12b). Pectoral fin use was shown to increase with the

momentum ratio with paired fin percentage time and percentage area being nearly 100% above a momentum ratio around one. While the pectoral fin usage was shown in Figure 5.3, similar increases in deployment area and time were noted to exist for the pelvic fin deployment as well.

Additionally, cylinder arrays were oriented either vertically or horizontally. As a result, eddies were predominantly oriented vertically downstream of vertical arrays or horizontally with horizontal arrays. These orientations were anticipated to create perturbations tending predominantly to challenge fish in yawing and pitching, respectively. Such effects were seen for both the medium and large cylinder array treatments.

The effect of eddy orientation resulted in differences in the pattern of pectoral-fin deployment. In flow regimes where eddies primarily rotated about a vertical axis, and therefore were expected to impart yawing perturbations on the fish, pectoral-fin deployment was asymmetric (i.e. in most cases only one pectoral fin was deployed), lateral to the body and perpendicular to the flow (Figure 5.4c). The asymmetric deployment of pectoral fins in a fore-aft direction is expected to cause a yawing moment about the fish center of mass. This same pattern of pectoral fin deployment has previously been described by Drucker and Lauder (2003) for yawing maneuvers and by Liao (2007) to maintain position in a vertically oriented (yawing) Karman vortex street. The lateral-perpendicular pectoral fin deployment in the presence of vertical eddies is therefore interpreted as a rapid counter-yawing technique which is accompanied by the self-correcting forces from the pelvic fin deployment.

Similarly, in the presence of horizontally rotating eddies, which are expected to impart pitching perturbations on the fish, both pectoral fins were deployed simultaneously either dorsally (curled above the pectoral-body base) or ventrally (curled below the pectoral-body base) and perpendicular to the flow (Figure 5.4b). This pattern of deployment is expected to induce pitching moments about the fish center of mass. The dorso-ventral perpendicular pattern, in concert with the pelvic fin deployment is therefore interpreted as a counter-pitching technique that is used in the presence of pitch-inducing turbulent eddies.

Pectoral-fin use for the control and small cylinder flow regimes were similar and predominantly followed the lateral-perpendicular pattern. For these flow regimes pectoral-fin use was low, yet it appears that when the fins were deployed, they were countering yawing perturbations. Given the small eddy momentum compared to the fish (momentum ratio < 1/50), it is likely that the pectoral fins were countering other destabilizing mechanisms such as the propulsion-based recoil rather than perturbations due to turbulence (Lighthill 1977, Webb 2003).

Unexpectedly, at the lowest $\bar{u}$, a third pectoral fin deployment pattern was observed. The lateral-horizontal pectoral fin deployment involved one or both pectoral fins being extended perpendicular to the body with the control surface oriented dorso-ventrally, with vertical beating (Figure 5.4a). The mechanics of this orientation should produce rolling moments and is therefore interpreted as a counter-rolling technique. The presence of this third pattern at the lowest swimming speeds across all three cylinder treatments suggests that other control deployments may produce extraneous rolling moments on the fish at low speeds. At higher speeds these same moments may or may not exist, yet under these conditions body trimming would likely play a larger corrective role.

Increased fin deployment time and area as seen in these experiments for the pectoral and pelvic fins was expected to lead to increased drag and hence increased aerobic costs as indicated by a reduction in the 2-min u_{crit}. However, while substantial increased fin deployment occurred in the medium cylinder array treatments no reduction in the 2-min u_{crit} was observed. The increase in fin deployment without a corresponding decrease in critical swimming speed implies that the costs of fin deployment are minimal compared to the costs of recovery from spills discussed in Chapter 3.

The role of the caudal fin in the presence of turbulent eddies was previously reported in Chapter IV. In the large cylinder flow regimes (where the momentum ratio approached unity) tail beat amplitude increased while tail beat frequency decreased. There was no distinction in these two parameters nor with body wavelength, tail angle of attack, or body depth across cylinder orientation ($p<0.05$). These parameters are all commonly associated with propulsion. The caudal fin also represents the control surface with the greatest area with respect to the flow and moment arm from the center of mass

for countering flow perturbations, especially for yawing moments. Fine-scale body/caudal fin motions such as fin ray kinematics (Lauder and Drucker 2004) may provide information on the caudal fin role in stability in turbulent flows. It is likely, however, that separating propulsion requirements from stability requirements will be as difficult as the classic problem of separating propulsive forces from drag forces in fish-like swimming (Schultz and Webb 2002).

References

Alexander, R. McN. (1965). The lift produced by the heterocercal tails of Selachii. *Journal of Experimental Biology* **43**, 131-138.

Aleyev. Y. G. (1977). *Nekton*. Junk, The Haque.

Archer, S. D. and Johnston, I. A. (1989). Kinematics of labriform and subcarangiform swimming in the Antarctic fish *Notothenia neglecta*. *Journal of Experimental Biology* **143**, 195-210.

Blake, R. W. (1979). The mechanics of labriform locomotion I Labriform locomotion in the angelfish (*Pterophyllum eimekei*): An analysis of the power stroke. *Journal of Experimental Biology* **82**, 255-271.

Blake, R. W. (1980). The mechanics of labriform locomotion II An analysis of the recovery stroke and the overall fin-beat cycle propulsive efficiency in the angelfish. *Journal of Experimental Biology* **85**, 337-342.

Brett, J. R. and Sutherland, D. B. (1965). Respiratory metabolism of pumpkinseed *(Lepomis gibbosus)* in relation to swimming speed. *J. Fish. Res. Bd Can.* **22**: 405-9.

Cada, G. F. and Odeh, M. (2001). Turbulence at hydroelectric power plants and its potential effects on fish. *Report to Bonneville Power Administration*, Contract No. 2000AI26531, Project No. 200005700, 1-37.

Cotel, A. J. and Webb, P. W. (2004). Why won't fish wobble? Proc. 17th ASCE Engineering Mechanics Conference, June 13-16, 2004, University of Delaware

Cotel, A. J., Webb, P. W. and Tritico, H. M. (2006). Do brown trout choose locations with reduced turbulence? *Transactions of the American Fisheries Society* **135**, 610-619.

Drucker E. G. (1996). The use of gait transition speed in comparative studies of fish locomotion. *American Zoologist* **36**, 555-566.

Drucker, E. G. and Lauder, G. V. (1999). Locomotor forces on a swimming fish: three-dimensional vortex wake dynamics quantified using digital particle image velocimetry. *Journal of Experimental Biology* **202**, 2393-2412.

Drucker, E. G. and Lauder, G. V. (2001). Wake dynamics and fluid forces of turning maneuvers in sunfish. *J of Exp. Bio.* **204**, 431-442.

Drucker, E. G. and Lauder, G. V. (2003). Function of pectoral fins in rainbow trout: behavioral repertoire and hydrodynamic forces. *J. exp. Biol.* **206**, 813-826.

Enders E C, Boisclair D, and Roy A G. (2003). The Effect of Turbulence on the Cost of Swimming for Juvenile Atlantic Salmon. *Canadian Journal of Fisheries and Aquatic Science* **60**, 1149-1160.

Farlinger, S. and Beamish, F. W. H. (1977). Effects of time and velocity increments in the critical swimming speeds of largemouth bass (*Micropterus salmoides*). *Transactions of the American Fisheries Society* **106**: 436-439.

Fish, F. E. and Shannahan, L. D. (2000). The role of the pectoral fins in body trim of sharks. *J. Fish Biol.* **56**: 1062-1073.

Fish, F. E. (2002). Balancing requirements for stability and maneuverability in cetaceans. *Integrative and Comparative Biology* **42**: 85-93.

General Pixels. (2000). *PixelFlow 2.1: Installation and User's Guide.*

Gharib, M. and Dabiri, D. (2000). An overview of digital particle image velocimetry in *Flow Visualization: Techniques and Examples* (ed Smits A and Lim T T) London: Imperial College Press.

Gibb A. C., Jayne B. C. and Lauder G. V. (1994). Kinematics of pectoral fin locomotion in the bluegill sunfish *Lepomis macrochirus*. *Journal of Experimental Biology* **189**, 133-161.

Harris, J. E. (1936). The role of fins in the equilibrium of swimming fish. I. Wind-tunnel tests on a model of *Mustelus canis* (Mitchell). *J. exp. Biol.* **13**, 476-493.

Harris, J. E. (1938). The role of the fins in the equilibrium of swimming fish II. The role of the pelvic fins. *J. exp. Biol.* **15**, 32-47.

Higham T. E. (2007). Feeding, fins, and braking maneuvers: Locomotion during prey capture in centrarchid fishes. *Journal of Experimental Biology* **210**, 107-117.

Huang, H., Dabiri, D. and Gharib. M. (1997). On errors of digital particle image velocimetry *Meas. Sci. Technol.* **8**: 1427-40.

Keast, A. (1985). The piscivore feeding guild of fishes in small freshwater ecosystems. *Environmental Biology of Fishes* **12(2)**, 119-129.

Korsmeyer, K. E., Steffensen, J. F. and Herskin, J. (2002). Energetics of median and paired fin swimming, body and caudal fin swimming, and gait transition in parrotfish (*Scarus schlegeli*) and triggerfish (*Rhinecanthus aculeatus*). *Journal of Experimental Biology* **205**, 1253-1263.

Lauder, G. V. and Drucker, E. G. (2004). Morphology and experimental hydrodynamics of fish fin control surfaces. *IEEE Journal of Ocean Engineering* **29(3)**, 556-571.

Liao, J. C. (2002). Swimming in needlefish (Belonidae): anguiliform locomotion with fins. *Journal of Experimental Biology* **205**, 2875-2884.

Liao, J. C. (2007). A review of fish swimming mechanics and behavior in altered flows. *Philosophical Transactions of the Royal Society B* **362(1487)**, 1973-1993.

Lighthill, J. (1977). Mathematical theories of fish swimming. In *Fisheries Mathematics* (J. H. Steele, Ed.). Academic Press, New York.

Lupandin, A. I. (2005). Effect of Flow Turbulence on Swimming Speed of Fish. *Biology Bulletin* **32(5),** 558-565.

Maxwell, S. E. and Delaney, H. D. (2004). *Designing experiments and analyzing data*. 2nd Edition. Lawrence Erlbaum Associates, Inc. Mahwah NJ.

McLaughlin, R. L. and Noakes, D. L. G. (1998). Going against the flow: an examination of the propulsive movements made by young brook trout in streams. *Can. J. Fish. Aquat. Sci*. **55,** 853–860.

Odeh, M., Noreika, J. F., Haro, A., Maynard, A., Castro-Santos, T. and Cada, G. F. (2002). Evaluation of the Effects of Turbulence on the Behavior of Migratory Fish. Final Report for the U S Department of Energy Bonneville Power Administration Department of Fish and Wildlife, DOE/BP-00000022-1.

Pavlov, D. S., Lupandin, A. I. and Skorobogatov, M. A. (2000). The Effects of Flow Turbulence on the Behaviour and Distribution of Fish. *Journal of Ichthyology* **40(S2**), S232-261.

Pedley, T. J. and Hill, S. J. (1999). Large-amplitude undulatory fish swimming: fluid mechanics coupled to internal mechanics. *Journal of Experimental Biology* **202**, 3431-3438.

Robinson, A. and Laurmann, J. A. (1956). *Wing theory.* Cambridge University Press, Cambridge.

Schultz, W. W. and Webb, P. W. (2002). Power requirements of swimming: Do new methods resolve old questions? *Integrative and Comparative Biology* **42**, 1018-1025.

Smith, D. L., Brannon, E. L. and Odeh. M. (2005). Response of Juvenile Rainbow Trout to Turbulence Produced by Prismatoidal Shapes. *Transactions of the American Fisheries Society* **134**, 741-753.

Standen, E. M. and Lauder, G. V. (2005). Dorsal and anal fin function in bluegill sunfish Lepomis macrochirus: three-dimensional kinematics during propulsion and maneuvering. *Journal of Experimental Biology* **208**, 2753-2763.

Standen E. M. and Lauder G. V. (2007). Hydrodynamic function of dorsal and anal fins in brook trout (*Salvelinus fontinalis*). *Journal of Experimental Biology* **210**, 325-339.

Thorson D. H. and Westneat M. W. (2005). Diversity of pectoral fin structure and function in fishes with labriform propulsion. *Journal of Morphology* **263(2)**, 133-150.

Tritico HM, Cotel AJ, and Clarke JN. (2007). Development, testing and demonstration of a portable submersible miniature particle imaging velocimetry device. *Measurement Science and Technology* **18**, 2555-2562.

Wang, Z. J. (2000). Vortex shedding and frequency selection in flapping flight. *Journal of Fluid Mechanics* **410**, 323-341.

Webb, P. W. (1998). Entrainment by river chub Nocomis micropogon and smallmouth bass Micropterus dolomieu on cylinders. *J. Exp. Biol*. **201**, 2403–2412.

Webb, P. W. (2002). Control of Posture, Depth, and Swimming Trajectories of Fishes. *Integrative and Comparative Biology* **42**, 94-101.

Webb, P. W. (2004). Response latencies to postural disturbances in three species of teleostean fishes. *The Journal of Experimental Biology* **207**, 955-961.

Webb, P. W. (2006). Stability and maneuverability. In *Fish Physiology* (eds R. E. Shadwick and G.V. Lauder), pp. 281-332. Elsevier Press, San Diego.

Weihs, D. (1972). A hydrodynamical analysis of fish turning maneuvers. *Proc. R. Soc. Land. B.* **182**, 59-72.

Weihs, D. (1993). Stability of aquatic animal locomotion. *Contemp. Math*. **141**, 443-461.

Weihs D. (2002). Stability versus maneuverability in aquatic locomotion. *Integrative and Comparative Biology* **42**, 127-134.

Wilga, C. D. and Lauder, G. V. (1999). Locomotion in sturgeon: function of the pectoral fins. *Journal of Experimental Biology* **202**, 2413-2432.

Wilga, C. D. and Lauder, G. V. (2002). Function of the heterocercal tail in sharks: quantitative wake dynamics during steady horizontal swimming and vertical maneuvering. *Journal of Experimental Biology* **205**, 2365-2374.

Chapter VI

Development, Testing, and Demonstration of a Portable Submersible Miniature Particle Imaging Velocimetry Device

Introduction

Eddy dynamics are expected to affect ecosystem function through mixing and momentum exchange processes ranging from predator-prey interactions to sediment transport capacities. There have been an increasing number of calls for studies which investigate the spatial scale of turbulence in natural aquatic environments (Landry et al 1995, Nikora et al 2003, Standen et al 2004). The most common device currently used for the investigation of turbulence in the natural aquatic environment is the Acoustic Doppler Velocimeter (ADV). ADVs provide high resolution temporal velocity data at a single point in the flow stream. They therefore provide excellent temporal resolution but spatial investigations must either work within the constraints of Taylor's frozen turbulence approximation or utilize arrays of ADVs which collect velocity data simultaneously (Roy et al 2004).

Successful attempts have been made in the past at developing submersible PIV systems but these systems have not been developed in such a way that they are easily transported or setup in natural environments. Submersible PIV systems have been developed to examine the bottom boundary layer of the ocean by Bertuccioli et al (1999) and Nimmo-Smith et al (2002). The PIV system used in these experiments was powered by ship main power and lowered to the sea floor using on-board cranes. The system utilized a 1024 by 1024 CCD camera (Kodak Megaplus XHF) at 30 fps in conjunction with a 350 mJ pulsed laser (Cynosure Inc.) operating at a wavelength of 594 nm. The laser light was supplied, via fiber optics, to the bottom of the ocean along with the camera system in a waterproof enclosure. The illuminated measurement area was approximately 20 cm by 20 cm (Bertuccioli et al 1999). Several years later, they re-designed the system

to record an illuminated area of 35 cm by 35 cm. This was done by using two 2048 by 2048 CCD cameras operating simultaneously (Nimmo-Smith et al 2002). On board the ship was a desktop computer with an Alacron frame grabber to store the gathered data. The largest reported speed is approximately 17 cm/s. Alternatively, miniature PIV systems have also been developed by Chetelat et al (2001) and others for the investigation of microscopic flow, however these systems are not designed for field use. We have successfully developed a PIV system which is both submersible and portable for specific field use, while keeping the cost and complexity of the system at a minimum.

System Overview

The newly developed PIV system works as follows: A one mega pixel high-resolution CCD camera collects images and outputs a TTL signal which is fed into a programmable microprocessor board (Figure 6.1a). This signal lets the microprocessor know when the images are being captured allowing for synchronization between the camera and a laser chopper wheel (Figure 6.1b). The chopper wheel chops the continuous emission from a handheld laser system into short asynchronous pulses which illuminate the flow in short durations at short pulse separation times. The pulse width and separation can be varied by changing the aperture and rotational velocity of the wheel, for the validation presented below pulse durations and pulse separations ranged from 6 to 20 ms. The short pulse durations avoid particle streaking in the images while the short pulse separation times reduce the distance particles travel between images. Reducing the distance particles travel between images allows the cross correlation integration windows to be smaller and reduces the frequency of particles moving into or out of the laser sheet (ghost particles) (Raffel et al 1998). The laser and timing systems are powered by on-board 3 volt and 9 volt batteries which were changed daily to ensure maximum and consistent power supply. Both systems have on/off switches to allow for reduced power demand. The laser camera system housings have a combined volume of 0.017 m^3 and weighs 7.5 kg which allows for easy transport and setup.

Camera System-A UniqVision UP-1830 10-bit black and white CCD camera was modified in two ways for PIV data collection and used in this system. The first camera modification enabled image data which have been transferred to the laptop to be

deleted rapidly (within 1 μs) in order to quickly free space for collection of the second laser pulse image (General Pixels 2000, UniqVision email communication). This modification allows for shorter pulse separation times leading to an increased range of flows which can be captured using PIV analysis (Gharib and Dabiri 2000, Dabiri 2003). The second modification changed the TTL output to be a continuous +5 Volt signal interrupted by a 2 ms 0 Volt signal 31 μs after the optical camera shutter opens allowing for synchronization of the image capture with laser pulsing. This specification allowed for synchronization between the camera and the laser chopper wheel. The camera captures 1 mega pixel images at a rate of 30 fps. The images are transmitted via a 10 meter Camera-Link cable to a PCMCIA frame grabber card. The user, either in a boat or on shore, controls the image acquisition through use of a laptop computer. The software for the card (FrameLink) is then used to capture and store images. A standard zoom lens

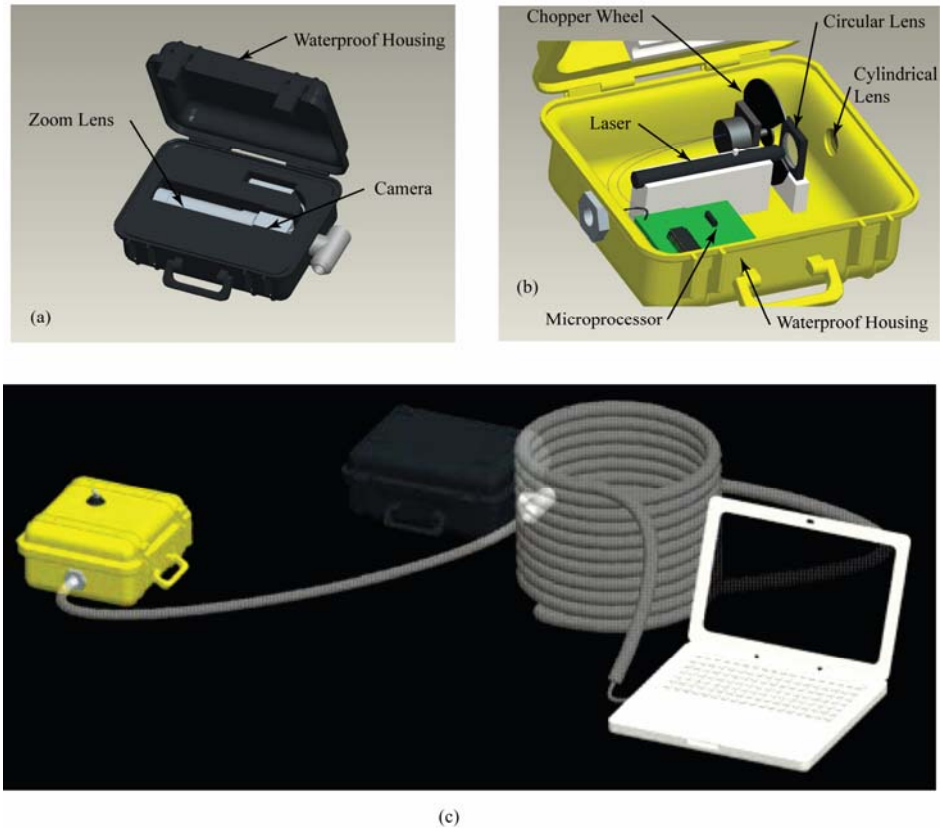

Figure 6.1: System Schematic a) Camera system and housing b) Laser system and housing c) System overview including laptop and connecting cables

(Toyo Optics 12.5-75 mm) is used and the camera is powered by a 12 volt battery. Use of a zoom lens, rather than a wide angle lens reduces parallax error. Additionally, the path that the laser light travels between the particle and camera lens is exactly the same as in standard PIV systems (particle → water → Plexiglas → air → lens) avoiding the need for additional corrections due to light refraction.

The camera depth of field is important in microscopic PIV investigations to determine the depth over which particles are tracked (Olsen and Adrian 2000, Malkiel et al 2003). In the case of field PIV systems the light sheet width (approximately 1 mm in this system) is the determining parameter. The depth of field does, however, determine whether unavoidable naturally occurring objects appear in the background of collected images. These background objects would show up on the PIV images as groups of static light or dark pixels reducing the calculated velocity from the cross-correlation analysis. Two steps were taken to avoid this potential error. First, a camera lens system was chosen such that the depth of field was less than three centimeters (aperture = f1.8, lens focal length = 75 mm, distance to light sheet = 1 m, and circle of confusion = 0.05 mm, Ray 2002). Additionally, during laboratory testing the system was run with all lights turned off and field collection was conducted at night to avoid illuminating background objects.

Laser System-The 90 mW hand held laser produces a 1.6 mm diameter circular beam which operates at 532 nm with a divergence angle of 0.9 mRad. It runs continuously once turned on via a switch on the waterproof housing. To create the sheet of light necessary to obtain PIV data, the beam is directed through a 1000 mm focal lens (which focuses the beam to less than 1 mm within the region of interest 1000 mm from the lens) and then through two 12.5 mm cylindrical lenses to create a sheet of light. At 1000 mm the laser sheet has a practical width of 8 cm. The chopper wheel is located in front of the optical lenses so that the laser beam is first chopped before being transformed into a laser sheet.

Timing System-The TTL signal from the camera is plugged into a microprocessor which drives a variable speed motor. The motor is attached to a chopper wheel which rotates to modulate the duration and timing of laser emission. The microprocessor allows the user to adjust the speed of the wheel, via a rheostat, to

accomplish this synchronization. The microprocessor and chopper wheel are powered using a 9 volt battery within the laser housing.

Housing System-The system is enclosed within two connected waterproof cases which were modified for the system. One case houses the laser, optics, beam chopper, and microprocessor; the other case the camera. The systems are inter-dependent in two ways. First, the camera TTL signal is fed, via coaxial cable, between the cases through a 2 meter hose, from the camera, to the microprocessor. Second, the camera case is connected to the shore/boat via a 10 meter hose which contains the power cord for the camera and the Camera-Link cable which transmits the raw images to a laptop.

The modifications made to the cases are as follows: Two holes were cut, one on each case, to allow for the hose between the cases. On the camera case there was a hole cut for the hose to the surface. There was also a hole cut in the side for the camera to capture images. The hole was covered with a square of ¼" Plexiglas and siliconed in place. On the laser case, a hole was cut in the top so as to allow for the installation of a wing nut-rod system which allows one to turn the laser on/off without opening the case. Also, a hole was cut in the side of the laser case so as to insert the two cylindrical lenses and allow the laser beam to pass through the case. This was done by placing the lenses back to back inside a small o-ring and sealing the lenses into the hole.

Post Processing-Standard post processing techniques may be used on the digital images (Huang et al 1997, Lang and Manglano 2004, Adrian 2005). The contrast of all images was increased using Adobe Photoshop® contrast tool in order to facilitate visual inspection of the appropriate region of interest changing the number of outlier correlations by less than 0.3%. The contrast was increased uniformly for all images so as to maintain consistency in pixel illumination between images. For the comparison in Section 2 and the demonstration in Section 3 the contrast was increased by 75 contrast units for all images. Image pairs were selected which had only a single exposure per frame in two sequential frames. These image pairs were uploaded into PixelFlow, a PIV collection and post processing software developed by General Pixels (Gharib and Dabiri 2000, General Pixels 2000). A cross correlation algorithm is performed on 32x32 pixel windows within each image pair to determine the average particle displacement. The 32x32 pixel windows are calculated every 16 pixels across the entire region of interest to

obtain a vector map of the flow. Outliers are removed if the resulting vector is ±3 pixels/s different than its neighboring vectors (General Pixels 2000, Bartol et al 2005, Samothrakis and Cotel 2006a) and a spatial smoothing algorithm is employed to remove discontinuities. PixelFlow is then used to calculate the vorticity field (General Pixels 2000, Bartol et al 2003) and the vector and contour maps are plotted using TecPlot®.

Validation

Validation of a new technology requires comparison of results with accepted measurement devices in canonical flows. Here we begin that process by investigating the flow behind a circular cylinder with a standard laboratory PIV and the newly developed underwater PIV system.

Laboratory PIV System-A PIV system developed by General Pixels (General Pixels 2000) was used for comparison purposes. The system consists of a 120 mJ NdYAG dual-head 532 nm pulsed laser (NewWave Gemini), timing box, 1 mega pixel 10-bit 30 fps UniqVision black and white CCD camera. The camera is driven by a dedicated PC which stores the digital images. The system is run by PixelFlow software also used to post-process the image pairs. The system has been used on a variety of flows (Huang et al 1997, Gharib and Dabiri 2000, Samothrakis and Cotel 2006b) and compares well with other flow measurement tools (Westerweel et al 1997, Huang et al 1997, Liu et al 1991).

Flow Set-up-Tests were conducted in a model 29899 low turbulence closed circuit water tunnel designed by Engineering Laboratory Design, Inc. The test section of the flume is 2.44 m long with a square cross section of 61 cm by 61 cm. Water depth was 60 cm and a single 1.6 cm diameter poly-vinyl chloride cylinder was placed horizontally in the flume at a depth of 30 cm. Tests were conducted at cross-sectionally averaged velocities of 5.5, 9.1, and 12.9 cm/s which correspond to discharge based Reynolds numbers of $3.3x10^4$, $1.4x10^5$, and $7.9x10^5$, respectively. The flume was seeded with 1.2 ppm titanium dioxide particles which had a mean diameter of 1.0 μm (Lin et al 2003).

PIV Set-up-The physical configurations of the underwater and laboratory PIV setups were similar. The laser sheet for each system was shone through the Plexiglas floor to illuminate the flow directly downstream of the cylinder while the camera for each

system was setup perpendicular to the laser sheet to capture images of the illuminated flow. The optics for the laboratory PIV were setup such that a region approximately 30 cm by 30 cm was illuminated downstream from the cylinder while the camera recorded a region approximately 20 cm by 20 cm resulting in an image magnification of 33 pixels/cm (Figure 6.2). The underwater PIV system necessarily illuminated a smaller region of the flow (5 cm by 7 cm) due to the lower intensity of the battery powered laser (Figure 6.2). The camera recorded a region of 10 cm by 10 cm resulting in an image magnification of 58 pixels/cm. The pulse duration for the laboratory PIV for all tests was set to 100 μs while the pulse separations were set to 9, 8, and 4 ms for, for Reynolds numbers of $3.3x10^4$, $1.4x10^5$, and $7.9x10^5$, respectively. The pulse duration for the underwater PIV was 20, 6, and 6 ms for Reynolds numbers of $3.3x10^4$, $1.4x10^5$, and $7.9x10^5$, respectively. The pulse separations for the underwater PIV were 20, 13, and 6 ms for Reynolds numbers of $3.3x10^4$, $1.4x10^5$, and $7.9x10^5$, respectively. The appropriate pulse separations for the underwater PIV were calculated such that the average particle displacement between image pairs would be less than one fourth of the integration window ($l_p \leq 0.25 l_w$) (Westerweel et al 1997, General Pixels 2000, Bernal 2003). The equation used and modified for the above units is:

$$\Delta t = \frac{250 \cdot LW}{M \cdot U_f} \tag{6.1}$$

Where Δt is the pulse separation in milliseconds, LW is the integration window in pixels, M is the magnification in pixels per centimeter, and U_f is the flow speed in centimeters per second. Pulse separations for the lab PIV system were originally determined using Equation (6.1) and subsequently shortened in order to minimize the number of outlier pixels. The pulse duration for the underwater PIV images was determined by balancing the need for increased illumination time for the low laser power system and the need to avoid particle streaking. It was determined by visual inspection of raw images that a minimum of 6 ms exposure was necessary to provide sufficient particle illumination. For the maximum flow inspected in this evaluation (15 cm/s) the particle displacement within each pulse is approximately 0.9 mm (5.2 pixels). Analysis of raw images collected at 15 cm/s indicate an apparent particle size of approximately 5 pixels along the flow path axis by 2 pixels in the transverse axis for an average particle diameter

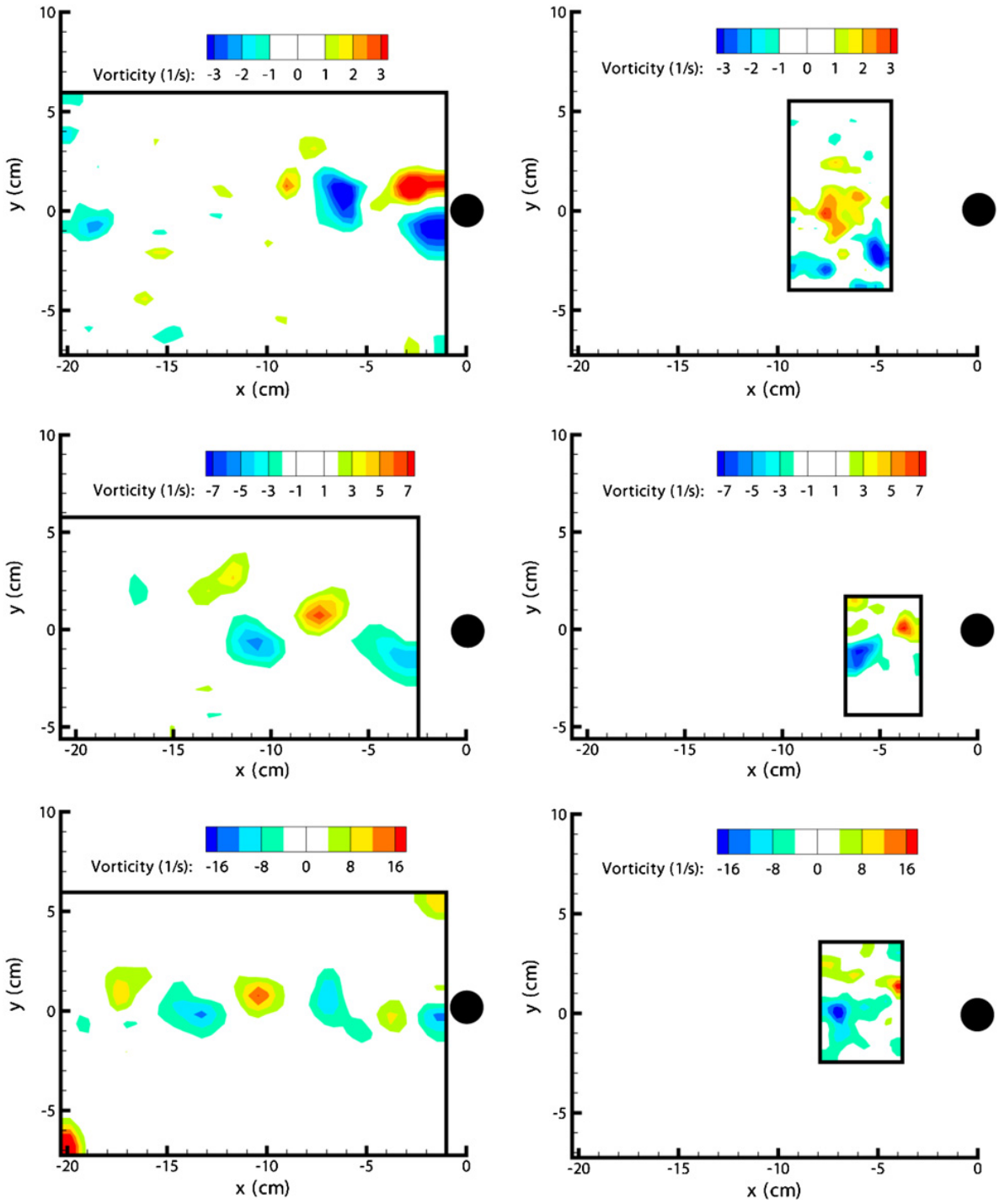

Figure 6.2: Selected vorticity plots from lab PIV (left) and underwater PIV (right) for discharge Reynolds numbers of a) 3.3×10^4 b) 1.4×10^5 and c) 7.9×10^5. The lab PIV illuminates a larger area than the underwater PIV. The black circle represents the obstruction cylinder; the x axis is the downstream distance from the cylinder while the y axis is the vertical distance from the cylinder centerline, flow is from right to left across the sheet. Vorticity scales are adjusted between flows but are the same between lab and underwater PIV images.

of 3.5 pixels. Huang et al 1997 found that apparent particle size did not affect mean bias or root mean square errors for the particles that they tested (1.4 and 3.6 pixels in diameter). For the 4 cm/s flow pulse durations could be increased to 20 ms due to the slower particle speed allowing for images to be collected using the camera shutter set to 20 ms. Due to the greater laser power in the lab PIV system particles could be illuminated with 100 μs pulse durations.

Validation Results-Image pairs were collected and analyzed using the methods described above. For each of the three flows 50 image pairs (100 images) were collected using the lab PIV. One hundred images were collected at 30 fps for each of the three flows using the underwater PIV, however, due to the nature of the chopper wheel only a portion of the 100 images corresponded to image pairs. For Reynolds number flows of $3.3x10^4$ the chopper wheel was not used due to the small velocities and 40 sequential velocity pairs were used to calculate flow variables. For the quicker flows at $Re=1.4x10^5$ and $7.9x10^5$ where the chopper wheel was used; 17 and 21 image pairs, respectively, were used for calculations. The mean and standard deviation velocity, vorticity, and average eddy diameter are reported for three flow conditions in Table 6.1 following Lorenco et al 1994, Koutsiaris et al 1999, Perrin *et a*l 2006, Saikrishnan et al 2006.

The mean velocities measured by the laboratory and underwater PIV systems were comparable for each of the three flows (Table 6.1). The average velocity was calculated over the entire interrogation window of the underwater PIV and compared to the average velocity from the lab PIV calculated over the same area (Figure 6.2). Mean velocities recorded by the underwater PIV were within 2% of the laboratory PIV values for Reynolds numbers of $7.9x10^5$ and $1.4x10^5$. The $3.3x10^4$ Reynolds number velocities measured by the underwater PIV were 0.5 cm/s (9.4%) greater than that of the laboratory PIV. The slight overestimation of velocity for the slowest flow is most likely due to the long pulse separation between images (Raffel et al 1998).

The average vorticity magnitude was also compared between systems with a maximum difference of 3.5% occurring at a Reynolds number of $7.9x10^5$. The average vorticity magnitude was calculated over the entire region of interest of the underwater PIV and compared to the average vorticity magnitude from the lab PIV calculated over

the same area. A sensitivity analysis was conducted on the effect of interrogation window size on vorticity magnitude. Doubling the underwater PIV interrogation window size from 32x32 pixels to 64x64 pixels resulted in a +1.1%, -2.1%, and +0.6% change in average eddy vorticity for the Re $7.9x10^5$, $1.4x10^5$, and $3.3x10^4$ flows, respectively.

Eddies were determined by setting a threshold vorticity equal to 33% of the maximum vorticity measured by the lab PIV which corresponded to 1, 2, and 4 s^{-1} (Figure 6.2). Vortex identification methods vary widely among investigations (Adrian et al 2000, Vollmers 2001, Camussi 2002) but generally produce qualitatively similar results as long as a consistent method and threshold are used across all of the data. The selection of 33% of the maximum vorticity is within the range of thresholds reported in the literature (Adrian et al 2000, Chagnaud et al 2006, Finn and Boghosian 2006) and was chosen as a threshold due to its ability to clearly identify individual eddies. Eddy diameters were determined by calculating eddy area and equivalent eddy diameter assuming that eddies have a 1 to 1 aspect ratio. Average eddy diameters measured by the underwater PIV were on average 26% less than the eddy diameters measured by the laboratory PIV. This is due to the smaller interrogation region available to the underwater PIV compared to the lab PIV. The smaller area of interrogation for the underwater PIV resulted in more partial eddies (i.e. the underwater illuminated a smaller area therefore many eddies were only partially captured causing a smaller recorded diameter). The average difference for the maximum eddy size is 4% across the three runs indicating consistency when only complete eddies are included.

Field Demonstration

The underwater PIV was field tested in the Huron River, Ann Arbor Michigan on January 10, 2007 (Figure 6.3). Average discharge during the data collection was 40.0 m^3/s and varied less than 2% during the data collection period. Flow data just downstream from a 1.2 cm diameter limb just upstream (10 meters) from USGS gauging station 04174500 was collected. Natural particles suspended in the Huron River were sufficient for flow illumination during field collection. Errors due to low particle density have been shown to be significantly reduced when illuminated particle concentrations are greater than 10 per interrogation window (Willert and Gharib 1991, Keane and Adrian

Table 6.1: Comparisons of free stream velocity, vorticity, mean eddy diameter and maximum eddy diameter between Laboratory and Underwater PIV for flow downstream from a 1.6 cm cylinder. Reynolds numbers are based on discharge. Values in parentheses represent ±1 standard deviation about the mean. Note that the standard deviations are not reported for the maximum eddy diameters since they represent the single largest eddy recorded.

	Laboratory PIV	Mini PIV	Percent Difference
Free Stream Velocity	Re $7.9x10^5$:15.3(2.5) cm/s $1.4x10^5$: 8.2 (1.1) cm/s $3.3x10^4$: 5.2 (1.2) cm/s	Re $7.9x10^5$:15.1 (3.4) cm/s $1.4x10^5$: 8.3 (1.6) cm/s $3.3x10^4$: 5.7 (0.9) cm/s	Re $7.9x10^5$: -1.7 % $1.4x10^5$: +1.9 % $3.3x10^4$: +9.4 %
Vorticity	Re $7.9x10^5$:10.77 (0.81) s^{-1} $1.4x10^5$: 4.41 (0.60) s^{-1} $3.3x10^4$: 1.72 (0.22) s^{-1}	Re $7.9x10^5$:10.40 (1.16) s^{-1} $1.4x10^5$: 4.31 (0.80) s^{-1} $3.3x10^4$: 1.69 (0.23) s^{-1}	Re $7.9x10^5$: -3.5 % $1.4x10^5$: -2.1 % $3.3x10^4$: -1.5 %
Mean Eddy Diameter	Re $7.9x10^5$: 1.3 (0.8) cm $1.4x10^5$: 1.7 (0.8) cm $3.3x10^4$: 1.1 (0.8) cm	Re $7.9x10^5$: 1.0 (0.8) cm $1.4x10^5$: 1.1 (0.9) cm $3.3x10^4$: 0.9 (0.8) cm	Re $7.9x10^5$: -24.8 % $1.4x10^5$: -36.6 % $3.3x10^4$: -17.0%
Max Eddy Diameter	Re $7.9x10^5$: 3.1 cm $1.4x10^5$: 3.5 cm $3.3x10^4$: 3.2 cm	Re $7.9x10^5$: 3.3 cm $1.4x10^5$: 3.0 cm $3.3x10^4$: 3.8 cm	Re $7.9x10^5$: +5.9 % $1.4x10^5$: -14.0 % $3.3x10^4$: +20.1 %

1992, Bertuccioli et al 1999). Water collected during field measurements had a turbidity of 37 NTU and had a concentration of 34.8 mg/L resulting in an average of 16 illuminated particles per interrogation window. The PIV system was set up such that the laser system was 1 m downstream and the camera system was 1.2 m transverse to the region of interest (Figure 6.3). This configuration ensured that any disturbances to the flow were convected downstream rather than into the region of interest. The two systems were set perpendicular to each other using right-angle squares though use of a rigid arm connector would simplify future field setups. Fifteen image pairs were collected with the underwater PIV over a single 3.3 second (100 images) data collection event; pulse separation and duration were set to 7 ms and image magnification was 33 pixels/cm.

Point velocity data were collected with an Acoustic Doppler Velocimeter (ADV) in addition to the underwater PIV (Figure 6.4). The ADV was setup 10 cm downstream from the submerged limb and data were collected at a frequency of 30 Hz for two PIV

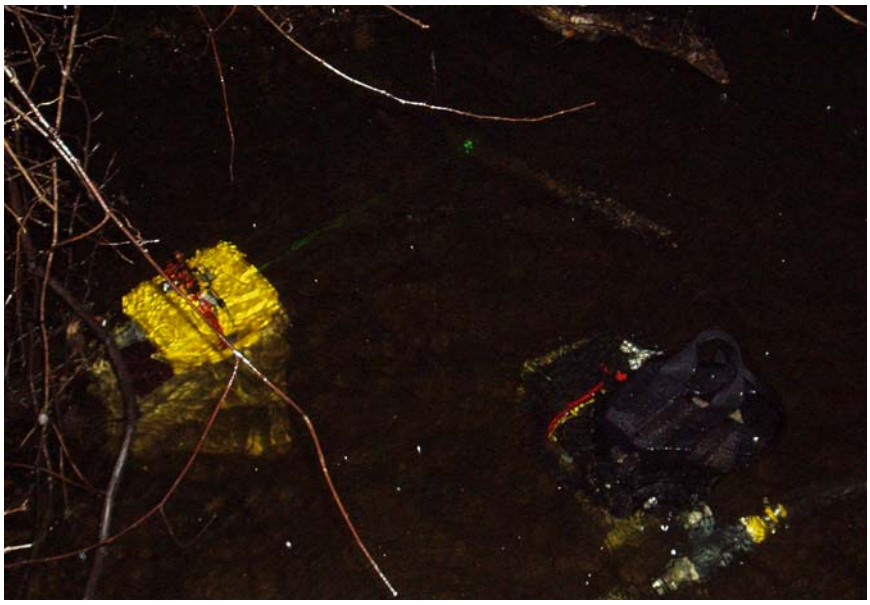

Figure 6.3: Image of underwater PIV being used in the Huron River, MI

parameters were calculated using the techniques described above. Average velocities were calculated for the 0.36 cm^2 area corresponding to the location of the ADV sample volume. Average velocities measured by the underwater PIV and ADV were 11.0 and 10.8 cm/s, respectively. The recorded temporal standard deviation of the velocity fluctuations were 5.0 and 4.8 cm/s for the PIV and ADV systems, respectively. The average eddy size recorded by the underwater PIV was determined to be 0.79 cm and the average vorticity magnitude was 4.0 s^{-1}.

Conclusions

This newly developed underwater and highly portable PIV system has been shown to provide comparable velocity, vorticity fields, and eddy length scales to a standard laboratory PIV system under low to moderate velocity conditions. Tests so far provide high confidence in the underwater PIV results for instantaneous velocities up to 15 cm/s which is a practical range for many lake and low gradient river systems, and boundary layer regions. Velocity measurements from the underwater PIV were within 10% of those recorded by a standard laboratory PIV while vorticity measurements were within 3.5%. Average eddy sizes recorded by the underwater PIV system were 26% less

a)

b)

c)

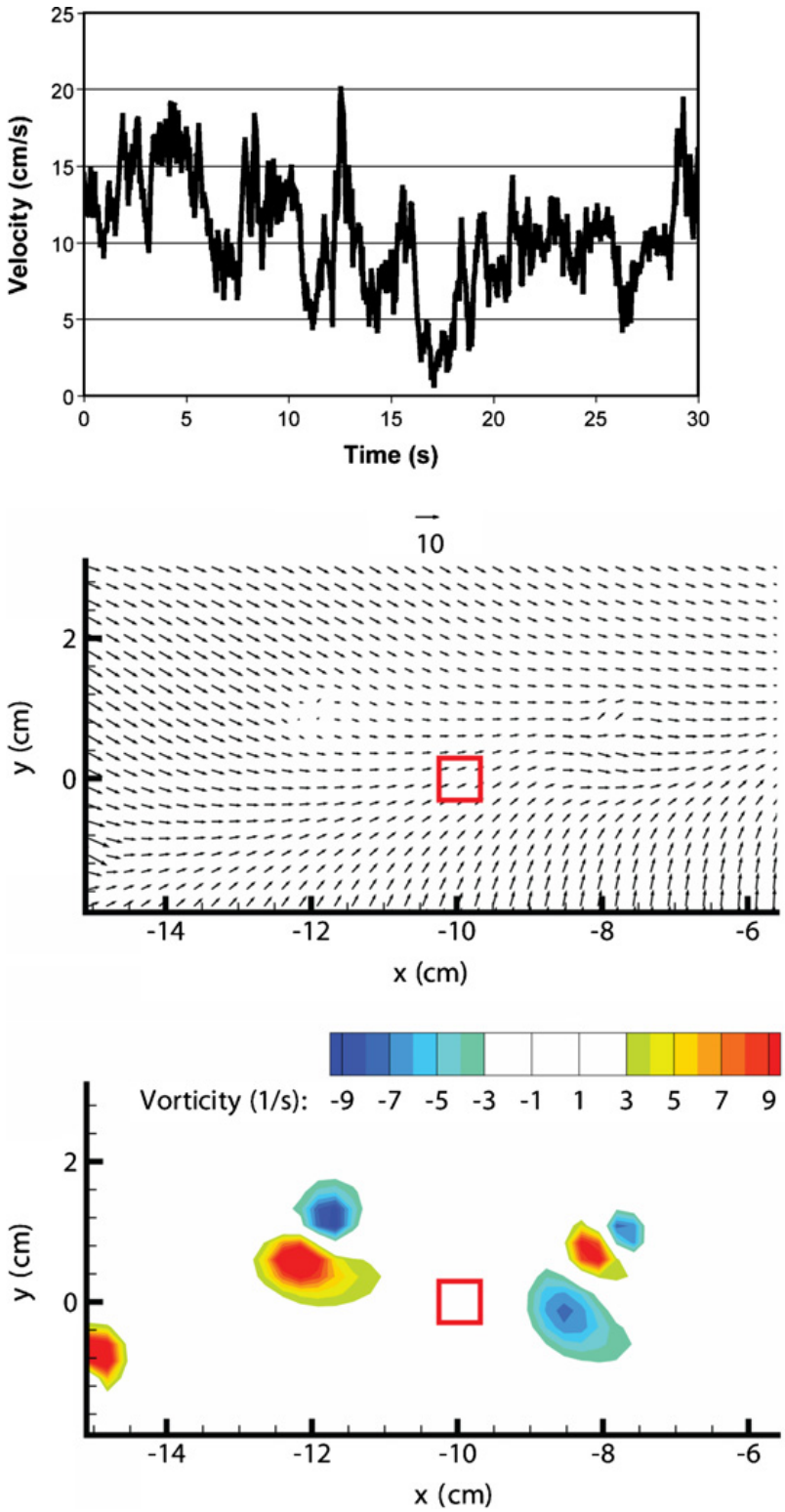

Figure 6.4: Field data. a) ADV timeseries – streamwise velocity plotted b) instantaneous vector field from underwater PIV – reference vector is 10 cm/s c) instantaneous vorticity field from underwater PIV. The limb is located at x=0 cm and the ADV control volume is indicated with a 1 cm^2 red box at x=-10 cm, y=0 cm. Two 2- minute time series data were collected at the same location 15 minutes apart.

than those recorded by the laboratory PIV due to eddy cropping and magnification effects. The system cost $7500 to develop (including laptop but excluding post processing software which can be developed by a user or purchased in addition to the system) and field data in the Huron River was collected using two people over 3 hours making the system comparable to existing ADV systems in price and portability. The spatial velocity maps from the underwater PIV can be used to calculate vorticity and eddy diameters with greater spatial resolution than previously published ADV investigations. The current system can be modified for a larger illumination region by incorporating a 300 mW laser rather than the 90 mW laser used in this study. A stronger laser coupled with shorter chopping times would also increase the range of velocities attainable. The underwater PIV was originally designed for investigations of ecologically relevant turbulence in natural environments. Other obvious uses include investigation of flow over naturally occurring bed forms and groundwater flow into surface water bodies. Another anticipated use is to validate theoretical and numerical models for unsteady flow in natural aquatic systems.

References

Adrian, R. J., Christensen, K. T. and Liu, Z. C. (2000). Analysis and interpretation of instantaneous turbulent velocity fields. *Exp. Fluids* **29**, 275-290.

Adrian, R. J. (2005). Twenty years of particle image velocimetry. *Exp. Fluids* **39**, 159-69.

Bartol, I. K., Gharib, M., Weihs, D., Webb, P. W., Hove, J. R. and Gordon, M. S. (2003). Hydrodynamic stability of swimming in ostraciid fishes: role of the carapace in the smooth trunkfish Lactophrys triqueter (teleostei: ostraciidae). *The J. Exp. Bio.* **206**, 725-44.

Bartol, I. K., Gharib, M., Webb, P. W., Weihs, D. and Gordon, M. S. (2005). Body-induced vortical flows: a common mechanism for self-corrective trimming control in boxfishes. *The J. Exp. Bio.* **208**, 327-44.

Bernal, L. P. (2003). Experimental Methods In Fluid Mechanics: Course Notes L3.5.

Bertuccioli, L., Roth, G. I., Katz, J. and Osborn, T. R. (1999). A submersible particle image velocimetry system for turbulence measurements in the bottom boundary layer. *J. Atm. and Ocean Tech.* **16**, 1635-46.

Camussi, R. (2002). Coherent structure identification from wavelet analysis of particle image velocimetry data. *Exp. Fluids* **32**, 76-86.

Chagnaud, B. P., Bleckmann, H. and Engelmann, J. (2006). Neural responses of goldfish lateral line afferents to vortex motions. *The J. Exp. Bio.* **209**, 327-42.

Chetelat, O., Yoon, S. Y. and Kim, K. C. (2001). Design and construction of a miniature PIV (MPIV) system. *Korean Soc. Mech. Eng. J.* **15(12)**, 1775-83.

Dabiri, D. (2003). On the interaction of a vertical shear layer with a free surface. *J. Fluid Mech.* **480**, 217-32.

Finn, L. I. and Boghosian, B. M. (2006). A global variational approach to vortex core identification. *Physica* A **362**, 11-6.

General Pixels (2000). PixelFlow 2.1: Installation and User's Guide

Gharib, M. and Dabiri, D. (2000). An overview of digital particle image velocimetry Flow Visualization: Techniques and Examples ed Smits A and Lim T T (London: Imperial College Press)

Huang, H., Dabiri, D. and Gharib, M. (1997). On errors of digital particle image velocimetry. *Meas. Sci. Technol.* **8**, 1427-40.

Keane, R. D. and Adrian, R. J. (1992). Theory of cross-correlation analysis of PIV images. *Appl. Sci. Res.* **49**, 191-215.

Koutsiaris, A. G., Mathioulakis, D. S. and Tsangaris. S. (1999). Microscope PIV for velocity-field measurement of particle suspensions flowing inside glass capillaries. *Meas. Sci. Technol.* **10**, 1037-46.

Lang, A. W. and Manglano, C. E. (2004). An experimental study of a turbulent shear layer at a clean and contaminated free-surface. *Exp. Fluids* **36**, 384-92.

Landry, F., Miller, T. J. and Leggett, W. C. (1995). The effects of small-scale turbulence on the ingestion rate of fathead minnow larvae. *Can. J. Fish. Aquatic Sci.* **52**, 1714-9.

Lin, C., Lai, W. J. and Chang, K. A. (2003). Siumltaneous particle image velocimetry and laser doppler velocimetry measurements of periodical oscillatory horseshoe vortex system near square cylinder-base plate juncture. *J. of Eng. Mech.* **129(10),** 1173-88.

Liu, Z. C., Landreth, C. C., Adrian, R. J. and Hanratty, T. J. (1991). High resolution measurement of turbulent structure in a channel with particle image velocimetry. *Exp. Fluids* **10**, 301-12.

Lourenco, L. M., Sivram, P. G. and LaSalle, R. T. (1994). On-line particle-image velocimeter: an integrated approach. *Appl. Optics* **33(13)**, 2465-70.

Malkiel, E., Sheng, J., Katz, J. and Strickler, J. R. (2003). The three-dimensional flow field generated by a feeding calanoid copepod measured using digital holography. *J. of Exp. Biol.* **206**, 3657-66.

Nikora, V. I., Aberlee, J., Biggs, B. J. F., Jowett, I. G. and Sykes, J. R. E. (2003). Effects of fish size, time to fatigue, and turbulence on swimming performance: A case study of *Galaxias maculatus*. *J. Fish Bio.* **63**, 1365-82.

Nimmo-Smith, W. A. M., Atsavapranee, P., Katz, J. and Osborn, T. R. (2002). PIV Measurements in the bottom boundary layer of the coastal ocean. *Exp. Fluids* **33**, 962-71.

Olsen, M. G. and Adrian, R. J. (2000). Out-of-focus effects on particle image visibility and correlation in microscopic particle image velocimetry. *Exp. Fluids* **Suppl.**, S166-74.

Perrin, R., Braza, M., Cid, E., Cazin, S., Moradei, F., Barthet, A., Sevrain, A. and Hoarau, Y. (2006). Near-wake turbulence properties in a high Reynolds number incompressible flow around a circular cylinder measured by two and three component PIV. *Flow Turb. Combust.* **77,** 185-204.

Raffel, M., Willert, C. and Kompenhans, J. (1998). Particle Image Velocimetry: A Practical Guide (Berlin: Springer-Verlag).

Ray, S. F. (2002). Applied Photographic Optics (Oxford: Focal Press).

Roy, A. G., Buffin-Belanger, T., Lamarre, H. and Kirkbride, A. (2004). Size, shape, and dynamics of large scale turbulent flow structures in a gravel bed river. *J. Fluid Mech.* **500**, 1-27.

Saikrishnan, N., Marusic, I. and Longmire, E. K. (2006). Assessment of dual plane PIV measurements in wall turbulence using DNS data. *Exp. Fluids* **41,** 265-78.

Samothrakis, P. and Cotel, A. J. (2006a). Finite volume gravity currents impinging on a stratified interface. *Exp. Fluids* **41**, 991-1003.

Samothrakis, P. and Cotel, A. J. (2006b). Propagation of a gravity current in a two-layer stratified environment. *J. Geophysical Res.* **111**, C01012.

Standen, E. M., Hinch. S. G., and Rand, P. S. (2004). Influence of river speed on path selection by migrating adult sockeye salmon. *Can. J. Fish. Aquatic Sci.* **61**, 905-12.

Vollmers, H. (2001). Detection of vortices and quantitative evaluation of their main parameters from experimental velocity data. *Meas. Sci. Technol.* **12**, 1199-207.

Westerweel, J., Dabiri, D. and Gharib, M. (1997). The Effect of a discrete window offset on the accuracy of cross-correlation analysis of digital PIV recordings. *Exp. Fluids* **23**, 20-8.

Willert, C. E. and Gharib, M. (1991). Digital particle image velocimetry. *Exp. Fluids* **10,** 181-93.

Chapter VII

Conclusion

This dissertation has explored the effects of turbulence on habitat selection and swimming kinematics of fish. Previous investigations into the impacts of turbulence on fish ecology (Mackenzie et al. 1994, Montgomery et al. 1996, Pavlov et al. 2000, Standen et al. 2002, Enders et al. 2003, Smith et al. 2005) have focused on the correlation between turbulent velocity fluctuations and ecological metrics of interest (e.g. gamete dispersal, predator/prey interactions, metabolic rates). Use of the temporal velocity fluctuations (specifically, the turbulence intensity, which is the standard deviation of the velocity about the mean divided by the mean) to describe turbulence assumes that turbulence is a random process only describable through the statistical variance in the distribution. Chapter 2 follows this conventional approach, showing that the turbulence intensity is lower in locations selected by brown trout than in otherwise suitable habitat. This finding is important in that it expands the findings of Smith et al. 2005, who reported similar results for juvenile salmonids in gravel-bed rivers, to include adult salmonids in sand-bed rivers. The correlation between reduced turbulence intensity and habitat preference, however, lacks explanatory strength since a coherent physical model explaining why temporal variations in velocity should affect habitat selection has yet to be proposed and vetted.

Since the 1970s (Brown and Roshko 1974, Hussain 1983, Williamson 1996) it has become increasingly apparent that turbulence is not primarily a random phenomenon. Turbulent flow is composed of coherent structures termed eddies. This dissertation has proposed and shown that by describing these vortical structures in turbulent flows, we can explain the impact of turbulence on fish swimming kinematics. Parts of this overall theory have previously been proposed. Specifically, the fact that the spatial scale of

turbulence should be important and is likely related to the fish length (L_f) has been proposed by Cada and Odeh (2001), Nikora et al. (2003), Biggs et al. (2005), and Lupandin 2005. Tritico and Hotchkiss (2005) proposed that the eddy orientation, while Liao (2007) proposed that the rate of rotation (vorticity - ω_e), would be important.

Turbulent eddies were described by their diameter (d_e), vorticity, convective velocity (u_{local}) and orientation. It was specifically shown in Chapter III that when the momentum of these eddies ($0.25m_e\omega_e d_e$ where m_e is the eddy mass) approached the momentum of the fish ($M_f V_f$ where M_f is the fish mass and V_f is the fish velocity and is equal to u_{local} when fish are station holding) the rate of spills increased. Fish spills were defined as rapid head rotations followed by downstream translation of the body. These spills occurred more frequently as the eddy vorticity and diameter increased. It was shown that the flow regime with the largest momentum ratio (Π_r) was the zone with the greatest spill rate. The momentum ratio of the 95th percentile eddy was slightly greater than unity (meaning that the eddy momentum was slightly greater than the fish momentum). Similarly, as the momentum ratio increased, the critical swimming speed of the fish decreased. Increasing eddy momentum was also correlated to greater percentage time and area of paired fin deployment.

The eddy orientation was also shown to affect the critical swimming speed, the duration of spills, the recovery sequence from spills, and the mode of pectoral fin deployment. The presence of large horizontal eddies resulted in a further reduction in the critical swimming speed compared to the presence of large vertical eddies; this concurred with the finding that recovery from pitching spills, resulting from horizontal eddies, lasted approximately 20% longer than yawing spills, resulting from vertically oriented eddies. Recovery from pitching spills took longer due to the tail orientation with respect to the rotational direction. The tail of creek chubs has a high aspect ratio such that there is a large control surface for countering yawing moments but a very small control surface for countering pitching moments. The lack of this large downstream moment arm for controlling pitching moments resulted in more frequent spills; furthermore, when pitching spills did occur, fish typically added two additional rolling maneuvers to the recovery sequence to allow the tail to be used as a control surface. Pectoral fins were observed to be deployed in three distinct patterns that correlated with the expected

moment on the body due to eddies (yawing, pitching) and internal static instability (rolling).

In the presence of large Π_r the tail beat frequency was less than, and tail beat amplitude was larger than, fish swimming in the control. These results were consistent with the findings of Liao et al. (2003) for fish swimming downstream from a single cylinder producing the highly predictable Kàrmàn vortex street ($Re_{cyl} = \frac{\bar{u}d_c}{\upsilon}$ where Re_{cyl} is the cylinder based Reynolds number, $\bar{u}$ is the cross-sectionally averaged velocity, d_c is the cylinder diameter, and v is the kinematic viscosity ranged from 5,600 to 20,000). From the description of Liao's vortex street it is apparent that even though their cylinder based Reynolds numbers are similar to the Reynolds numbers in Chapters III through V (Re_{cyl} ranged from 340 to 45,000) the flows in the current were much more complex due to the range of eddy diameters and vorticity in the flow. Results differed from Liao's work such that in these more chaotic flows fish did not match the eddy shedding frequency of the cylinder with tail beat frequency. Instead, it was shown that for a given eddy diameter the tail beat frequency was proportional to the eddy vorticity. In a uni-modal Karman vortex street the eddy vorticity and shedding frequency are linearly proportional to each other. As the simple Karman vortex street breaks down a continuum of eddy sizes and vorticity result. This research therefore suggest that Liao's observations of the link between shedding frequency and tail beat frequency may be generalized to more complex flow situations through a linear proportionality of tail beat frequency to eddy vorticity. This conclusion was arrived at through recognition of a linear relationship between the fish based persistence parameter and the fish based Strouhal number with dimensional analyses. The fish based persistence parameter ($T_f = \frac{\omega_e \cdot L_f}{4\pi \cdot V_f}$) measures the number of rotations that an eddy makes while traveling the length of a fish body and is a measure of the stationarity of turbulent eddies with respect to an interface. The fish based Strouhal number ($St_f = \frac{F_f \cdot A_f}{V_f}$ where F_f is the tail beat frequency and A_f is the tail beat amplitude) is a measure of the amount of work required for the fish to swim at a given speed.

In order to transfer the results for the effects of turbulent eddies on fish swimming kinematics back to a fluvial environment, turbulent eddy diameter and vorticity needed to be quantifiable in the field. A portable, submersible, miniature particle image velocimetry device (PIV) was developed to address this need. The device used the same imaging techniques as laboratory based PIV devices but submersed a battery powered laser and a laptop-driven camera in waterproof housings. The underwater PIV device was tested against a laboratory PIV for flow downstream from a circular cylinder. Vorticity and velocity results were similar to that of the laboratory PIV (within 4% and 9%, respectively). The eddy diameter was calculated to be smaller in the underwater PIV due to portions of eddies being chopped off by the restricted imaging zone (due to the reduced laser power). The underwater PIV was demonstrated in the Huron River, MI USA downstream from a 1.2 cm diameter submerged limb. This demonstration resulted in the imaging and processing of the first underwater PIV-analyzed eddies in a fluvial environment. As a result of the successful demonstration of this device, it is anticipated that future studies into the effects of eddy diameter and vorticity on fish in streams will be possible.

The primary results of this dissertation are therefore:

- Turbulence intensity is lower in locations selected by brown trout than in otherwise suitable habitat.
- Spills occurred more frequently as the eddy vorticity and diameter increased.
- When eddy momentum approached the momentum of the fish, critical swimming speed decreased, while spill rates along with the time and area of paired fin deployment increased.
- Large horizontal eddies, with respect to the fish, resulted in more frequent spills, a longer recovery time, reduced critical swimming speed, and different pectoral fin deployment patterns compared to large vertical eddies.
- A device for measuring underwater eddies in fluvial environments has been developed, tested, and demonstrated.

One of the goals of this dissertation work was to clarify the apparently inconsistent effects of turbulence on fishes as described in Chapter I (Table 1.1). The primary method for accomplishing this task was to move the discussion of turbulence-

fish interactions away from a velocity fluctuations model of turbulence to a turbulent eddy based model of turbulence. The eddy-based theory of the effects of turbulence on swimming fishes may be summarized to state that:

> Turbulent eddies with a diameter equal to the fish length which also have a high vorticity (and hence momentum) will have the greatest impact on fish locomotion. Furthermore, due to the asymmetry of the fish body and fin forms, the eddy orientation will also determine the outcome of fish-eddy interactions.

This theory, which has been proposed before by Cada and Odeh (2001) and Liao (2007), among others, has largely been validated by the results in this dissertation. While these results only represent a single series of experiments, it is anticipated that since the theory is based on the physical mechanisms of interaction between fish and turbulent eddies in the flow, it is likely to be validated across many other scenarios.

Future Work

The experiments in Chapters III, IV, and V produced eddies which were less than or equal to the fish length. A component of the fish/eddy theory that remains untested is the effects of eddies which are larger than the fish on swimming performance. The theory predicts that at some large diameter, eddies will cease to produce stability challenges and will instead act as large secondary currents. Work by Enders et al. (2003) may provide guidance to expected results as they have tested the effects of unsteady *primarily* rectilinear flow (pulsed pump flow) on fish metabolism. The connection between the Enders et al. (2003) research and large eddy flow may be relevant near the edges of the large eddies. At the edges of large eddies, flow is only mildly curved due to the large distance to the core, and the unsteady effects might be similar to unsteady rectilinear flow swimming.

Future work should also focus on expanding these results to other species and body/fin forms. The lab experiments have shown the importance of turbulent eddies on the swimming kinematics of creek chub as a model North American fusiform fish. Other swimming species (both fish and other) with varying propulsive and control surface patterns, body forms, and lengths should be investigated to understand the interplay of

these parameters with turbulent eddies on swimming performance. Work by Eidietis et al. (2002) on the differences in ability to counter rolling torques on three species of fish – creek chub (*Semotilus atromaculatus*), blue gill (*Lepomis macrochirus*), and large mouth bass (*Micropterus salmoides*) showed that creek chub were able to counter greater rolling torques than the other two species. While the researchers expected that creek chub would be least adept at countering rolling perturbations, due to small fin area and fusiform body shape, body depth did not relate to ability to resist rolling. Furthermore, in spite of the smaller fin surface area of the creek chub, the ventral placement of the paired fin system was attributed to the greater performance of creek chub compared with the centrarchid species which had more laterally placed paired fins. These results indicate that body depth (and hence metacentric height) may not be important in countering turbulent perturbations but that the fin placement pattern and orientation is likely to be important.

Similarly, the effect of turbulent eddy momentum ratio and the persistence parameter on predator/prey interactions, habitat selection, and reproduction should be investigated in the field. Previous research into the effects of turbulence on habitat selection (Pavlov et al. 2000, Smith et al. 2005, Cotel et al. 2006), predator/prey interactions (Landry et al. 1995, Mackenzie and Kiorboe 2000) and reproduction (Crowder and Diplas 2000) have used point velocity measurement devices to characterize the temporal variations in velocity. Pavlov et al. (2000), Cada and Odeh (2001) and others proposed that the relative size of turbulent eddies to fish would be important. Support for this theory has been provided in Chapters III through V in laboratory experiments and is also expected to be true in fluvial environments. In order to test the impact of turbulent eddy diameter on parameters such as habitat selection and reproduction in the field an underwater PIV device has been developed and demonstrated (Chapter VI). Future studies should mimic those by Smith et al. (2005) and Cotel et al. (2006) using both an Acoustic Doppler Velocimeter (ADV) and the underwater PIV to characterize the flow. The side-by-side comparison will allow the strength of correlation between habitat selection and the results from the underwater PIV device to be compared to the correlation strength between habitat selection and data from the ADV device. Additionally, the side-by-side comparison will help to contextualize each approach by

providing insight into the connection between point measurement results and turbulent eddies in fluvial environments.

The role of turbulence in habitat selection of adult brown trout adds further support for including turbulence as an important index in developing habitat models. Results from Chapters II through V suggest that regions of a stream which have been designated as suitable habitat based on standard habitat suitability indices for adult brown trout may be further restricted based on the eddy momentum ratio. The areas that are most likely to be affected by including the eddy momentum ratio as a habitat suitability index are areas at the upper range of the suitable average velocity range for brown trout which also have high eddy momentum ratios where the eddies are primarily horizontal in orientation. The suitability of such areas for habitat could be increased by decreasing the eddy momentum ratio through decreasing eddy diameter by, for example, installing small diameter flow obstructions upstream from the region of interest. The proportion of horizontal eddies in a region could be reduced by introducing vertical flow obstructions. This theory could readily be tested in the laboratory or field setting by installing horizontal and vertical cylinder arrays to determine if there is a preference at higher flow rates. A similar test has been conducted by Webb (1998) which found that river chub (*Nocomis micropogon*) and smallmouth bass (*Micropterus dolomieu*) did not entrain on individual horizontal and vertical cylinders at different rates. While this study indicates that there may not be an effect of cylinder orientation on flow preference the study did not explicitely allow for choice between cylinder orientations (which would have involved placement of both a horizontal and vertical cylinder in the flow simultaneously), nor was an array of cylinders placed in the flow which, rather than providing a single source of eddy orientations would more broadly influence the flow.

As the case for the importance of turbulent eddies increases, engineering guidelines and best management practices should be developed to provide practitioners guidance in the design of more successful fishways and restoration projects. Current fisheries engineering designs (e.g. fish ladders, fish screens) are based on mean velocity values even though many of these structures are highly turbulent. Turbulence in fish ladders, for instance, is often used to reduce mean velocities in these high slope conditions. The results from this dissertation provide guidance to fish passage designers

because it shows that not all turbulence affects fish equally. Specifically, turbulent eddies of large momentum with respect to the fish momentum will have the greatest impact on the fish. Additionally, horizontal eddies have been shown to provide a greater stability challenge than vertical eddies, therefore specific care should be shown in avoiding designs which produce horizontal eddies of the same diameter as the fish length. Similar to fish passage design, stream restoration designs that focus on micro-habitat such as rock barbs and large woody debris can be adjusted to avoid creating turbulent eddies that will make otherwise suitable habitat too unstable for swimming.

References

Biggs, B. J. F., Nikora, V. I. and Snelder, T. H. (2005). Linking Scales of flow variability to lotic ecosystem structure and function. *River Research and Applications* **21**, 283-298.

Brown, G. L. and Roshko, A. (1974). On Density Effects and Large Structure in the Turbulent Mixing Layers. *Journal of Fluid Mechanics* **64**, 775-816.

Cada, G. F. and Odeh, M. (2001). Turbulence at hydroelectric power plants and its potential effects on fish. *Report to Bonneville Power Administration*, Contract No. 2000AI26531, Project No. 200005700: 1-37.

Cotel, A. J., Webb, P. W., and Tritico, H. M. (2006). Do Brown Trout Choose Locations With Reduced Turbulence? *Transactions of the Am. Fisheries Soc.* **135**, 610-619.

Crowder, D. W. and Diplas, P. (2000). Evaluating Spatially Explicit Metrics of Stream Energy Gradients using Hydrodynamic Model Simulations. *Canadian J. Fisheries and Aquatic Sci.* **57(7)**, 1497–1507.

Enders E C, Boisclair D, and Roy A G. (2003). The Effect of Turbulence on the Cost of Swimming for Juvenile Atlantic Salmon. *Canadian Journal of Fisheries and Aquatic Science* **60**, 1149-1160.

Hussain, A. K. M. F. (1983). Coherent structures – reality and myth. *Physics of Fluids* **26(10),** 2816.

Landry, F., Miller, T. J. and Leggett, W. C. (1995). The effects of small-scale turbulence on the ingestion rate of fathead minnow larvae. *Canadian Journal of Fisheries and Aquatic Sciences* **52**, 1714-1719.

Liao, J. C. (2007). A review of fish swimming mechanics and behavior in altered flows. *Philosophical Transactions of the Royal Society B* **362(1487)**, 1973-1993.

Liao, J. C., Beal, D. N., Lauder, G. V. and Triantafyllou, M. S. (2003). Fish Exploiting Vortices Decrease Muscle Activity. *Science* **302**, 1566-1569.

Lupandin, A. I. (2005). Effect of Flow Turbulence on Swimming Speed of Fish. *Biology Bulletin* **32(5)**, 558-565.

Mackenzie, B. R. and Kiorboe T. (2000). Larval Fish Feeding and Turbulence: A Case For the Downside. *Limnology and Oceanography* **45**, 1-10.

Mackenzie, B. R., Miller, T. J., Cyr, S. and Leggett, W. C. (1994). Evidence for a Dome Shaped Relationship Between Turbulence and Larval Fish Ingestion Rates. *Limnology and Oceanography* **39(8),** 1790-1799.

Montgomery, D. R., Buffington, J. M., Peterson, N. P., Schuett-Hames, D. and Quin, T. P. (1996). Stream-bed Scour, Egg Burial Depths, and the Influence of Salmonid Spawning on Bed Surface Mobility. *Canadian Journal of Fisheries and Aquatic Sciences* **53**, 1061-1070.

Nikora, V. I., Aberlee, J., Biggs, B. J. F., Jowett, I. G. and Sykes, J. R. E. (2003). Effects of Fish Size, Time to Fatigue, and Turbulence on Swimming Performance: A Case Study of Galaxias maculatus. *Journal of Fish Biology* **63**, 1365-1382.

Pavlov, D. S., Lupandin, A. I. and Skorobogatov, M. A. (2000). The Effects of Flow Turbulence on the Behaviour and Distribution of Fish. *Journal of Ichthyology* **40(S2)**, S232-261.

Smith, D. L., Brannon, E. L. and Odeh, M. (2005). Response of Juvenile Rainbow Trout to Turbulence Produced by Prismatoidal Shapes. *Transactions of the American Fisheries Society* **134**, 741-753.

Standen, E. M., Hinch, S. G., Healey, M. C. and Farrell, A. P. (2002). Energetic Costs of Migration through the Fraser River Canon, British Columbia, in Adult Pink and Sockeye Salmon as Assessed by EMG Telemetry. *Canadian Journal of Fisheries and Aquatic Sciences* **59**, 1809-1818.

Tritico, H. M. and Hotchkiss, R. H. (2005). Unobstructed and Obstructed Turbulent Flow in Gravel Bed Rivers. *Journal of Hydraulic Engineering* **131(8)**, 635-645.

Webb, P. W. (1998). Entrainment by river chub Nocomis micropogon and smallmouth bass Micropterus dolomieu on cylinders. *J. Exp. Biol*. **201**, 2403–2412.

Williamson, C. H. K. (1996). Vortex dynamics in the cylinder wake. *Annual Review of Fluid Mechanics* **28**, 477-539.